ISSN: 1813-1786
Volume No. 16
Indexed in:
ULRICH'S P. D.
PASTIC

TECHNICAL JOURNAL

2011

University of Engineering and Technology
Taxila

ISSN: 1813-1786
Volume No. 16
Indexed in:
ULRICH'S P. D.
PASTIC

TECHNICAL JOURNAL

2011

University of Engineering and Technology Taxila

EDITORIAL BOARD

CONTENTS

Discover papers in this journal online http://techjournal.uettaxila.edu.pk
Indexed in Ulrich Periodical Directory, Directory of Periodical PASTIC

Determining Critical Condition for Initiation of Bed Load Transport

Dr. Muhammad Ashiq[1] and Zahra Kharal[2]

Abstract

This investigation was designed to develop bed load transport initiation model. The data from four UK sites (Northern England Region), two USA sites (Rocky Mountains Region) and from a flume study (carried out in old brewery hydraulics laboratory, University of Newcastle Upon Tyne, UK) were collected and analyzed. By using this data a bed load transport initiation model based on the maximum lower size (MLS, the largest size for which all smaller tracers moved) was developed, using individual particle sizes (i.e. fractional sizes) along with the discharge based approach (initially introduced by Schoklitsch). This model comprised bed material size gradation parameter (D84/D16), shape factor (SF) and slope (S) parameters (three parameters that play a significant role in the initiation of motion). The performance of the model (hereafter called MLS model) was compared with the collected field and laboratory data. It performed quite satisfactorily with the Roaring River data (upstream site), as generated data points were located in the close proximity of the line of perfect agreement (LPA) and 10% margin lines. Likewise, its performance was found well with the four flume data sets as majority of the generated points were situated close to LPA and within 10% margin lines. In another comparison test with MUS model its performance was found much better. All the comparisons have showed encouraging results. However, the data used for model development and testing was limited; more data therefore need to be collected to generalize the application of the model further.

Keywords: Critical condition, Discharge theory, Initiation, Maximum upper size, Maximum Lower Size Models, Model performance, Relative position

Introduction

The critical/threshold condition at which initiation (i.e. beginning of movement of bed particles that were stationary some time before) of bed load transport starts has been described by different investigators. DuBoys [1] stated "excess of some quantity above the critical level at which transport begins"; Simons and Sentürk [2] said "when the flow over movable boundaries of a channel has hydraulic conditions exceeding the critical condition for motion of the bed-material, sediment transport will start"; also they mentioned that "most transport equations calculate the sediment transport as a function of the excess of some flow quantity, such as shear stress or discharge, above the critical level"; Carson and Griffiths [3] described this condition as "some critical or threshold level of discharge, velocity or related parameter must be attained before the gravel on a channel bed will start to move downstream"; Klingeman and Matin [4] stated that "transport initiation process requires larger flows that must exceed the threshold-motion values"; Dancey et al. [5] said it is “beginning of movement of bed particles that previously were at rest and that subsequently roll or slide along the bed”; and Dey [6] stated it “condition being just sufficient to initiate sediment motion”. However, this “critical condition” as described by the well known scientists is an assumption that there is no sediment transport at lower flows. In reality there can be, but of such a small amount that in practical terms it can be ignored [7]. How can this critical condition be determined accurately? Why is there a need to determine it? A large variety of models are available for determining this condition, so why is it necessary to develop another model? These are the likely questions that could arise in minds of the sediment investigators/scientists working in this field. To find answers to these questions this study was designed, with special emphasis on the first question how this condition can be determined accurately. This was answered through the development of an optimal model that incorporates effects of all the significant parameters relevant to initiation process. To achieve this objective two models, based on the maximum lower size (MLS, the largest size for which all smaller tracer particles moved) and maximum upper size (MUS, absolute maximum size of moved tracer particles), were developed by using individual particle size and discharge based theory - a theory which is more practical and used (relatively) infrequently in the available models and found better (i.e. more practical) than the other theories (i.e. shear stress, stream power and velocity) in the recent studies [8]. The MUS model was developed for the purpose of comparison

[1] Civil Engineering Dept., University of Engineering and Technology Lahore, [2] Civil Engineering Dept., University of Toronto. Canada.

and to prove that how results could fluctuate with the use of model based on the maximum upper size of moved bed particles. Data used in the development of these models were collected from four UK sites (Harwood Beck Upper and Lower sites at Harwood, River Wear site at Stanhope, and South Tyne River site at Alston - all sites located in the Northeast England) and two USA sites (Ypsilon Lake Trail Bridge site, upstream site, and Alluvial Fan Road Bridge site, downstream site, located at the Roaring River in the Rocky Mountain National Park Colorado, USA - collected during July 1995). The performance of the MLS based model was compared with the MUS based model and with the laboratory data (collected at the Newcastle University, UK) and field data (collected from the Roaring River during May-June 1995 period); these data which were not used in the development of the models.

Why to Investigate Initiation Process?

The following salient features described by different investigators highlight the significance of the process and reflect why it is important to understand and further investigate initiation phenomena, especially, in coarse bed-material rivers [7].

1. For determining maximum flows required to flush out the fine sized sediment and organic matter present on the river bed among the gravel particles. The presence of these fine size sediment particles reduces the permeability by filling the spaces between the gravels necessary for aquatic habitat.
2. For maintaining bed stability in navigational channels that otherwise may be affected by the waves generated by the ships or boats.
3. To explain the difference between river bed stability and mobility.
4. To provide premises for the analysis and design of stable river beds.
5. For creating certain types of bed form on river beds that may be useful for the dual purpose of flood control and navigation.
6. For maintaining the stability of toxic substances hazardous for human and aquatic life when present in river beds.
7. To understand the bed load process which is necessary in the development of bed load transport functions/models.

Effects of Particles Position on Their initiation

It was observed (frequently) during this investigation at the UK and USA sites and in the flume channel investigation that larger bed particles (tracers) moved while smaller ones didn't, depending upon their position across and along the channel bed. The position of particles played a role in their movement in two ways.

a) Their position relative to other particles: The tracer particles which were located behind larger particles or located in depression or located in small pools were moved infrequently compared with those located without any shelter or those which were not hidden or situated outside the pools, having the same sizes and experiencing the same water discharge.

b) Their position relative to flow currents/flow depths: The tracer particles which were facing (relatively) stronger water currents, especially, those located in flow threads moved earlier compared with those which were facing weaker water currents or located outside the threads, even though the particle sizes and flow rates were the same. As in natural rivers slope changes (commonly) across the channel width and along the channel length, therefore, particles located in the shallower places/depths did not move with the same value of water flow rates as those located at places with greater water depths.

Model Development

Bases for Model Development

Owing to the advantages associated with the discharge based approach (e.g. more practical) and certain flaws/problems with available models, such as not including particle shape effect (SF, a significant parameter to account for the particle shape effects) while some only account for the absolute grain size. Also, these models have been developed using the maximum upper size of the moved particles with the maximum value of water discharge. This is not a realistic approach to deal with the initiation condition as it is possible that with the same value of water discharge larger size particles may move earlier due to their position in the channel bed, whereas smaller size particles move later or do not move at all. A particle located in a flow thread is likely to move earlier than a particle located out of the flow thread or located at a shallow place. Because of these and other reasons when the existing critical discharge theory based (initiation) models are applied to the real field conditions they generally perform poorly and the computed critical discharge values differ drastically from the observed ones. The poor basis of the existing models [4] suggests a need to develop a model (or models) that can predict critical condition accurately for the initiation of bed material movement in coarse bed material rivers. Two such models, therefore, are suggested below, one based on the maximum lower size (MLS, largest size for which all smaller tracers moved) and other on the maximum upper sizes (MUS, absolute maximum size of tracer moved) of the moved tracer particles. These models are

$$q_{ci(MLS)} = \alpha_{MLS} \left(D_{i\ (MLS)}\right)^{\beta_{MLS}} \quad (1)$$

$$q_{ci(MUS)} = \alpha_{MUS} \left(D_{i\ (MUS)}\right)^{\beta_{MUS}} \quad (2)$$

where $q_{ci(MLS)}$ and $q_{ci(MUS)}$ are the critical unit water discharges (m^3/sec/m) required to move the maximum lower size (MLS) and maximum upper size (MUS) of the bed material particles, respectively; α_{MLS} and β_{MLS} are the coefficient and exponent for the maximum lower size based model; α_{MUS} and β_{MUS} are the coefficient and exponent for the maximum upper size based model; and $D_{i(MLS)}$ and $D_{i(MUS)}$ are the ith maximum lower and maximum upper sizes of the moved particles with $q_{ci\ (MLS)}$ and $q_{ci(MUS)}$ discharges, respectively.

For determining the parameters (i.e. α_{MLS}, β_{MLS} α_{MUS}, and β_{MUS}) of these models (i.e. Equations (1) and (2) - hereinafter called as MLS model and MUS model) data collected from the four UK and two USA sites have been used and following steps were taken.

Step - I

Development of Individual Models Using Maximum Lower Size (MLS) of Moved Particles:

Various empirical models defining the relationship between the unit critical water discharge and the maximum lower size (MLS) of the moved particles were developed for the UK and US sites data. For each of the UK sites five different models were developed, because a high flood passed on 31 January 1995 altering the channel cross-sections and bed material formation. These five models were developed for five different data cases for each site: a) combined data (using combined data for before flood, BF; after flood, AF; and flood point, F), b) before 31 January 1995 (BF, before flood), c) after 31 January 1995 (AF, after flood), d) before 1 February 1995, and e) after 30 January 1995. For demonstration purpose out of these five cases models based on the combined data (i.e. for the South Tyne River site) and those based on post 31 January data (i.e. for River Wear site) are depicted here in Figure 1, whereas the models themselves for all the five cases are given in Table 1. For the River Wear site after 31 January data were used for model development because of the significant variations

in channel cross-section and bed material formation caused by the high flood passed on 31 January 1995. As a result of these variations the river channel characteristic changed and the river could have acted as if it was two different channels before and after the flood. The involvement of only one single flood point caused substantial variation in the coefficient and exponent values of the models, which is evident from the difference in cases 'c' (data after 31 January 1995) and 'e' (data after 30 January 1995). Likewise, a significant effect of a single flood point is also evident for the different cases 'b' (i.e. data before 31 January 1995) and 'd' (i.e. data before 1 February 1995).

On the other hand for each of the USA sites these models were developed using three data cases as a very high flood that passed after the May-June 1995 study period significantly changed the channel cross-sections and bed material formation. These three cases were: a) combined data (before + after flood i.e. May-June 1995 and July 1995 periods together); b) before flood, BF (May-June 1995 period); and c) after flood, AF (July 1995 period). The developed models for both of the USA sites for the three cases are given in Table 1. The effects of the high flood on model parameters (i.e. coefficient and exponent values) are evident from difference of cases 'b' (before flood) and 'c' (after flood), in comparison with the case 'a' (combined data).

As is evident from Table 1 (for maximum lower size), variations in the model exponent values between sites and at-a-site generally do not have any specific trend except that the exponent values for the UK sites are generally larger than the exponent values for the USA sites, which are 1 for all the three cases. The lack of any specific trend in the exponent values is mainly because each river has characteristics of its own and the number of data points for each case was different. The value of exponents (for combined data case 'a') varies between 0.80 and 1.58 (Table 1) for the UK sites. The variations in exponent values found for the maximum lower size (Table 1) are less than the variations for the maximum upper size (Table 2). Nevertheless, the maximum lower size based exponents has a realistic base, as movement of bed particles does not only depend on the absolute and relative grain size effects but also their position on channel bed relative to the flow current/flow depth. It should be remembered that the relationships (given in Table 1) based on less than four data points may have little meaning and are included for completeness only. Thus no physical interpretation should be made of equations based on less than four data points. Figures plotted (not given) based on combined data, which include the flood peak, for the UK sites showed that the maximum lower size (MLS) and maximum upper size (MUS) data points are situated close to each other at very high flows. This showed a possibility of equal mobility of bed material at very high flows. The results of equal mobility at very high flows are in agreement with the results of Ashworth and Ferguson [9] who said that "precise equal mobility of small and large particles was approached in the data set with the highest shear stresses and transport rates". These results partly supported the view point of Ferguson [10], when he mentioned the recent consensus of opinion (based on Ashworth and Ferguson [9], Wilcock [11] study results) according to which transport may approach equal mobility at high excess stresses and transport rates. These field investigations regarding equal mobility of bed material were different than those observed in the flume channel investigation in the Old Brewery Hydraulics Laboratory (Civil Engineering Department, Newcastle University, UK). In the flume investigation it was observed that after the movement of few particles just with 5-10 % increase in water discharge the whole bed material started to move. The probable reason for this equal mobility could be the smaller size distribution variation of bed materials (used in experiments) as the values of D84/D16 were 1.46, 1.93, 1.49 and 1.64 for the I, II, III and IV set of materials, respectively. On the other hand D84/D16 values for the field sites were 6.03, 5.07 and 5.53, respectively. Beside the D84/D16 parameter, other parameters that may have played an important role in the mobility of bed material are the shape factor (SF, which incorporates the effect of long, median, and short axes of the bed material particles) and slope (S) parameters, as these parameters were considerably different for the field and flume investigations.

Step-II

Development of Individual Models Using Maximum Upper Size (MUS) of Moved Particles:

Similar to the maximum lower size (MLS) case the empirical models were also developed for the maximum

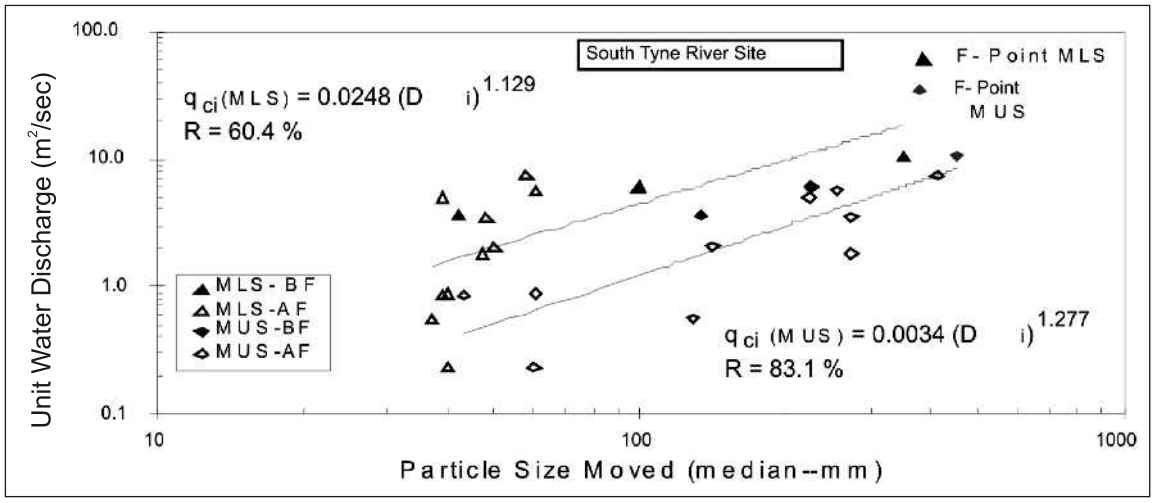

(a)

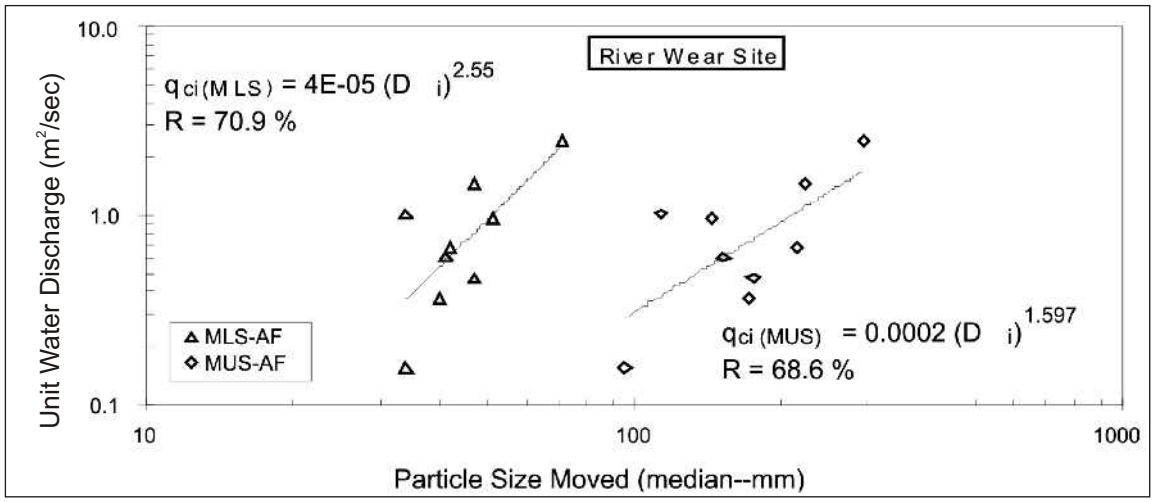

(b)

Figure 1: Relationship between unit water discharge and maximum lower size (MLS) and maximum upper size (MUS) of the moved tracer particles for: a) combined flow case of South Tyne Riversite; and b) after flood case for River Wear site (i.e. for after 31 January.

upper size (MUS) of the moved particles for the UK and USA sites and are presented in Table 2. For demonstration purpose these models for the South Tyne River and River Wear sites for the combined data case are shown in Figure 1.

Like the MLS model for the MUS model the exponent values for the UK sites were generally greater than the exponent values for the USA sites (i.e.$\leq$ 1.1). The value of exponents for the UK sites, which include the flood peaks, vary between 1.28 and 1.47. On the other hand the exponent values for the Roaring River (Colorado), during three different periods in 1984-1985 (recorded by Bathurst [12]), ranged between 0.20 and 0.39 [10]. Inpasihardjo [8] recorded the exponent value of 0.54 for the Pitzbach (Austria), whereas for the UK sites his values ranged between 0.93 and 1.17. All these exponent values, recorded by three different researchers, have been obtained using a discharge based approach. From these values a significant difference in the exponent values (within and between rivers) is evident. Bathurst [12] developed a function for the exponent value (exponent, $b=f\ n(D_{84}/D_{16})$ which was subsequently modified by Inspasihardjo [8], however their functions do not explain the variations, therefore further explanation is needed which may be achieved by incorporating other parameters (e.g. shape).

Table 1: Models defining relationship between critical unit water discharge and maximum lower size (MLS) of moved particles for the UK and USA sites.

Site	Data Points	Function	R (%)
Harwood Beck Upper			
a. Combined data (i.e. before and after flood)	14	$q_{ci(MLS)} = 0.0021 (D_i)^{1.580}$	73.42
b. data before 31 January (flood date) 1995	3	$q_{ci(MLS)} = 0.050 (D_i)^{0.898}$	99.89
c. data after 31 January 1995	10	$q_{ci(MLS)} = 0.0001 (D_i)^{2.308}$	63.56
d. data before 1 February 1995	4	$q_{ci(MLS)} = 0.027 (D_i)^{1.052}$	99.85
e. data after 30 January 1995	11	$q_{ci(MLS)} = 0.001 (D_i)^{1.709}$	77.97
Harwood Beck Lower			
a. Combined data (i.e. before and after flood)	13	$q_{ci(MLS)} = 0.0383 (D_i)^{0.800}$	51.28
b. data before 31 January (flood date) 1995	3	$^{*}q_{ci(MLS)} = 3.0E+6(D_i)^{-4.162}$	65.27
c. data after 31 January 1995	9	$q_{ci(MLS)} = 1.0E-5 (D_i)^{2.881}$	47.11
d. data before 1 February 1995	4	$q_{ci(MLS)} = 0.143 (D_i)^{0.603}$	93.06
e. data after 30 January 1995	10	$q_{ci(MLS)} = 0.009 (D_i)^{1.126}$	67.31
River Wear at Stanhope			
Table 1 Continued	13	$q_{ci(MLS)} = 0.0025 (D_i)^{1.524}$	82.34
a. Combined data (i.e. before and after flood)	3	$q_{ci(MLS)} = 2.0E-6 (D_i)^{3.412}$	99.50
b. data before 31 January (flood date) 1995	9	$q_{ci(MLS)} = 4.0E-5 (D_i)^{2.550}$	70.92
c. data after 31 January 1995	4	$q_{ci(MLS)} = 0.025 (D_i)^{1.057}$	97.67
d. data before 1 February 1995	10	$q_{ci(MLS)} = 0.002 (D_i)^{1.522}$	85.73
e. data after 30 January 1995			
****South Tyne River at Alston**			
a. Combined data (i.e. before and after flood)	13	$q_{ci(MLS)} = 0.0248 (D_i)^{1.129}$	60.42
c. data after 31 January 1995	10	$q_{ci(MLS)} = 5.0E-08 (D_i)^{4.572}$	71.41
d. data before 1 February 1995	3	$q_{ci(MLS)} = 0.588 (D_i)^{0.496}$	99.65
e. data after 30 January 1995	11	$q_{ci(MLS)} = 0.022 (D_i)^{1.133}$	60.25
U/S Site Roaring River			
a. Combined data (i.e. before and after flood)	7	$q_{ci(MLS)} = 0.007 (D_i)^{1.053}$	96.95
b. Data before flood (May-June 1995 period)	3	$q_{ci(MLS)} = 0.072 (D_i)^{0.408}$	82.64
c. Data after flood (July 1995 period)	4	$q_{ci(MLS)} = 0.425 (D_i)^{0.064}$	4.24
D/S Site Roaring River			
a. Combined data (i.e. before and after flood)	7	$q_{ci(MLS)} = 0.007 (D_i)^{0.993}$	78.87
b. Data before flood (May-June 1995 period)	3	$^{*}q_{ci(MLS)} = 0.425(D_i)^{-0.185}$	54.86
c. Data after flood (July 1995 period)	4	$q_{ci(MLS)} = 0.236 (D_i)^{0.181}$	84.68

*The reason for these models having negative exponents is too few data to define a realistic relationship.

** South Tyne River don't have model for case b, as there were only two data points for this case.

NB: In all these models confidence levels were fixed at 95 % which provided significance levels = 0.05.

The main possible factors for difference in the exponent values within and between rivers are:

a) Bed sediment size distribution that could vary temporally and spatially. A good example of the temporal variation in the exponent values is the difference of values obtained by Bathurst [8] using Roaring River data and the values obtained by the author using the same river site but with data recorded in 1995 [6, 9]. Likewise, the difference of exponent values obtained by the author and Inpasihardjo or Bathurst indicated the effect of spatial variations. The effects of temporal and spatial variation in the bed size distribution on the exponent values for different sites are also evident from Figure 2;

b) Shape of sediment particles, which could vary with the geology of the catchment. The effect of geology on the exponent values is evident from the difference of exponent values obtained by the author (using UK river data) and those obtained by the Inpasihardjo (using Austrian data) - data from

two different catchments. However, the exponent values obtained by the Bathurst and Inpasihardjo (for Austrian data) are based upon data that were collected using the Helley-Smith sampling technique, while the author's data were collected by using the tracer technique. Another example of the shape effect on the exponent values is clear from difference of exponent values obtained by the first author and the Inpasihardjo, although both used the UK data and same sampling technique was followed but with different sites.

The effect of the above mentioned factors on the exponent values is also evident from the discussion by Ferguson [10]. In contrast to the discharge based approach, investigators including Andrews and Erman [15], Ashworth and Ferguson [9] used a shear stress based approach (using maximum particles size moving with different flows) to determine the exponent value [10]. Their exponent values varied between 0.65 and 1.00. By using the same shear stress approach Parker and Klingman [13] obtained the exponent value of 0.98 (for Oak Creek, using subsurface grain size distribution), which was revised to 0.90 (based on surface grain size distribution). Based on the results by different researchers, Ferguson [10] said "critical stress to move an individual particle depends far less on its own size than on the ambient size, or perhaps (in the case exponent = 1) entirely on the latter and not at all on the individual size. In this case, termed equal mobility' by Parker and Klingman [13], particles of all sizes will move at the same stress and by implication the same critical discharge;

c) Sampling technique followed for data collection may have affected the collected data (i.e. whether data were collected by using the tracer technique or Helley-Smith sampling technique) [14].

d) Lack of data points may be a reason to affect the exponent values, as it affected the exponent values in Tables 1 and 2.

Step – III

Development of Models' (Equation 1 and 2) Parameter: In order to determine the values of parameters (i.e. α_{MLS}, $\beta_{MLS,}$ α_{MUS}, and β_{MUS}) of Equation (1) and (2) only the combined case models were taken (from Tables 1 and 2) for the three UK sites, no considerable variations occurred in the channels' cross-section for these sites during the 31 January 1995 flood. For the River Wear site significant changes in channel cross section and bed material size distribution were recorded after a high flood passed on 31 January 1995. Also, more data points were available for the after flood case compared with the before flood case. Therefore the after flood (AF) model is used for the River Wear site. The selected models in terms of coefficient (α) and exponent (β) for both of the MLS and MUS sizes are given in Table 3 along with some other parameters.

Likewise, for the USA sites out of the three cases (given in Table 1 and 2) only the after flood case (i.e. for July 1995 period) was taken, as the high flood which passed after the May-June 1995 study period altered the channel cross-sections and coarsened the bed material. Also, the after flood case has more data points. The selected cases and other corresponding variables that were used to develop functions for parameters (i.e. α_{MLS} and β_{MLS}) of Equation (1) and parameters (i.e. α_{MUS} and β_{MUS}) of Equation (2) are given in Table 3. The statistical technique used for the development of these functions was multi-variative analysis.

As explained earlier and found during the field and flume investigations the bed material gradation parameter (D_{84}/D_{16}), shape factor (SF) and slope (S) play an important roles in bed material movement. These results are supported by the results depicted in Figure 2 (based on data given in Tables 3 and 4. In this figure data points from the UK sites (recorded by [3] and [16]) are located far above the other than UK data points. The reason for this different data distribution may be that UK rivers have different particle shapes (as evident from shape factor values in Table 3) compared with the other data in main cluster, which are mostly from the USA sites. Thus in the development of functions (for Equation (1) and Equation (2)) beside the D_{84}/D_{16} parameter other parameters such as shape factor (SF), slope (S), channel width (W) and reference particle size (D_r) have to be involved to account for effects of all the significant variables. The developed functions are

For Maximum Lower Size

α_{MLS} (R = 93.2 %)

$$\alpha_{MLS} = \left(-26.9 - 156S - 1.38\frac{D_{84}}{D_{16}} + 83.1SF\right)\left(\frac{\sqrt{g}D_r^{1.5}}{W^{\beta_{MLS}}}\right) \quad (3)$$

β_{MLS} (R = 85.7 %)

$$\beta_{MLS} = 6.66 - 11.5SF \quad (4)$$

Maximum Upper Size

α_{MUS} (R = 95.3 %)

$$\alpha_{MUS} = \left(-0.58 + 36.2S + 0.101\frac{D_{84}}{D_{16}}\right)\left(\frac{\sqrt{g}D_r^{1.5}}{W^{\beta_{MUS}}}\right) \quad (5)$$

β_{MUS} (R = 89.1 %)

$$\beta_{MUS} = 7.16 - 13.28SF \quad (6)$$

where SF = shape factor = $c/(ab)^{0.5}$, c = shortest particle axis, b = intermediate axis, and a = longest axis); and D_r = reference particle size (m), represents the relative size effects of the mixture and equals D_{50} for log-normal size distribution and D_{63} for non log-normal size distribution. For these functions (Equations (3) to (6)) channel slopes used ranged between 0.008 and 0.047 (m/m), D_{50} of the bed material ranged between 0.065 and 0.140 m, and channel width (mean) between 6 and 30 m.

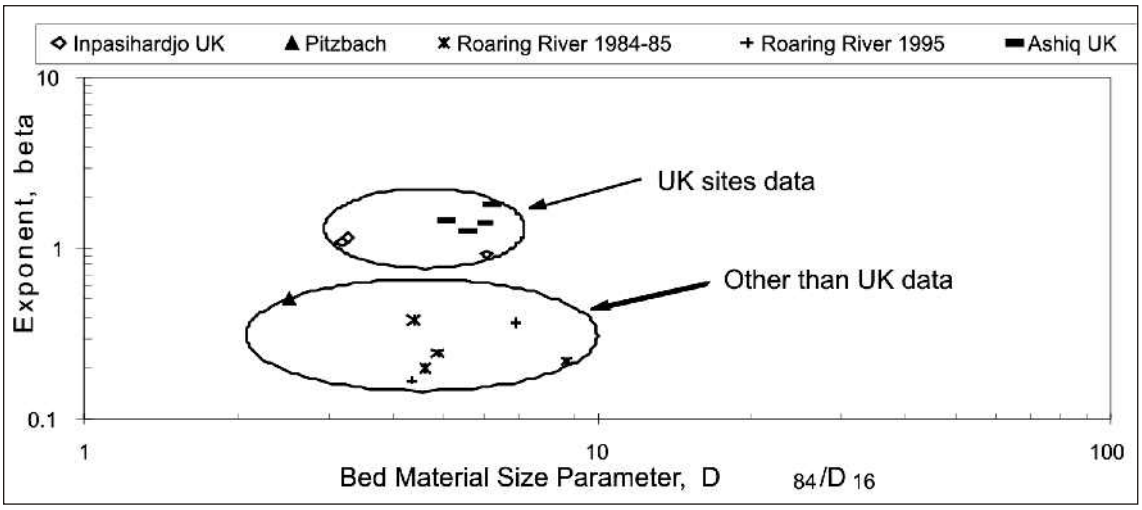

Figure 2: Relationship between exponent, beta and bed material size parameter, D84/D16 using UK sites data and other than UK sites data.

Table 3: Variables used for the development of models (Equation 1 and 2) parameter (α_{MLS}, β_{MLS}, α_{MUS}, and β_{MUS}).

Site	Slope (S) (m/m)	D_{84}/D_{16}	Shape Factor (SF)	Maximum Lower Size (MLS)		Maximum Upper Size (MUS)	
				α	β	α	β
(1)	(2)	(3)	(4)	(5)	(6)	(7)	(8)
Harwood Beck Upper (Combined Data Case)	0.008	6.03	0.454	0.0021	1.580	0.0008	1.399
Harwood Beck Lower (Combined Data Case)	0.0189	5.07	0.478	0.0383	0.800	0.0004	1.465
River Wear (After 31 Jan. 1995 Data Case)	0.0162	6.02	0.447	4.0E-05	2.550	0.0002	1.597
South Tyne River (Combined Data Case)	0.0105	5.53	0.482	0.0248	1.129	0.0034	1.277
U/S Site Roaring River (July 1995 Data Case)	0.0350	6.92	0.541	0.425	0.064	0.098	0.366
D/S Site Roaring River (July 1995 Data Case)	0.0473	4.36	0.585	0.236	0.181	0.234	0.167

Table 4: Parameters of Equation, $q_{ci} = \alpha (D_i)^{\beta}$ fitted for each site and corresponding reference particle size.

Site	Equation Parameters		Equation R^2 (%)	Reference Particle Size (mm)	Bed Material Size Gradation Parameter(D_{84}/D_{16})
	α	β			
1	2	3	4	5	6
(a) Bathurst's [8] Roaring River Data					
Ypsilon Lake Trail Bridge 1984 and 1985	0.0967	0.378	63.7	91	4.37
Fall River Road Bridge					
15/6 - 24/7/84	0.103	0.219	54.9	67	8.68
18/5 - 27/5/85	0.0944	0.241	93.3	76	4.88
27/5 - 6/6/85	0.170	0.199	72.2	95	4.32 - 4.88
(b) Inpasihardjo's [16] Data					
Table 4 continued Kilder Burn	0.0444	0.921	83.9	164	6.09
Glen	0.0095	1.164	93.6	75	3.26
South Tyne	0.0149	1.096	91.8	184	3.16
Pitzbach	0.0486	0.500	71.2	88	2.50
(c) Ashiq's [3] Data -UK sites					
Harwood Beck Upper site at Harwood, 1994 -1996	0.0008	1.399	0.735	97	6.03
Harwood Beck Lower site at Harwood,1994-1996	0.0004	1.465	0.774	112	5.07
River Wear Site at Stanhope, 1994 - 1996	7.00E-05	1.816	0.757	115	6.154
South Tyne River site at Alston, 1994 - 1996	0.0034	1.277	0.690	130	5.53
(d) Ashiq's [3] Data -USA sites					
Ypsilon Lake Trail Bridge (i.e. downstream site) July 1995	0.098	0.366	0.707	130	6.97
Alluvial Fan Road Bridge (i.e. downstream site) July 1995	0.234	0.167	0.461	111	4.35
In above mentioned equation q_{ci} has dimensions $m^3 s^{-1} m^{-1}$; D_i has dimensions mm					

Performance Test of Developed Models

The performance of the developed models (Equation (1) and (2)), in conjunction with the model parameters (i.e. α_{MLS}, β_{MLS}, α_{MUS} & β_{MUS} - Equations (3) to (6), respectively), was tested using both the flume and field data. The flume data used were that collected in the Old Brewery Hydraulics Laboratory and comprised four set of materials, whereas the field data used were from the upstream (u/s) and downstream (d/s) sites of the Roaring River for the period of May-June 1995. These data were not used in the development of the models and comprised long, median, and short axes of the bed material particles, required for determining the shape factor (SF, values for flume data are given in Table 5) - a parameter used in the models. In this performance test values of the unit critical water discharges ($q_{c(c)}$) were computed using both the flume and field data. These computed discharges were than compared with the measured (observed) critical water discharge ($q_{c(m)}$) values. The values of mean error (ε_m) and root mean square error (ε_{rms}) were determined by using Equations (7) and (8). Also, values of mean discrepancy ratio (DR, ratio of computed to observed discharges) and standard deviation

(SD) were determined to further verify the performance of the models.

Mean Error (ε_m)

$$\varepsilon_m = \sum_{i=1}^{n} \frac{q_{ci(m)} - q_{ci(c)}}{n} \qquad (7)$$

Root mean square error (ε_{rms})

$$\varepsilon_{rms} = \left[\sum_{i=1}^{n} \frac{\left(q_{ci(m)} - q_{ci(c)}\right)^2}{n} \right]^{1/2} \qquad (8)$$

Where

$q_{ci(m)}$ = measured (observed) unit critical water discharge (m^2/sec) for particle size D_i; $q_{ci(c)}$ = computed unit critical water discharge (m^2/sec) for particle size D_i; and n = total number of observations.

MLS Model Performance Test

Model (Equation (1), in conjunction with the Equations (3) and (4)) performance was first tested by using four sets of flume data. As is evident from Figure 3 the data points generated by this model are mostly scattered close to the line of perfect agreement (LPA) and within the 10 % margin lines. Generally, a mixed pattern of overestimation and underestimation is evident from these figures. However, during the tests with the flume data, in some cases, the variation in the computed critical discharge was small. A possible reason for this is that the model is based on mixed-size (non-uniform) bed material data while the data used for testing (i.e. flume data) were somewhat uniform in nature.A performance test was then made with the Roaring River tracer data for May-June 1995 (Figure 4a) which shows good agreement for the upstream (u/s) site data, as data points are scattered close to the LPA.

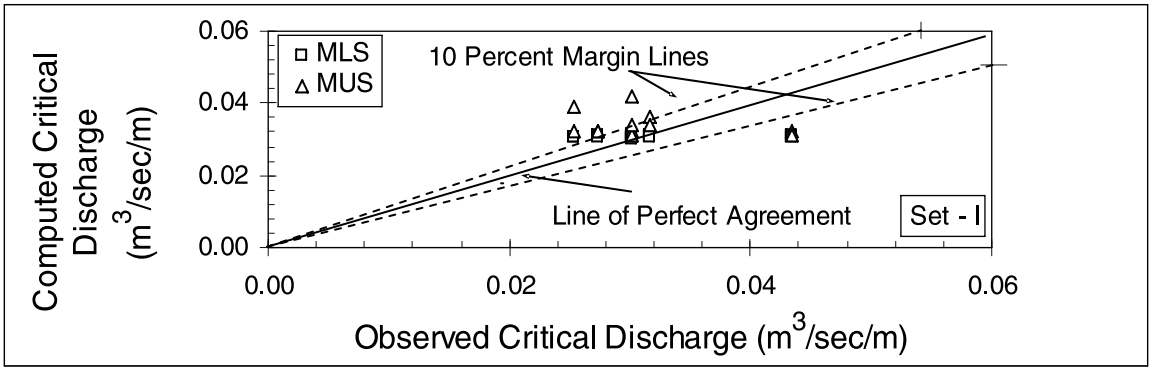

(a)

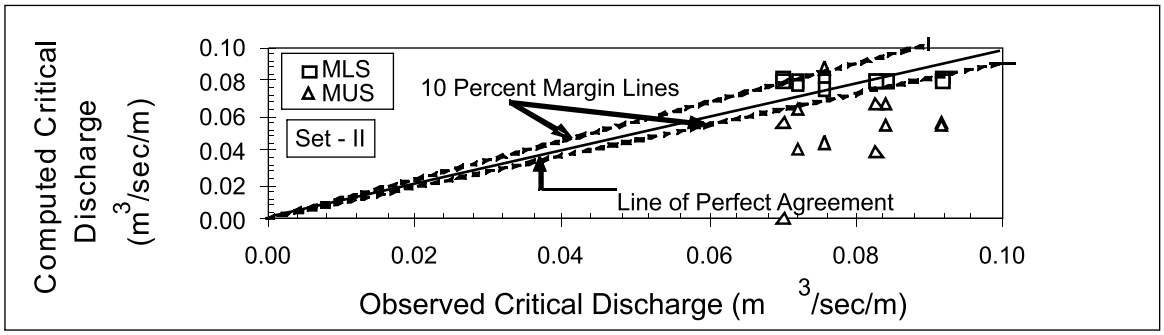

(b)

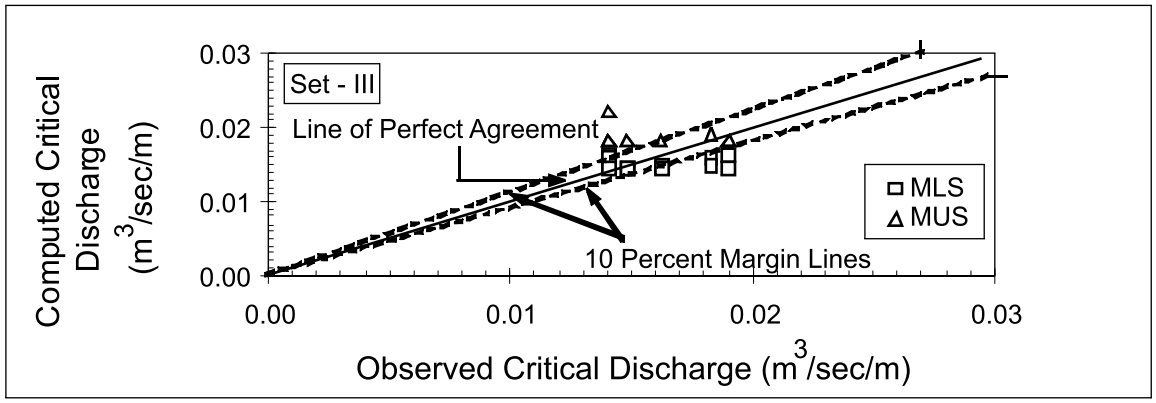

(c)

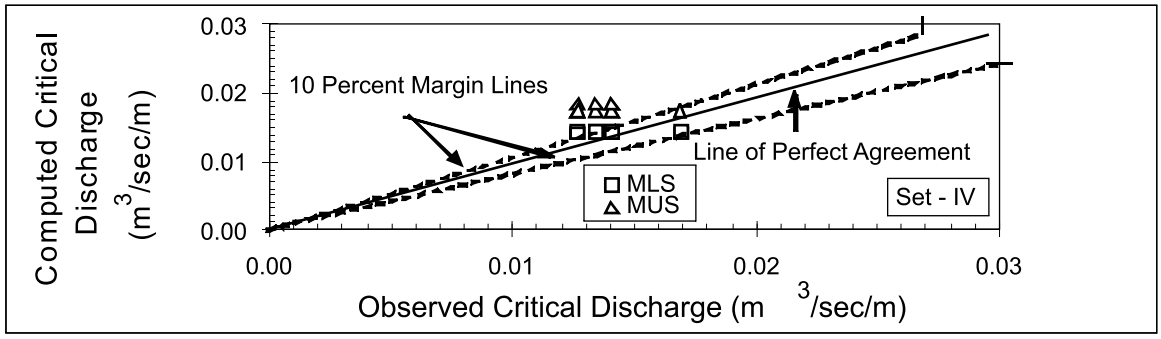

(d

Figure 3: Comparison of computed (by MLS and MUS models) and observed unit water discharges using flume data (having four sets of material) collected in the Old Brewery hydraulics laboratory: (a) Set - I; (b) Set -II; (c) Set - III; and (d) Set - IV.

On the other hand, for the downstream site data (Figure 4b), this model did not perform well as data points are located below the 10 % margin line. For this site the data scatter is nearly horizontal, which shows that model is not very sensitive for the data. However, test data are too few to comment on the model trend. The performance of the model is also highlighted by the mean error (ε m) and root mean square error (ε rms) values given in Table 5. Mean DR (discrepancy ratio, ratio of computed to observed values) values vary between 0.759 and 1.004 (Table 5) which shows that the model has performed satisfactorily. Similarly, the model's validity is evident by the SD (standard deviation) values.

Performance Test of Developed Models

The performance of the developed models (Equation (1) and (2)), in conjunction with the model parameters (i.e. α_{MLS}, β_{MLS}, α_{MUS} & β_{MUS} - Equations (3) to (6), respectively), was tested using both the flume and field data. The flume data used were that collected in the Old Brewery Hydraulics Laboratory and comprised four set of materials, whereas the field data used were from the upstream (u/s) and downstream (d/s) sites of the Roaring River for the period of May-June 1995. These data were not used in the development of the models and comprised long, median, and short axes of the bed material particles, required for determining the shape factor (SF, values for flume data are given in Table 5) - a parameter used in the models. In this performance test values of the unit critical water discharges ($q_{c(c)}$) were computed using both the flume and field data. These computed discharges were than compared with the measured (observed) critical water discharge ($q_{c(m)}$) values. The values of mean error (ε_m) and root mean square error (ε_{rms}) were determined by using Equations (7) and (8). Also, values of mean discrepancy ratio (DR, ratio of computed to observed discharges) and standard deviation

(SD) were determined to further verify the performance of the models.

Table 5. Mean error (ε_m) and root mean square error (ε_{rms}) in the prediction of critical water discharges using MLS and MUS models for the flume and field data, along with the values of mean DR and SD.

Site	Errors, Mean DR Values and SD of DR Values							
	MLS Model				MUS Model			
(1)	ε_m (m^2/sec) (2)	ε_{rms} (m^2/sec) (3)	Mean DR (4)	SD of DR (5)	ε_m (m^2/sec) (6)	ε_{rms} (m^2/sec) (7)	Mean DR (8)	SD of DR (9)
Flume Data								
a) Set-I	0.00076	0.00584	1.004	0.140	-0.0028	0.00794	1.124	0.211
(SF=0.582)	-0.0006	0.00743	1.016	0.098	0.0266	0.03320	0.660	0.280
b) Set-II	0.00092	0.00224	0.960	0.126	-0.0027	0.00362	1.187	0.177
(SF=0.595)	-0.0003	0.00144	1.030	0.098	-0.0038	0.00413	1.290	0.132
c) Set-III(SF=0.572)	0.0581	0.0597	0.880	0.045	-0.4270	0.4280	2.362	0.182
d) Set-IV(SF=0.575)	0.0521	0.0535	0.759	0.053	0.02290	0.02560	0.896	0.059
Field Data								
a) u/s site Roaring River								
b) d/s site Roaring River								

During this performance test it has been found that the model is quite sensitive to the shape factor (SF) value, therefore SF value should be determined accurately, otherwise results could fluctuate considerably. As, at this stage it was not possible to test the model performance with sufficient (mixed-size material) data, due to the non availability of data (with measured short, median and long axes), therefore further model tests are suggested before generalizing it for the common use.

MUS Model Performance Test

Like the MLS model, the performance of this model was investigated using the flume data and field data. Computed unit critical water discharges (qc) were compared with the observed unit water discharges (qc), as depicted in Figure 3 (for flume data) and in Figure 4 (for field data). A relatively wide range of data scatter was found for this model compared with the MLS model, as is evident from the figures. This model has significantly underestimated the computed values for the dataset II (Figure 3b) of the flume study and overestimated for the upstream site data of the Roaring River (Figure 4a), as data points are scattered below and above the line of perfect agreement (LPA). However, the overall performance of the model was not very satisfactory as mean DR values for the upstream site were greater than 2. These results are also supported by the mean error (εm) and root mean square error (εrms) values given in Table 5. Average grade

performance of the model is also evident from the SD values (Table 5). This model, in-contrast to its rival the MLS model, overestimated the computed discharges, possibly due to two reasons: a) movement of particles on the channel bed is affected not only by the absolute and relative grain size effects but also influenced by the position of particles relative to the flow currents/flow depth; and b) a lack of test data points (only three).

Large variations in the MUS model's performance for the laboratory and field data showed how unreliable it is to use this model for the computation of critical discharge values. The reason for the fluctuation in the model's performance was that initiation of motion of maximum particle sizes depends not only upon the discharge value but also upon the particle position across/along the channel bed. Many times during this study the larger size tracer particles were moved but smaller ones were not. This condition depended upon the location of the tracer particles in the channel bed. Therefore, it is more likely to find fluctuation in the computed results with the use of the MUS model, while the MLS model by its very nature is likely to produce better results. Like the MLS model the MUS model was also found to be very sensitive to the shape factor (SF) values, therefore it should be determined carefully

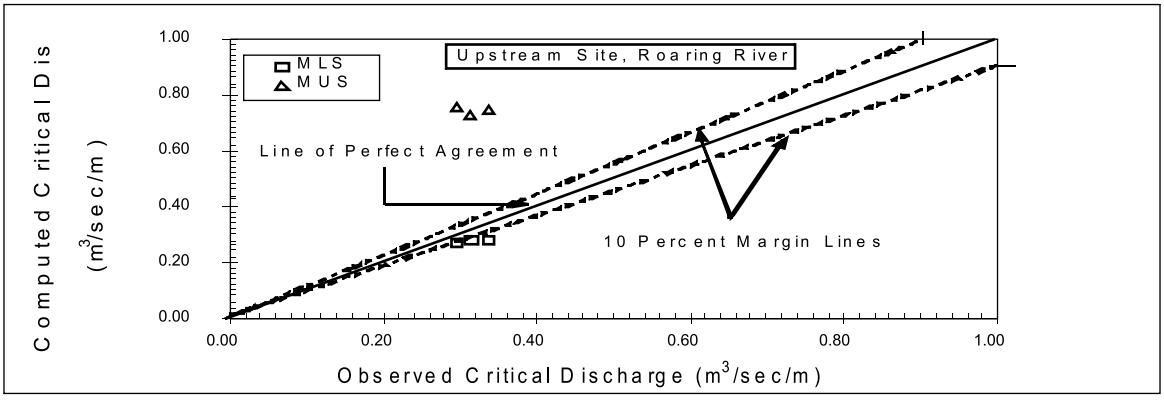

(a)

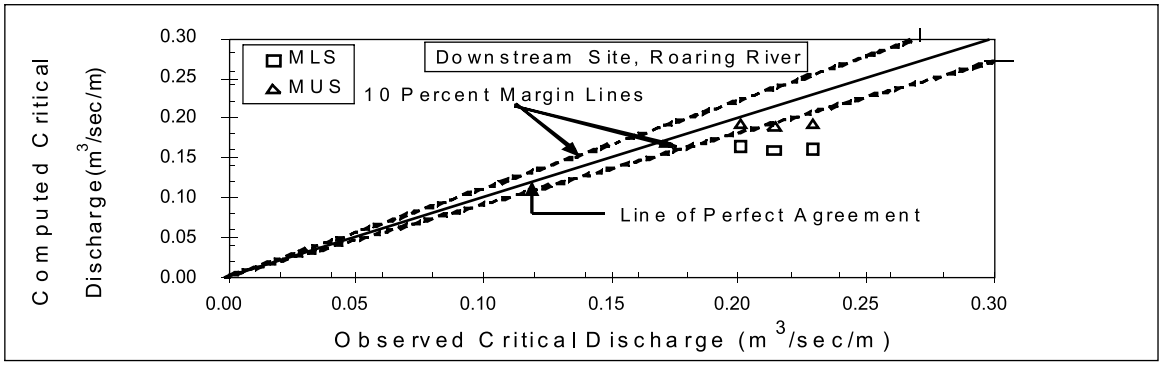

(b)

Figure 4: Comparison of computed (by MLS and MUS models) and observed unit water discharges using field data collected from the Roaring River (Colorado, USA) during May-June 1995 period: (a) upstream site; and (b) downstream site.

Results and Discussion

The performance of the existing bed load transport initiation models, based on critical discharge theory and individual particle sizes, was investigated using data from the four UK sites (i.e. Harwood Beck Upper and Lower sites, River Wear site and South Tyne River site). Among the tested models Bathurst's [12] model performed (relatively) better, even though its performance was not satisfactory. In this investigation the models performed poorly, partly because:

1) They need to incorporate other process e.g. particle shape effects - a parameter that plays a significant role in the bed material movement;
2) Their basis on absolute maximum size is inaccurate;
3) Different authors use different measurement techniques for data collection (which are used for model development and testing) whose compatibility is unknown [14].

The significance of the particle shape for the bed material movement has also been proved by Li and Komar [17] and Gomez [16]. Li and Komar [17] while investigating the pivoting angle applications to the selective entrainment of gravel stated that "order of increasing difficulty of entrainment is spheres, ellipsoidal grains, angular grains, and imbricated grains". The effects of particle shape have also been proved by Gomez [16] who described that hiding functions likely vary with particle shape. He further stated that "for a given imposed shear stress the order of increasing nominal particle diameter is flat, angular, and rounded gravels".

The second probable reason for the poor performance of the models was that they have been developed by using the absolute maximum size of the moved tracer particles which is not a realistic approach. Initiation of bed material movement depends not only upon particle size but it also upon particle position on the channel bed relative to other particles and flow depth/flow current. Wilcock [11] mentioned this source of error in his criticism of the classic concept of flow competence. He stated that "the larger errors and unknown bias suggest that the largest sampled mobile grain is not a reliable predictor of either critical shear stress or flow magnitude".

Particle shape plays a significant role in bed load initiation and it could vary from catchment to catchment. Therefore, two models were developed for determining the critical condition for the initiation of bed load transport, both including a shape factor (SF) parameter to account for the particle shape effects. One of these models is based upon the maximum lower size (MLS) (Equation (1) in conjunction with Equations (3) and (4)) of moved tracer particles, while the other is based on the maximum upper size (MUS)(Equation (2) in conjunction with Equations (5) and (6)) of moved tracer particles. The performance of these models was verified in an independent test with the flume and field data. The MLS model performed well compared with the MUS model, which showed considerable fluctuation in the results. However, before further generalisation the models need to be tested with more field data. In this study, due to the shortage of shape data (with measurements of particle long, median and short axis), it was not possible to carry out further performance tests, since most available data sets have just median particle axis.

Conclusions

The following specific conclusions may be drawn from this study.

1. To strengthen the existing weak data base (and to test performance of the existing and developed models) field and laboratory data (under uncontrolled and control conditions, respectively) were collected from the four UK and two US sites and from the Old Brewery Hydraulics Laboratory.

2. Before developing the new model for the initiation of bed load transport the performance of existing critical discharge theory (as this theory was used in model development) based models was tested with the four UK sites' data. In this performance test both the models (generally) performed poorly, however, Bathurst model's performance was relatively better.

3. Considering the poor performance of the available bed load initiation models a model (Equation (1) along with Equations (3) and (4)) based on the maximum lower size of moved tracer particles (MLS model) and discharge theory was developed using the collected field data. This model applies to each size fraction in a non-uniform distribution. This model is valid for channel slope ranging between 0.8 and 4.7% and D50 of bed material between 0.065 to 0.140 m. It showed encouraging results in an independent test (with the collected laboratory data and field data) with mean discrepancy ratio ranging between 0.759 and 1.004.

Acknowledgements

The help of Dr. James Bathurst (Principal Research Officer, Water Resources Systems Research Unit, and Department of Civil Engineering) of the Newcastle University, during the study, is gratefully acknowledged. Thanks are also due to the National River Authority (presently: Environmental Agency) for providing water discharge data for the UK river sites. Likewise, co-operation of the Rocky Mountain National Park staff (especially Dr Ken Czarnowski, Research Administrator) during the data collection from the Roaring River (Colorado, USA) is highly appreciated.

Notation

(L = length; M = mass; T = time; (-) = dimensionless)

a	longest particle axis;
b	intermediate particle axis;
c	shortest particle axis;
D_i	diameter of ith size fraction (L);
D_r	reference particle size (L);
D_{16}	particle size for which 16% of the sediment mixture is finer (L);
D_{35}	particle size for which 35% of the sediment mixture is finer (L);
D_{50}	particle size for which 50% of the sediment mixture is finer (L);
D_{63}	particle size for which 63% of the sediment mixture is finer (L);
D_{65}	particle size for which 65% of the sediment mixture is finer (L);
D_{84}	particle size for which 84% of the sediment mixture is finer (L);
D_{90}	particle size for which 90% of the sediment mixture is finer (L);
g	acceleration due to gravity (LT-2); LPA line of perfect agreement;
MLS	maximum lower size of moved tracer particles (L);
MUS	maximum upper size of moved tracer particles (L);
n	total number of observations;
q^{bi}	unit bed load for ith size fraction (L2T-1);
q^c	critical unit water discharge (L2T-1);
q_{ci}	critical unit water discharge for ith size fraction (L2T-1);
$q_{ci(c)}$	computed unit critical water discharge (m2/sec) for particle size Di;
$q_{ci(m)}$	measured (observed) unit critical water discharge (m2/sec) for particle size Di;
$q_{ci(MLS)}$	critical unit water discharge for ith size fraction for the maximum lower size of the moved tracer particles (L2T-1);
$q_{ci(MUS)}$	critical unit water discharge for ith size fraction for the maximum upper size of the moved tracer particles (L2T-1);
R	correlation coefficient (-);
S	slope (-);
SD	standard deviation;
SF	shape factor (-);
W	channel width (i.e. surface flow width of channel) (L);

$\sum$ summation (-);

α coefficient (-);

α_{MLS} intercept value for the maximum lower size of the moved tracer particles (-);

α_{MUS} intercept value for the maximum upper size of the moved tracer particles (-);

β exponent (-);

β_{MLS} exponent value for the maximum lower size of the moved tracer particles (-);

β_{MUS} exponent value for the maximum upper size of the moved tracer particles (-);

ε_m mean error; and

ε_{rms} root mean square error.

References

[1] M. P. DuBoy, 1879 "Etudes du Regime et 1" Action Exercee par les Eaux sur un lit a Fond de Graviers Indefiniment affouilable", Annales de Ponts et Chausses, Ser. 5, Vol. 18, 141-195.

[2] D.B. Simons and F. Sentürk, "Sediment transport technology", 1977, Water Resources Publication, Fort Collins, Colorado, 807 pp.

[3] M. A. Carson and G. A. Griffiths, 1987 "Bed load transport in gravel channels", Journal of Hydrology (N.Z), Vol. 26, No.1.

[4] P. C. Klingeman and M. Matin, 1993 "Incipient motion in gravel-bed rivers", Proc. ASCE Conference on Hydraulic Engineering, San Franscio, California (USA), July 25-30, Edited by Hsieh WenShen, S. T. Su, and Feng Wen, Vol. 1,.

[5] C.L.Dancey, P. Diplas, A. Papanicolaou, and M. Bala, 2002 "Probablity of individual grain movement and threshold condition", J. of Hydraulic Engineering, ASCE, Vol. 128, No.12, 1069-1075.

[6] S. Dey, 2003 " Threshold of sediment motion on combined transverse and longitudinal sloping beds", J. Hydraulic Research, 41(4), 405-415.

[7] M. Ashiq, 2001 "Initiation of bed material movement in coarse bed material rivers –a literature based investigation", Journal Institution of Engineers, Malaysia. Vol. 62, No.1, 45-58.

[8] K. Inpasihardjo, 1991"Bed load transport of nonuniform size sediment in mountain rivers", Ph.D. Thesis, Department of Civil Engineering, University of Newcastle Upon Tyne, UK, 454 pp.

[9] P. J. Ashworth and R. I. Ferguson, 1989 "Size-selective entrainment of bedload in gravel bed streams", Water Resour. Res. 25, 627-634.

[10] R. I. Ferguson, 1994 " Critical discharge for entrainment of poorly sorted gravel" , Earth Surface Processes and Landforms, Vol. 19, 179-186.

[11] [P. R. Wilcock, 1992"Bed-load transport of mixed-size sediment", Dynamics of Gravel-Bed Rivers, P. Billi, R. D. Hey, C. R. Thorne, and P. Tacconi, eds., John Wiley and Sons, Ltd. Chichester, UK, 109-131.

[12] J. C. Bathurst, 1987 "Critical conditions for bed material movement in steep, boulder-bed streams", Proceedings of the Corvallis Symposium, Erosion and Sedimentation in the Pacific Rim. IAHS Publ. no. 165, 309-317.

[13] [G. Parker and P. C. Klingeman, 1982"On why gravel bed streams are paved", Water Resource. Res., 18(5), 1409-1423.

[14] M. Ashiq, 2002 " Dams: sediment inflow problem, compatibility of the inflow measurement techniques". Proceedings of HYDRO-2000, an International Conference on 'Development, Management, Performance of Hydropower and Dams', by Aqua-Media International Ltd (Surrey - UK), Turkey, November 4-7.

[15] [E. D. Andrews and D. C. Erman, 1994 "Persistence in the size distribution of the surficial bed material during an extreme snowmelt flood", Water Resour. Res., 22, 191-197, 1986. [16]B. Gomez, "Effects of particle shape and mobility on stable armour development", Water Resources Research, Vol. 30, No. 7, 2229-2239.

[16] B. Gomez, 1994 "Effects of particle shape and mobility on stable armour development", Water Resources Research, Vol. 30, No. 7, 2229-2239.

[17] Z. Li, and P. D. Komar, 1986 "Laboratory measurements of pivoting angles for applications to selective entrainment of gravel in a current", Sedimentology, 33, 413 - 423.

Influence of Diaphragm action Upon the Seismic Response of High Rise moment resisting Building Frames

Saeed Ahmad [1], Asim Gulzar [2], and Huma Pervaiz [3]

Abstract

Diaphragm or horizontal bracing system is a horizontal system transmitting lateral forces to the vertical lateral load resisting elements. Under lateral loading floor slabs in reinforced concrete building perform as diaphragms to transfer lateral forces to load resisting frames. The objective of present study is to evaluate how a structure behaves when the reinforced concrete slabs are included in the structural analysis. In current study, two regular building model having 6 bays in each principle direction, each bay of 15ft length. In this way the plan dimensions become 90ft x 90ft.Total stories are 10, each having a height of 11ft except the plinth level which is 10ft in height .In this way the total height of the structure becomes 109ft. Diaphragms are modeled as rigid elements, thus the effect of their in plane movement relative to the vertical lateral load resisting system is neglected. It was found that the considering the effect of slabs in the structural analysis of case study buildings will give smaller values of storey displacements & storey shears, larger values of support reactions, column reinforcement & torsional forces transferred to beams, a mixed behavior for modal time period etc.

Keywords: Diaphragm, Seismic response, Lateral forces

Introduction

The effect of the slab panels is not considered in reinforced concrete structural analysis because designers neglect their contribution in lateral load resistance. Their contribution is neglected in the structural analysis because they show large complexity in structural behavior. Mostly, the construction carried out in Pakistan is reinforced concrete with slabs providing the useable floor area. During an earthquake, these slabs will increase the lateral earthquake load resistance significantly. As they form a large part of structural system, therefore designers should get benefit from their large in plane stiffness. So in this study the response of two essentially same structures, with and without consideration of stiffness of slabs were evaluated and compared on the basis of different structural parameters listed in research objectives.

Research findings of this case study are model with slab gives higher values of modal time period for first three modes as compared to model without slabs (Table 1 & Figure 7). This means that for first three modes model without slabs will give the critical results whereas for higher modes model with slab will give the critical results. Lower values of displacements are observed in model with slab because of higher stiffness of slab panels (Table 3 & Figure 9). Higher values of storey shear are observed in model without slabs (Table 2 & Figure 8). Support reactions are more in the case of model with slab (Figure 10 & 11). True torsional forces are transferred to beams in case of model with slabs. Smaller storey displacements give rise to smaller end forces in beams which generates an economical design for the case of model with slabs. Higher percentage of reinforcement is observed in columns for the case of model with slab (Figure 12).

Diaphragm effects in rectangular reinforced concrete building are also dicussed by Joel M.Barron & Mary Beth D.Hueste [1].

His objective of study was to evaluate how flexible diaphragm behaves in reinforced concrete design of building. As case study three story and five story buildings are evaluated using guidelines for seismic rehabilitation of buildings FEMA 273-nehrp. Models are then studied by assuming rigid diaphragm behavior and then by flexible diaphragm. He found that for low rise reinforced concrete building flexible design should be considered having an aspect ratio of 3:1 or larger.

Colin A. Rogers & Robert Tremblay studied the “impact of diaphragm behavior on the seismic design of low rise steel buildings [2].

This paper provides a description that how steel roof diaphragm behaves in low rise steel buildings. Diaphragm transfer lateral forces to vertical members. A vertical member yields in case of braced steel

[1,3] Civil Engineering Dept., University of Engineering and Technology Taxila, [2] Nespak, Islamabad.

frames. Vertical bars behave as energy dissipating fuse element. To avoid failure of diaphragm special means must be taken to ensure that deformation capacity will be properly distributed over the diaphragm area.

Research Objectives

In this comparative evaluation study, the seismic performance of two multistory reinforced concrete building, one with modeled slabs to account for its stiffness and other without it, shall be investigated by Elastic Response Spectrum Analysis using UBC-97.The objectives of the study are summarized in following:

1. To study effect of slabs as diaphragm on the performance of high rise ductile moment resisting frames under seismic loads and to get a quantitative idea o this effect based on different structural parameters like, but not limited to:
   a) Time Period
   b) Base Shear
   c) Story Drifts
   d) Relative Story Displacements
   e) Support Reactions
   f) Member End Forces (Shears, Moments, Torsion etc)
2. By comparing it with another same structure but without modeling the slabs.
3. To understand the need to account the stiffness of slabs.
4. To understand how much it is important to consider the diaphragm action against lateral seismic forces in order to ensure its serviceable performance level without extensive cracking so that its stiffness contribution should remains there.

Case Study Buildings

Influence of diaphragm action upon the seismic response of high rise moment resisting building frames is determined by taking a regular building model having 6 bays in each principle direction, each bay of 15ft length. In this way the plan dimensions become 90ft x 90ft.Total stories are 10, each having a height of 11ft except the plinth level which is 10ft in height .In this way the total height of the structure becomes 109ft.

Two models are used in the research study. One modeled with slabs & the other one without slabs. Load is applied in the form of member load upon beams in the case of model without slabs. The brief description of these models and graphical views are given below.

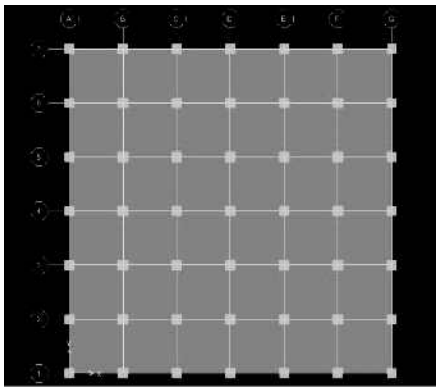

Figure 1: Plan of with slab

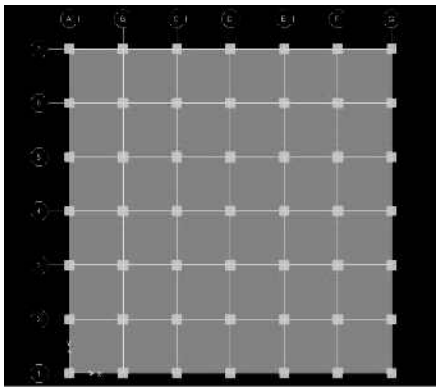

Figure 2: Plan of without slab

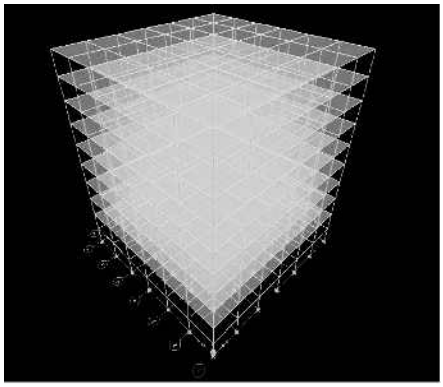

Figure 3: 3D view with slab

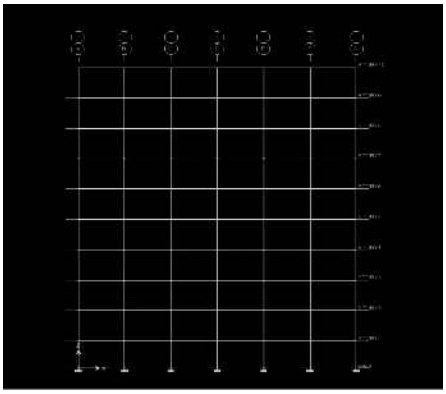

Figure 4: Elevation view without slab

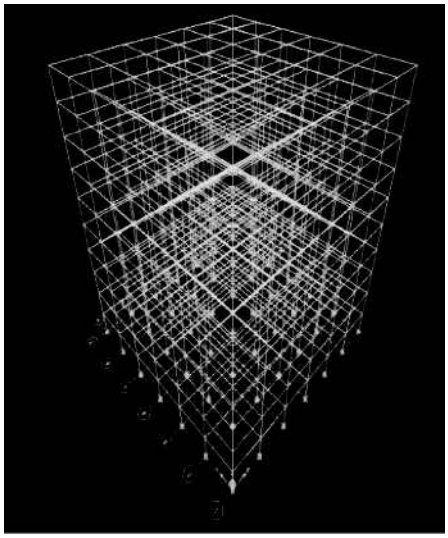

Figure 5: 3D view without slab

Method of Analysis

As prescribed earlier, dynamic analysis is performed response spectrum analysis method by using standard UBC response spectra whose peak values corresponds to Ca & Cv values zone 2B as per UBC. Eigen vector analysis type is used to generate different possible no of modes.

In modal analysis, SRSS (square root of sum of squares) technique is used for modal combinations in which 8 no of modes are considered since mass participation appears to be 99% for 8th mode in both principle directions. SRSS technique is also used for directional combinations.

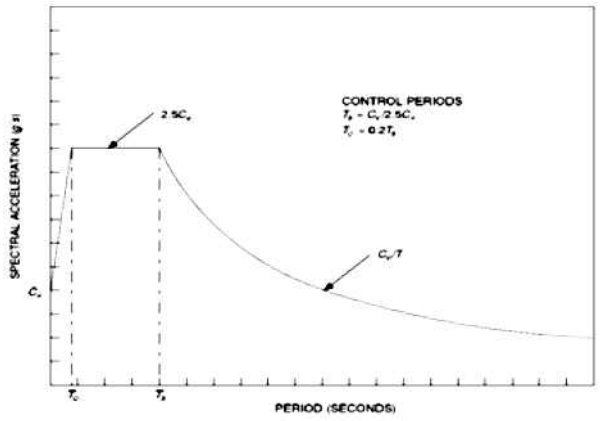

Figure 6: UBC response spectra

Results and Discussion

After performing the dynamic analysis of the two example models, their behavior will be analyzed & compared in terms of the following parameters.

1) Modal time period.
2) Storey shears.
3) Storey displacements.
4) Support reactions.
5) Reinforcement %age of columns

The comparison of results in terms of the above parameters will be given in terms of tables & graphs in the coming paragraph.

Modal Time Period

The time required to complete one complete cycle of vibration is called time period. Under free vibration the structure always vibrates in single mode called its fundamental mode and the corresponding time period is called fundamental period of the structure. The fundamental period is the longest period of the structure. The no of modes depends upon the no of degrees of freedom.

Table 1: Modal time periods of modeled slab and without slab

MODAL TIME PERIODS		
Mode	**Period(with slabs)**	**Period(without slabs)**
1	**1.43**	**1.34**
2	**1.43**	**1.34**
3	**1.33**	**1.26**
4	**0.50**	**0.88**
5	**0.50**	**0.68**
6	**0.47**	**0.68**
7	**0.30**	**0.49**
8	**0.30**	**0.47**

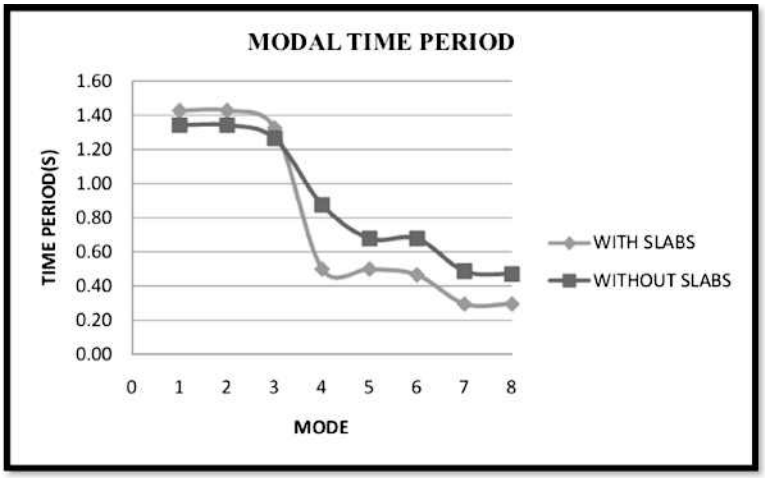

Figure 7: Comparison of time period against mode

Support Reaction

The reactions at the base level of the building with fix supports are assigned to the structure, for each load combinations for which foundation has to be designed are called support reactions. Following graphs will represent the comparisons of the two structures for support reactions.

1=Axial force (kip), 2=Moment in x dir (kip.ft), 3=Moment in y dir (kip.ft)

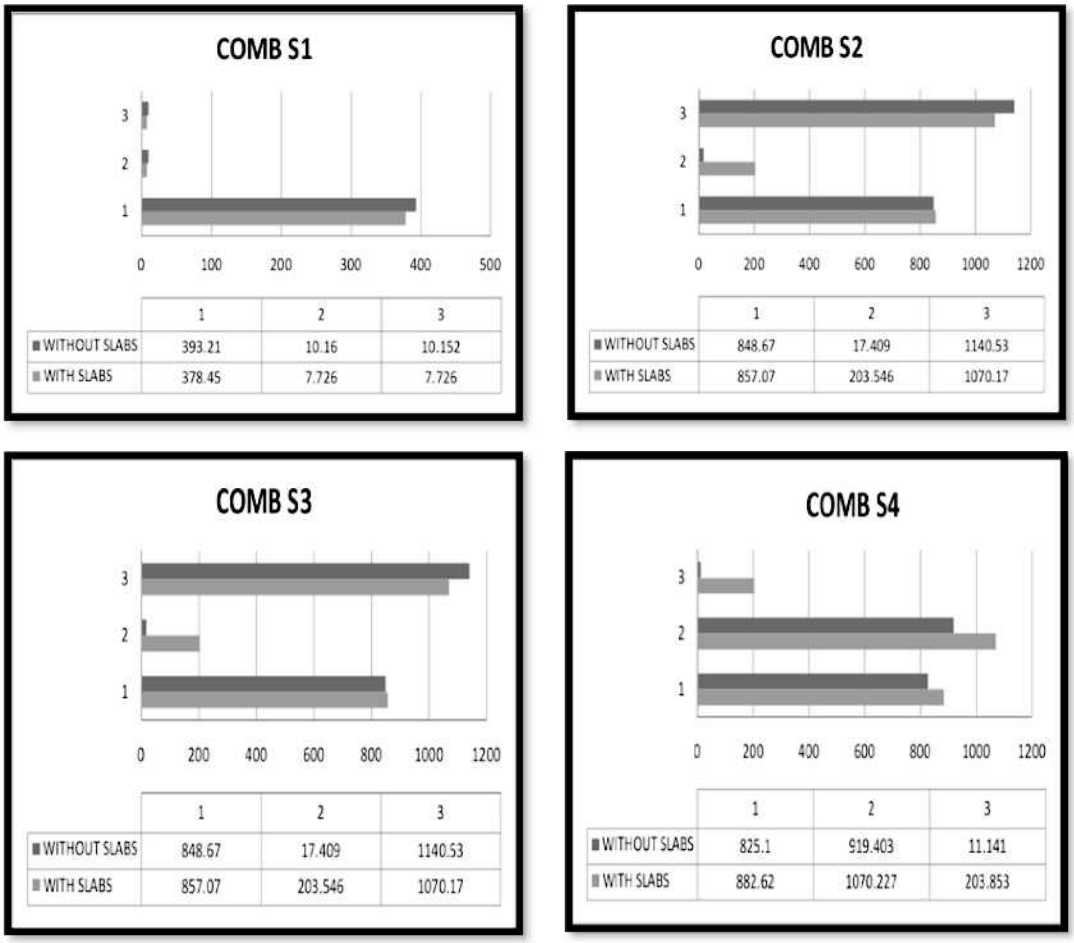

Figure 10: Support reaction (service load cases) of modeled slab and without slab

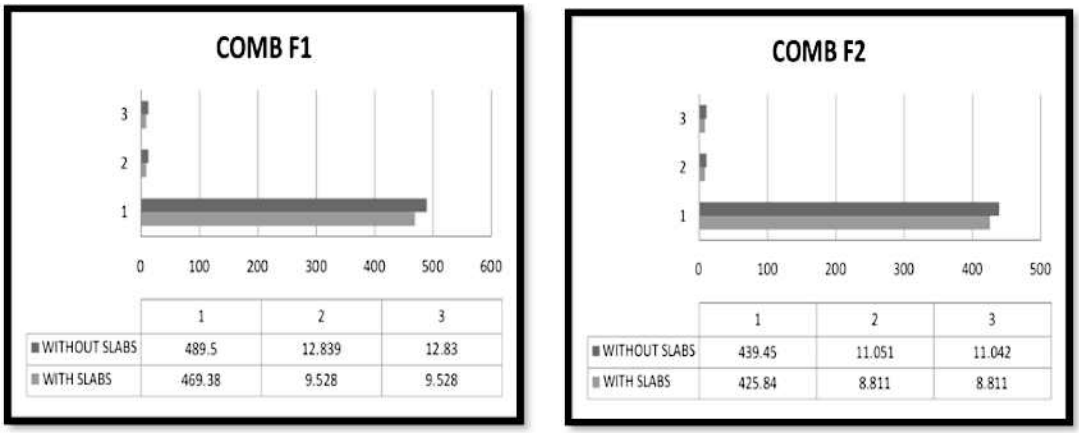

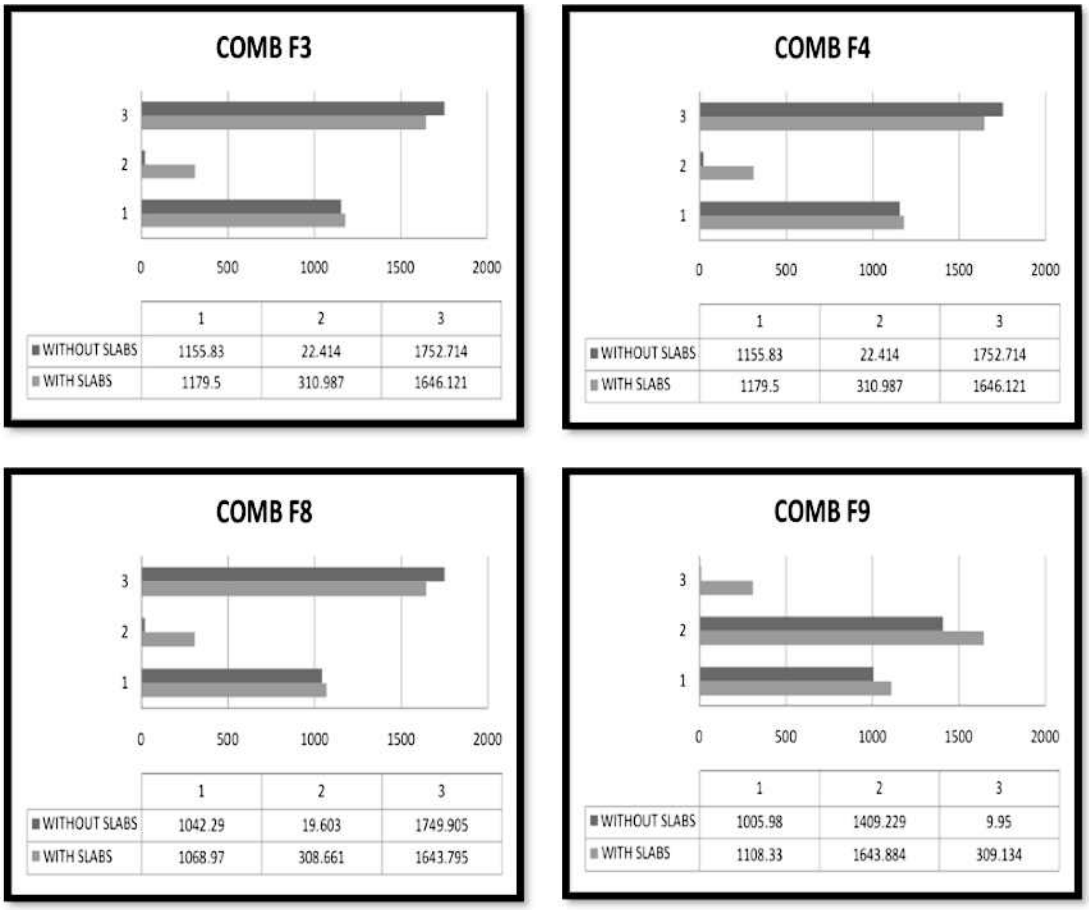

Figure 11|: Support reaction (factored load cases) of modeled slab and without slab

Column Reinforcement

Longitudinal reinforcement of the column will be prepared in the subsequent section:

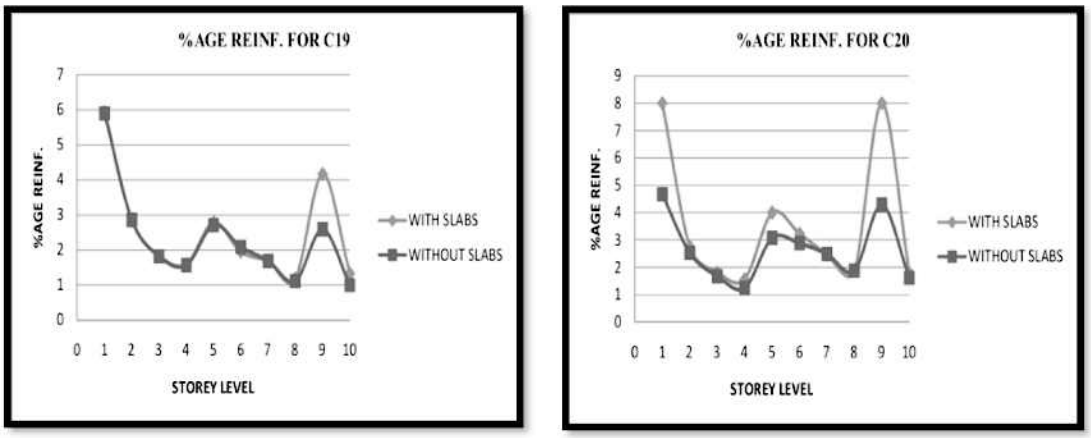

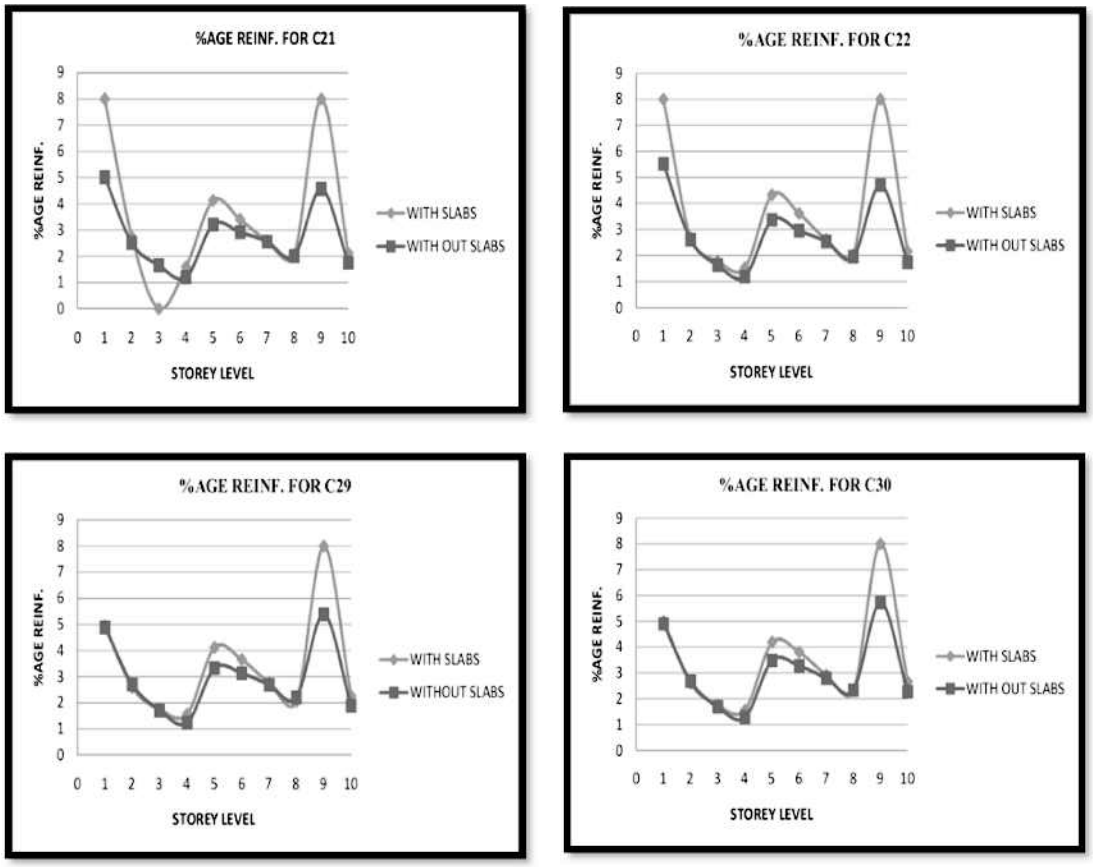

Figure 12: Column reinforcement of modeled slab and without slab

Conclusions

1. For the first three modes structure with slabs has higher periods as compared to without slabs. Whereas the condition is exactly opposite for the rest of the modes. By looking at response spectrum curve, it can be observed that lower the value of time period higher the value of g, which results in higher value of story shears. Hence, the structure should be analyzed for both cases in order to get the critical results.
2. Difference of time periods for the two cases is small for the first three modes, whereas the difference is large for the mode 4 & onward. This means that for higher modes the structural behavior becomes critical for models with slabs.
3. Story shear of the structure modeled without slabs are quite larger than that modeled with slabs. Thus, the model without slab will give the critical results.
4. Although the displacements for the structure with slabs are lower as compared to structure without slabs, but the difference can be ignored if some designer wants to. The lower value of displacements in the case of model with slabs indicates the effect of higher stiffness of slabs in structure. If designer consider their effect during the analysis & design phase of project, this will lead to economical design of structure.
5. For the case of model with slab the support reactions are more as compared to model without slabs. Therefore, for safe design of foundations slabs should be considered in the analysis & design of structure.
6. For all types of member forces, member end forces are generally of smaller value (although the %age decrease is of varying magnitude) in the structure in which stiffness of slabs are considered as compared to the other structure without slabs. The reason of smaller end forces are quite clear

from the fact that since story displacements are smaller in the structure of modeled with slabs which in turns yields smaller value of end forces. Hence it can be concluded that the stiffness of slabs yield economical design.

For all types of member forces, member end forces are generally of smaller value (although the %age decrease is of varying magnitude) in the structure in which stiffness of slabs are considered as compared to the other structure without slabs. The reason of smaller end forces are quite clear from the fact that since story displacements are smaller in the structure of modeled with slabs which in turns yields smaller value of end forces. Hence it can be concluded that the stiffness of slabs yield economical design.

7) However at floor level, the results of the torsional forces appears to be reversed which is certainly due to the effect of true torsional forces transferred to beams by the slabs. Hence it is necessary for the structural engineer to must consider its stiffness and must have a close look on the high torsion forces of beams since this important aspect can be overlooked in case of analysis without slabs and yields unsafe design at floor levels.

8) Columns are critical for the case of structure modeled with slabs. As column is the critical & most important component of the structure, therefore it is of utmost importance to consider the effect of slabs in the structural analysis & design.

9) The critical reinforcement varies in the story levels due to dynamic model analysis while in static analysis the reinforcement decreases uniformly in the upper stories; hence it is necessary for the structural engineers to perform dynamic analysis to get the critical results.

References

[1] Joel M. Barron & Mary Beth D. Hueste, A technical paper titled “Diaphragm effects in rectangular reinforced concrete buildings”.

[2] Colin A. Rogers & Robert Tremblay, “Impact of diaphragm behavior on the seismic design of low rise steel buildings”.

[3] Uniform Building Code-1997.

[4] ACI 318-02, Building Code Requirements for Structural Concrete.

Effects of Changes in the Management System of Lower Chenab Canal Building Frames

Muhammad Sulman[1] and Muhammad Ashiq[2]

Abstract

To resolve problems like inadequate maintenance of water conveyance conduits (irrigation channels) and associated hydraulic structures, unauthorized usage of water, and inequitable distribution of water, the Irrigation and Power (I&P) Department of Punjab Government handed over the Lower Chenab Canal System (East Circle), having 119 distributaries with total canal command area of 1.85 million acres, to Farmers Organizations (FOs) as a pilot project. To study the effects of this irrigation management transfer (IMT) on the Lower Chenab Canal System, this study was designed.

To investigate the IMT impacts, the daily head and tail discharge data from 2006 to 2009 were collected from the Project Monitoring and Implementation Unit (PMIU) of the Irrigation & Power Department. Based on this data the Delivery Performance Ratio (DPR), Capacity Factor (CF) and status of supply at tails of channels were determined. Besides that, assessment of impact of supplies at the tails after IMT was made. Relative DPRs for crop seasons of Kharif 2006, Rabi 2006-2007, Kharif 2007, Rabi 2007-2008 and Kharif 2008 were computed as of 0.72, 0.68, 0.87, 0.86 and 0.76 respectively. Results showed that there was an increase in supply at the channels tail during Kharif 2007 and Rabi 2007-2008. The analysis showed that the percentage of tails, in term of average number of channels, which remained dry during Kharif 2006, Kharif 2007, Kharif 2008 and Kharif 2009 season were 18%, 12%, 16% and 5.7% respectively; despite the fact that channels run as per authorized head discharge. The data of Abiana (water revenue) collection for different seasons were collected and impact of IMT on the Abiana collection and assessment was investigated. A general trend of decline in revenue collection was noticed.

This study would be helpful for the understanding of the reforms process and to make the improvements in the management system. It would provide findings how to improve the method of Abiana assessment and collection and to enhance the equitable distribution of supply at the tails of the channels.

Keywords: Lower Chenab, Tail, Head, Capacity Factor, DPR

Introduction

Like many other canal systems of Pakistan, Punjab in particular, or many other developing countries in general, Lower Chenab Canal (East) system has also been facing several problems. As stated by PIDA, Punjab Irrigation and Drainage Authority (2005a) [1], these problems were “overall deterioration of system management, shortage of water, inequitable distribution of irrigation water, general lack of agency responsiveness, increasing water theft, inadequate maintenance of the canal system, lack of farmers participation in decision making and management, delay in settlement of water disputes, wrong assessment of water revenue (locally known as Abiana), and lack of awareness among farmers about their water rights”. In order to take care of the stated problems, a new reform system was introduced by the province of Punjab.

Under this reform system, the Punjab province started the major institutional reforms, including decentralization and transformation of old irrigation system/practices from purely government control topublic participatory control to improve the efficiency of the old age system – known to be the world’s 2nd biggest irrigation system.The purpose of these reforms was to make improvement in the delivery of Irrigation supplies with respect to quality, quantity and operation/maintenance of irrigation channels. For the overall supervision of the IMT system, Punjab

Irrigation and Drainage Authority (PIDA) was established. Under this Authority a pilot Area Water Board (AWB) for the canal command area of the Lower Chenab Canal System (LCC) was established, along with the Farmers Organizations (FOs) at the distributary levels and Khal Panchayat at water course level to tackle irrigation water supply problems of the farmers. Under these reforms, farmers and other stakeholders have been participating/contributing and making decisions at all levels of irrigation system management. This farmers’ based management share the responsibilities according to a legal framework.

[1] Punjab Irrigation and Power Department, Lahore, [2] Civil Engineering Dept., University of Engineering and Technology Lahore

According to the reforms process, the Provincial Irrigation Department would control main regulation and provide technical support in policy making. On the other hand PIDA being an autonomous body would be responsible for the improvement of irrigation performance, optimizing water use efficiency, introducing the concept of participatory management, undertaking measures to improve assessment and collection of Abiana, and making the authority self sustaining. PIDA would perform its' responsibility through the Area Water Board at canal command level. It would devise such programs that will promote the formation and enhancement of FOs, which would be responsible for the operation and management of the distributaries in their command along with the maintenance and repair of canals and associated structures. Other responsibilities of these FOs would be to get water from the major canals and then distribute it to farmers on equitable basis. Beside these responsibilities, they would also take care of water disputes among the farmers, assess and collect Abiana (PIDA 2007) [2].

The aim of this part of the research work (and paper) was to study the impact of Irrigation Management Transfer to Farmers Organizations on the Lower Chenab Canal System (East). It mainly deals with the estimation of delivery performance ratio at heads and tails of the channels, development of equations, estimation of relative delivery performance ratio for the assessment of equitable distribution of irrigation water, computation of capacity factor for canal system, effect of farmers participation in decision making, assessment and collection of Abiana, and performance of FOs and their impact on water supply of irrigation channels.

Brief Description of Study Area

The main focus of this study is of Lower Chenab Canal (East) Circle, Faisalabad area. This partly covers areas of district Sheikhupura, Toba Tek Singh, Hafizabad, Jhang and Faisalabad. There are four branch canals in LCC (East) Circle, Faisalabad. These branch canals are Burala branch, Mian Ali branch, Lower Gugera branch and Upper Gugera branch. The LCC was constructed in 1892 and it is off taking from Head Khanki at the Chenab river in the Gujrat district. The LCC (and the associated Area Water Board, AWB) consists of total area of 2.262 million acres with grass command area (GCA) of 2.122 million acres and canal command area (CCA) of 1.85 million acres. The proposed discharge is 11229 cusecs and existing discharge is 8249 cusecs. Length of the main canals and branch canals is 297 miles. The numbers of distributaries in LCC are 119 and the Farmers Organizations (FOs) are 85. The major crops in study area are cotton, maize, sugarcane, rice, wheat, and oilseed and fodder (PIDA 2005b) [3]. The index plan of LCC (East) is shown in Figure 1.

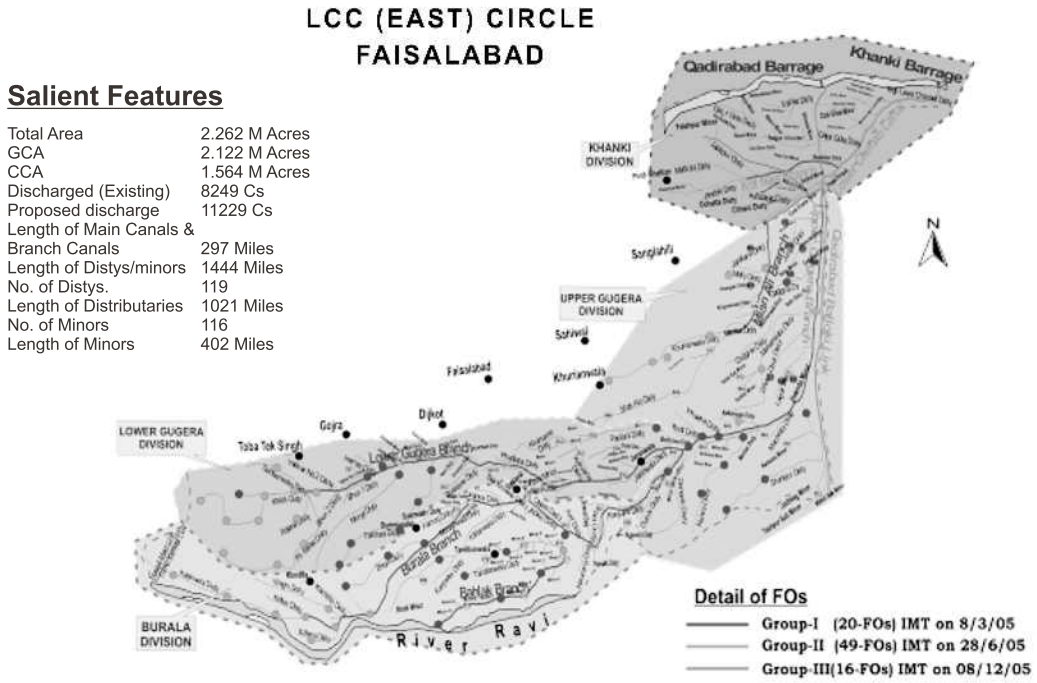

Figure 1: The index plans of LCC (East) [adopted from PIDA 2005b] [3]

Delivery Performance Ratio (DPR) and Relative Delivery Performance Ratio (RDPR)

Delivery Performance Ratio

Delivery Performance Ratio, DPR (ratio of actual discharge to designed discharge) of a channel is a very important hydraulic performance indicator to judge the performance of channels in an irrigation system as that of LCC (East). For this system two types of DPRs were computed i.e. Tail DPR (ratio of actual tail discharge to authorized tail discharge) and Head DPR (ratio of actual head discharge to authorized head discharge) for five different crop seasons including Kharif 2006, Rabi 2006-2007, Kharif 2007, Rabi 2007-2008 and Kharif 2008. A specimen table (Table 1), as given below, shows the computed values of Tail and Head DPRs for 13 different channels of LCC for Karif 2006 and Kharif 2007 seasons.

Table 1: Delivery Performance Ratios (DPR) at heads and tails for thirteen channels of LCC (East) for two Kharif seasons

Name of Channel	Kharif 2006			Kharif 2007		
	DPR at Head	DPR at Tail	Relative DPR	DPR at Head	DPR at Tail	Relative DPR
High Level Disty	0.135	0.173	1.280	0.293	0.000	0.000
Alipur Minor	0.442	0.449	1.017	0.532	0.304	0.571
Ram Nagar Minor	0.374	0.232	0.621	0.497	0.018	0.035
Kot Hara Sub Minor	0.381	0.032	0.085	0.264	0.077	0.292
Manchar Disty	0.340	0.226	0.665	0.534	0.292	0.547
1-R Minor	0.411	0.365	0.887	0.386	0.508	1.315
Fateh Pur Disty	0.000	0.000		0.629	0.015	0.024
Vanike Disty	0.473	0.233	0.492	0.633	0.304	0.480
Dhilwan Minor	0.525	0.410	0.782	0.487	0.486	0.996
Chak Ghazi Minor	0.572	0.394	0.689	0.587	0.617	1.052
Ramke Minor	0.564	0.395	0.701	0.635	0.681	1.072
Kharak Sun Minor	0.407	0.318	0.782	0.509	0.277	0.544
Mehdiabad Minor	0.587	0.227	0.387	0.625	0.597	0.956

Relationship Between DPRs at Tails and Heads of Channels: In order to find relationship between Delivery Performance Ratio at channel tails (DPRT) and Delivery Performance Ratio at channel heads (DPRH) different equations, given below, were developed for Kharif seasons of 2006-2009 for channels of Lower Chenab Canal (East) System. Plots in this regard may be seen in Figure 2.

a. Kharif 2006: DPRT = 0.81 DPRH - 0.053
b. Kharif 2007: DPRT = 0.53 DPRH - 0.226
c. Kharif 2008: DPRT = 0.8 DPRH - 0.012
d. Kharif 2009: DPRT = 0.91 DPRH - 0.005

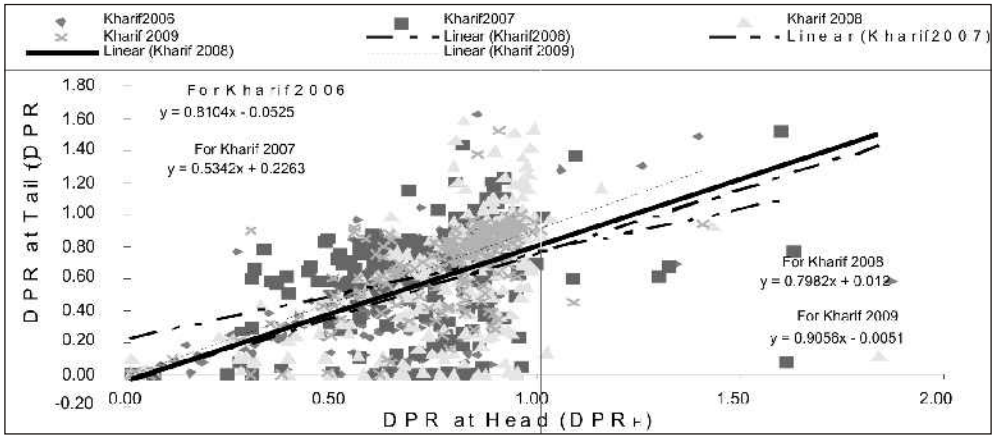

Figure 2: Relationship between Head DPR and Tail DPR for Kharif seasons of LCC (East)

Relative Delivery Performance Ratio

Relative Delivery Performance Ratio, LDPR (ratio of Tail DPR to Head DPR), which is used to measure Equity Performance Indicator, were computed by using the computed Tail DPRs and Head DPRs for all the channels in the LCC (east). A set of specimen LDPR values for eighteen channels of LCC (East) are given in Table 2. Afterwards, average of all the LDPRs for all channels was computed for all the five seasons. An ideal value of LDPR was one, which means that every changed flow condition at a sub-system head are proportionately distributed among the shareholders regardless of their location along the distributaries.

The summary of the average relative delivery performance ratio calculated for Lower Chenab Canal (East) System is shown in Table 3 and its variation is depicted in Figure 3.

Table 2: Relative Delivery Performance Ratio (LDPR) for eighteen channels of LCC (East) for five different seasons

Channel Name	RDPR Kharif 2006	RDPR Rabi 2006-2007	RDPR Kharif 2007	RDPR Rabi 2007-2008	RDPR Kharif 2008
Ramke Minor	0.33	0.62	1.14	0.62	0.96
Sagar Disty - I	1.00	0.92	0.86	0.74	0.87
Sagar Disty - II	1.89	0.94	0.88	0.87	0.84
Shah Jamal Distrobutory - II	0.83	0.35	0.81	0.59	0.98
Shah Jamal Distrobutory -I	0.09	0.38	0.72	0.28	0.42
Vanike Disty	0.81	0.51	0.35	0.00	0.58
Wazira Minor	0.52	0.78	0.75	0.50	0.82
Bassi Minor	0.22	0.03	0.40	0.00	0.00
Bath Disty	0.48	0.00	0.00	0.30	0.34
Bijwana Sub Minor	0.54	0.04	0.26	0.15	0.00
Chukeri Minor	0.29	0.57	0.43	0.28	0.11
Chutala Sub Minor	0.60	0.87	0.95	0.84	0.80
Dangali Disty	0.59	0.61	0.57	0.38	0.92
Gajjiana disty	0.36	0.11	0.19	0.29	0.33
Ghour Dour Disty	0.01	0.04	0.79	0.09	0.09
Haripur Minor	0.93	0.51	0.92	0.97	1.00
High Level Channel Disty	0.03	0.13	0.12	0.00	0.22
Innuana Disty	0.62	0.92	0.88	1.01	0.97

Table 3: Summary of the Average Relative DPR Values

Sr. No.	Name of System	Crop/Flow Season				
	LCC East	Kharif 2006	Rabi 2006-2007	Kharif 2007	Rabi 2007-2008	Kharif 2008
1		0.72	0.68	0.87	0.87	0.77

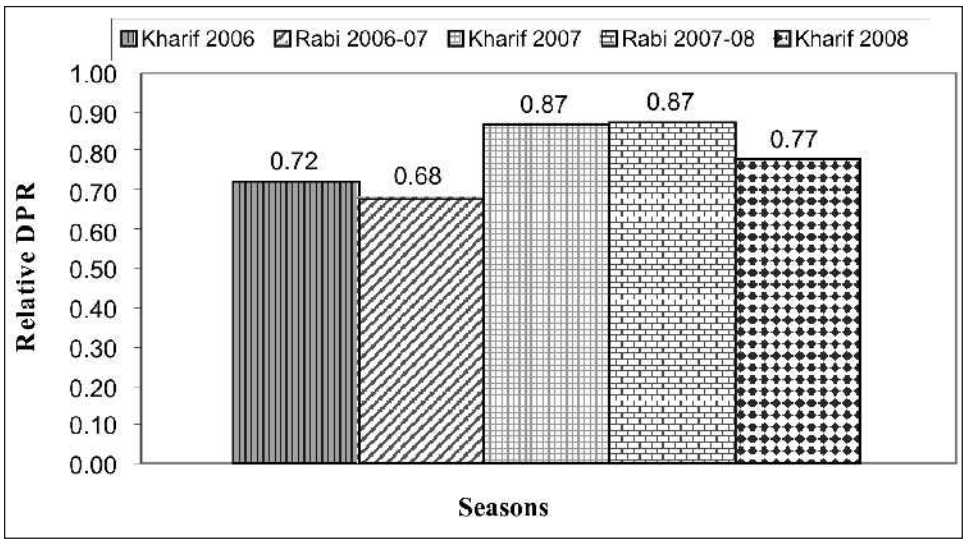

Figure 3: Variation of the Relative DPRs for LLC (East) channel system for five different Kharif seasons

Summary of the relative DPR shows that there was some improvement in the water supply for Kharif 2007 and Rabi 2007-08 seasons. For both of the seasons the Relative DPR is same as of 0.87, which is higher than the other crop seasons with an average relative DPR value of 0.72 for Kharif 2006, 0.68 for Rabi 2006-07 and 0.77 for Kharif 2008.

Capacity Factor for LCC (East) System

Average of Capacity Factor (ratio of sum of actual head discharges to sum of designed discharge) was computed for the Kharif seasons between years 2006-2009 for this Canal System. The values of average capacity factor for these seasons are given in Table 4. It showed improvement in supplies at the head of the channels of LCC (East) system for year 2007 and 2009, as compared to supply position in 2006 and 2008 respectively. This improvement is not sufficient enough and it is based upon a short span of time. To make some finding based on such a short time span would be a hasty conclusion. The variation of the average Capacity Factor for the Canal System is depicted in Figure 4.

Table 4: Summary of the Average Capacity Factor for all channels of LCC (East).

Sr. No.	Name of System	Kharif 2006	Kharif 2007	Kharif 2008	Kharif 2009
1	LCC East	0.86	0.91	0.87	0.91

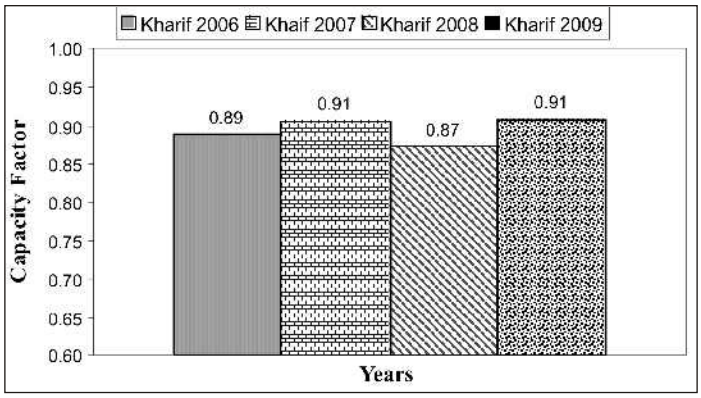

Figure 4: Variation of the Capacity Factors for LCC (East) channel system for different Kharif seasons

Status of Water Supply at Tails

The daily head and tail water supply data of all channels of LCC (East) for the Kharif seasons for years 2006-2009 were obtained from the Project Management Investigation Unit (PMIU) of I&P Department. The collected data were evaluated on monthly basis to find average water supply status at the tails. It was found that the percentage of tails, in term of average number of channels, that remained dry for Kharif 2006, Kharif 2007, Kharif 2008 and Kharif 2009 was 18, 12, 16 and 5.7, respectively; despite the fact that channels were running as per Authorized Head Discharge during these seasons which showed inequity of supply. This showed that there was some improvement in the dry tail status for Kharif 2007 than Kharif 2006. For Kharif 2008, dry channels were 4% more than the Kharif 2007. For Kharif 2009 season there were 5.7% tails remained dry which were 10% less as compared to dry tails for Kharif 2008. The criterion used for defining tail status is given in Table 5 whereas the data summary/analysis is given in Table-6. On the other hand the tail status variations are depicted in Figure 5.

Table 5: Criterion used for defining the type of tail status for LCC (East) system

Authorized Head	95% of Authorized Head Discharge
Dry Tail	Less than or equals 30% of Authorized Tail Discharge
Short Tail	Greater than 30% and Less than 90% of Authorized Tail Discharge
Authorized Tail	Greater or equals 90% of Authorized Tail Discharge & Less than 115% of Authorized Tail Discharge
Excessive Tail	Greater than 115% of Authorized Tail Discharge

Table 6: Water supply position for Kharif seasons for years 2006-09.

		Average No. of Channels			
Head Status	Tail Status	Kharif 2006	Kharif 2007	Kharif 2008	Kharif 2009
Channel	Excessive Tail	6	13	15	4
Run as per	Authorized Tail	74	77	71	140
Authorized	Short Tail	28	28	35	21
Head	Dry Tail	24	16	23	10
Closed Channels		55	59	42	38

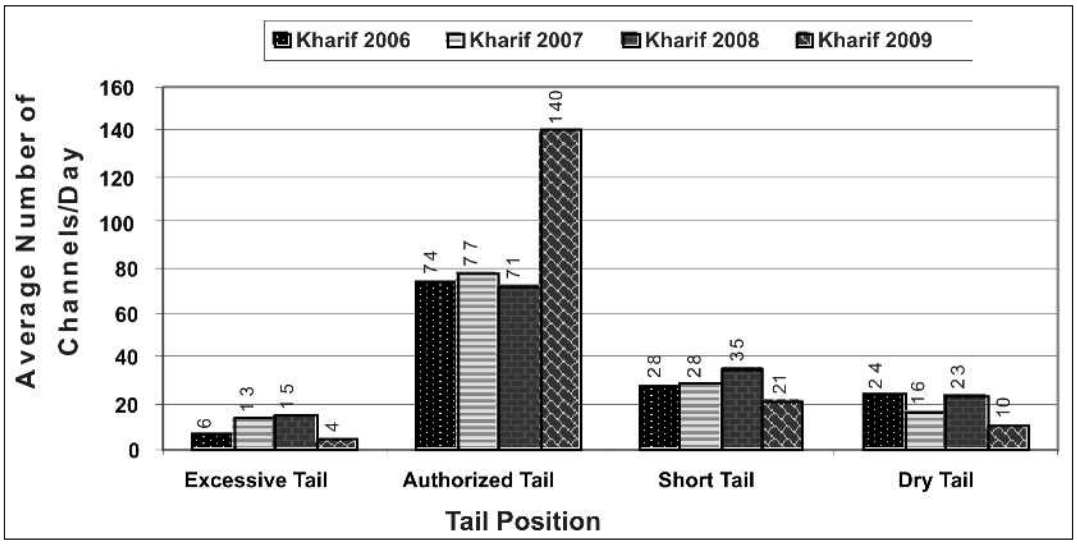

Figure 5: Status of water supply at tails during the Kharif seasons of 2006-09

Status of Abiana (Water Charges) Collection

The assembled data for different crop seasons showed that the highest percentage of Abiana collected was 87% for Rabi 2004-05 and the second highest value was 84% for Rabi 2006-07. On the other hand, for Rabi 2008-09 Abiana collections was only 31% which showed a significant drop. The cropwise progress of FOs regarding assessment and collection of Abiana until the end of October 2009 is given in Table 7. The variation in Abiana collection over the period is depicted in Figure 6.

As evident from Figure 6, for the first year of the project the revenue collection was at its highest level for Rabi 2004-05 season. Afterwards, there was a general trend of decline in Abiana collection with an exception of Rabi 2006-07 season (fifth year of project). It showed that the collection of Abiana was continuously falling with the passage of time and reached at its lowest value for Rabi 2008-09 season, when it dropped to 31%. Apparent reasons for the decline in Abiana collection could be that:

a) some of the Khal Panchayat Chairmen did not deposit the collected amount of Abiana to the FOs;

b) non-implementation of revenue laws for the collection of Abiana;

c) some of the farmers did not pay Abiana with reason of not getting their due share of water;

d) inadequate incentive for the Khal Panchayt Chairmen, which made them disinterested; and

e) lack of technical training of FOs representatives, which is required for better management.

Further, as mentioned in PIDA (2008), [4] report under the social survey of FOs functioning and AWB, the farmers (end users) were not very much satisfied with the performance of the pilot project and their dissatisfaction has been increasing with the passage of time. It has also been reported under the overall performance ranking that only 23% of the FOs' performance was good, 33% satisfactory, 27% adequate and 17% poor.

Some of the proposals regarding improvement in Abiana collection could be a development of realization in farmers that the sustainability of the Irrigation System and its equitable service delivery depends largely on the funds generated through their water charges, therefore, timely Abiana payments in this regard are necessary. Also, Abina collection system, which involves Khal Panchayt Chairmen, FAOs etc., should be improved.

Table 7: Status of Abiana collection upto 31st October 2009

Sr. No.	Cropping Seasons	Assessed Abiana Rs.	Remission given for relief Rs.	Net Assessed Abiana Rs.	Collected Abiana Rs.	% age of collect - ion
1	Rabi 2004-05	51,742,962	3,307,972	48,434,990	42,252,654	87.24
2	Kharif 2005	123,641,577	7,667,009	115,974,568	91,810,112	79.16
3	Rabi 2005-06	68,082,076	5,106,922	62,975,154	48,184,778	76.51
4	Kharif 2006	123,575,997	8,708,331	114,867,666	76,528,977	66.62
5	Rabi 2006-07	68,179,753	4,439,251	63,740,502	53,503,714	83.94
6	Kharif 2007	123,224,393	11,685,643	111,538,750	70,676,739	63.37
7	Rabi 2007-08	67,927,291	7,672,354	60,254,937	34,015,794	56.45
8	Kharif 2008	125,813,476	11,730,830	114,082,646	61,930,712	54.29
9	Rabi 2008-09	69,285,696	-	69,285,696	21,271,527	30.70
	Sub Total	821,473,221	60,318,312	761,154,909	500,17500,7	65.71

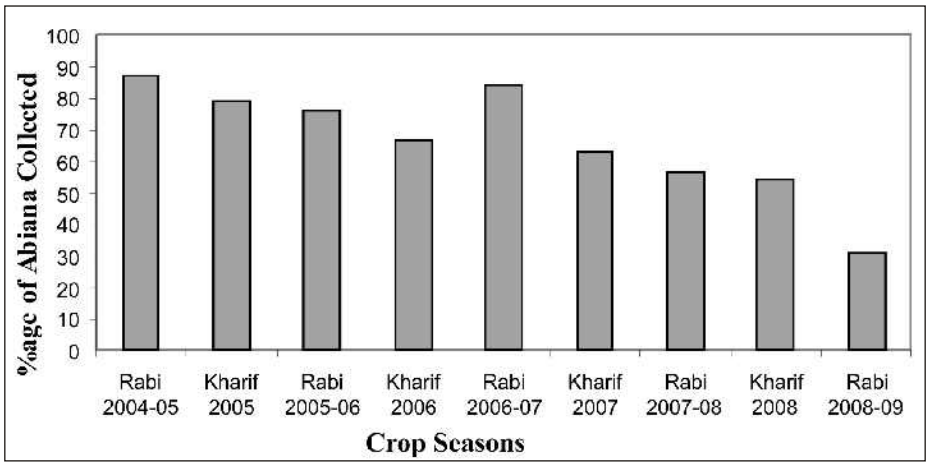

Figure 6: Percentage of Abiana collection for different crop seasons for LCC (east).

Conclusions

The following specific conclusions may be drawn from this study.

1. The computed values of relative DPR showed some improvement in the water supply for Kharif 2007 and Rabi 2007-08 seasons. Little improvement was found in the dry tail status during Kharif 2006, Rabi 2006-2007 and Kharif 2008 seasons. On the average basis, the results were not encouraging and no consistent pattern of improvement was recorded.
2. A random type variation was recorded in the average Capacity Factor for different Kharif seasons from 2006 to 2009 and it ranged from 0.86 (for Kharif 2006) to 0.91 (for Kharif 2007 & 2009). It did not show a consistent pattern of improvement in supplies.
3. A general trend of decline in Abiana collection was recorded, starting from Rabi 2004-05 season to Rabi 2008-09 season, with an exception of Rabi 2006-2007 season. This decline in revenue collection was excessive and it dropped two-third over the study period - which showed decreasing efficiency of FOs.
4. In general, based upon this LCC (East) study results and the data available till now, the reform program introduced by the Irrigation and Power Department of Government of Punjab through PIDA (which involved AWB, FOs, Khal Panchayt and its Chairmen etc) has not been doing well as it was initially anticipated. Thus it needs extensive review.

References

[1] PIDA. 2005. Scheme for Transfer of Irrigation Management, Farmers Organizations in Punjab. A Report prepared by PIDA. PIDA Headquarters, Irrigation Secretariat, Lahore.

[2] PIDA. 2007. Survey for Categorization of Farmers Organizations in LCC (East), Punjab, Pakistan. A Survey Report prepared by Development Consulting Services (DCS) for PIDA and JICA.

[3] PIDA. 2005.Reforms in Irrigation Sector (Vision, Strategy, Implementation, Achievements).A Report prepared by PIDA, PIDA Headquarters, Irrigation Secretariat, Lahore.

[4] PIDA.2008 Performance of Farmers Organizations and Area Water Board, LCC (East), Faisalabad. A PIDA Report, PIDA Headquarters, Irrigation Secretariat, Lahore.

Dynamic Behavior Of Rotor Surrounded By Outer Casting with Small Annular Clearance

Sagheer Ahmad [1] and M.K.K.Ghauri [2]

Abstract

Vibration response of a rotor surrounded by an outer casing is investigated. For the analysis, a six-degree-of-freedom dynamic model of a shaft and disk is established using Lagrangian equations. While deriving the differential equations of motion, gyroscopic effect was taken into account and the solution of equations and response was obtained in MATLAB. Results demonstrate that rotor-stator rubbing may occur in a variety of forms and circumstances. It is shown that the inclusion of gyroscopic effect in the vibration model is useful in revealing the nature of vibration response.

Keywords: Rotor, contact, Vibrations, Lagrangian, Gyroscopic effect

Introduction

For high thermal efficiency of turbo-machinery, the clearance between the rotating and stationary elements is kept very small. During malfunctioning, the stationary and rotating elements come in contact with each other resulting in partial or full rub. Rotor-casing rub has been the area of interest of many researchers. Much research has been carried out to understand the rotor/casing motion and to find ways to prevent serious damages resulting from the unstable rubbing vibration. Bazen [1] discussed the effects of friction and alignment on vibration response of interacting surfaces. The mathematical model presented by Currami [2] relates the rotor stiffness to parametric instability. Special attention was given by Choy et al [3] to determine the effects of casing stiffness, friction coefficient, mass imbalance and damping characteristics on the response. Large rub forces were experienced by increasing the casing stiffness and imbalance of the rotor. But damping tends to retard the initiation of backward whirl. It was proved by Zhang [4] that dry friction is the main cause of whirl during rubbing due to which instability occurs. Choy [5] observed the vibration response for the cases of blade loss and varying bearing clearances. Crandall [6] and Childs [7] investigated that large clearance between rotor and casing is needed for the occurrence of dry friction whirl and whip. Wu and Flowers [8] concluded that severity of rub depends on lubrication of interacting surfaces and acceleration of rotor. Goldman and Muszynska [9] showed that increase in temperature results in oscillation of rotor. Chu and Lu [10] concluded that rubbing results in increased stiffness of interacting surfaces. Feng et al [11] demonstrated that forward whirling of rotor results in the absence of friction and full rubbing behaves as backward whirling due to friction. It was demonstrated by Karpenko et al [12] that increased intensity of out-of-balance generates full annular rub. Qin et al [13] showed that chaotic motion is due to increase in the external damping of rotor-casing system. Jiang et al [14] studied the effects of different system parameters such as stiffness, damping and mass imbalance on the vibration behavior. Jiang [15, 16] included in his vibration model the effect of dry friction and predicted the self-excited vibrations of the rotor with the amplitude fluctuating around the critical value of the deflection. It is interesting to note from the above described survey that the details of early warning response characteristics prior to interaction of rotating and stationary elements are missing in the published literature.

Effect of gravity on rotor in the analyses. In the present study, rotor considered is vertical and effect of gravity has been considered. Gyroscopic effect has also been included, which, to the authors' knowledge has not been taken into account in a vertical rotor system in the past conducted researches. In this paper, the dynamic response of a vertical flexible rotor before its interaction with the outer casing has been presented. The aim is to contribute to the development of efficient method for understanding the behavior of a rotor system under the influence of certain system's parameters which have been frequently used by the past researchers

Rotor-Stator Model

The test rig (Figure-1) consisted of a flexible shaft vertically clamped, coupled with driving motor at the

[1&2] Mechanical Engineering Dept., University of Engineering & Technology, Taxila, Pakistan.

upper end through a flexible coupling and carrying a disk at the lower end. The shaft is rigidly connected to the foundation (outer casing) through a set of horizontal springs and viscous dampers at a distance of three quarter of shaft's length from the upper end. A suitable gap of 10 mm is kept between disk and the outer casing. Eddy current type displacement transducers and accelerometers (ENDEVCO 100 mv/g) were used for obtaining the signals from the rotor/casing system. For data acquisition and analysis, a Fast Fourier Transform (FFT) analyzer made by Bruel & Kajeer was arranged from Directorate of Nuclear Power Engineering Reactor, Pakistan Atomic Energy Commission, and Islamabad, Pakistan.

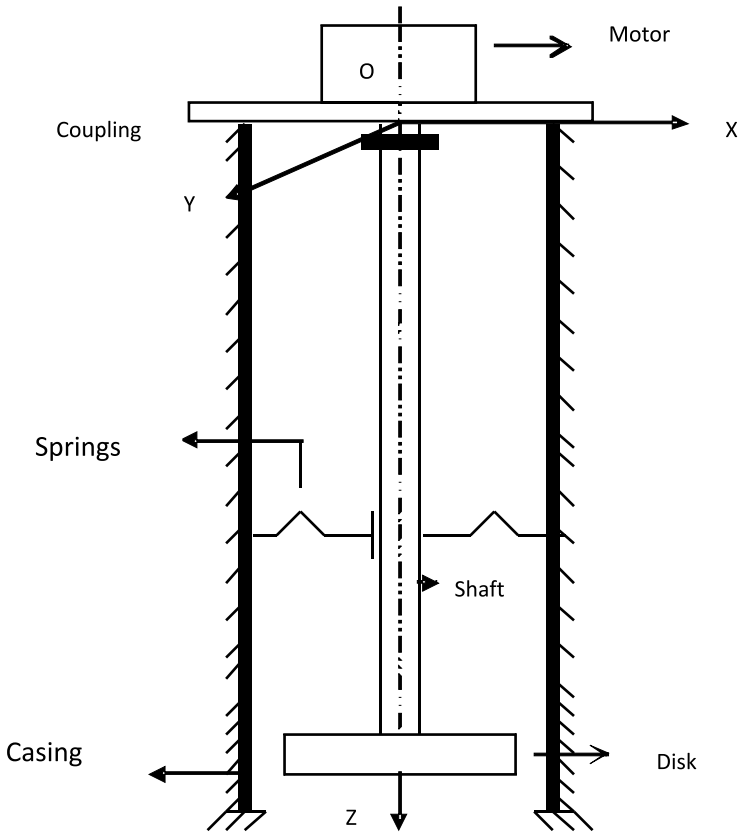

Figure 1: Physical model of the system

The dynamic motion of the system is described by six degrees-of-freedom as θx, θy , Xs1, Xs2, Ys1 and Ys2 as shown in (Figure-2). In the rigid pendulum like mode, the degrees-of-freedom are θx and θy. Whereas Xs1, Xs2 and Ys1, Ys2 represent the degrees-of-freedom in the 1st shaft flexing mode and in the 2nd shaft flexing mode respectively. The physical characteristics of the model and complete nomenclature are given in the appendix.

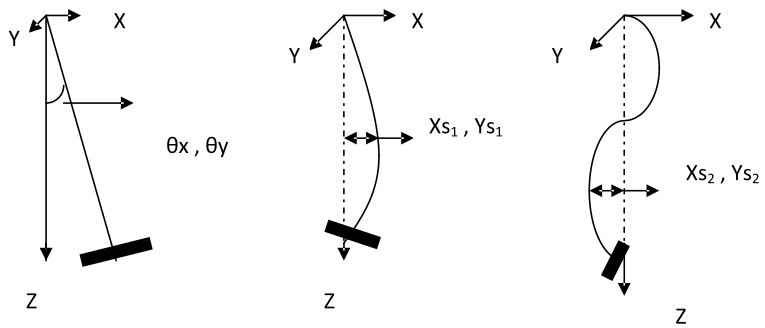

Figure 2: Degrees-of-freedom of the model and gyroscopic effect

Mathematical Model

In developing the rotordynamic model, radial symmetry is assumed. i.e., Kx = Ky and Cx = Cy . Springs and Viscous dampers are assumed to be linear and all the deflections in the considered modes of vibrations are assumed to be very small. Gyroscopic effect is taken into account by considering the turning motion of the disc about the X- and Y-axes during its rotation about the Z-axis (Figure-2) resulting from gyroscopic couple. Three modes of vibrations namely, the rigid pendulum like mode, 1st shaft flexing mode and the 2nd shaft flexing mode are considered In the context of this paper, it is impractical to write all the steps involved in the derivation of differential equations of motion. However, for the purpose of clarity, the main steps are discussed here.

The motion of the system is described in the reference frame OXYZ (Figure-1) using six generalized coordinates. Lagrange's equations are used for obtaining differential equations of motion.

$$\frac{d}{dt}\left(\frac{\partial T}{\partial \dot{q}}\right) - \frac{\partial T}{\partial q} + \frac{\partial U}{\partial q} + \frac{\partial D}{\partial \dot{q}} = Q \qquad (1)$$

where $\{q\}^T = \left[\theta_y, X_{s1}, X_{s2}, \theta_x, Y_{s1}, Y_{s2}\right]$ is the vector of generalized coordinates.

T, U and D represent total kinetic energy, total strain energy and energy dissipation function of the system respectively. The equations are written in matrix form with **M, C** and **K** as mass, damping and stiffness matrices. The resulting linearized equations of motion are:

$$\mathbf{M}\ddot{q} + \mathbf{C}\dot{q} + \mathbf{K}q = Q \qquad (2)$$

where $\mathbf{C} = \mathbf{C}^D + \mathbf{C}^G$

$\mathbf{C}^D$ = damping matrix due to external viscous damping

$\mathbf{C}^G$ = damping matrix due to gyroscopic effect.

and $\{Q\}^T = \left[1, 0, 0, -i, 0, 0\right].me\,\omega^2 e^{i\omega t}$

is the vector of forces due to mass imbalance 'me' in the disc.

The mass matrix **M** is given as

$$\begin{bmatrix}
\left(\frac{m_s l^2}{3} + m_d l^2 + m_s r^2 + m_d r_d^2\right) & -\frac{m_s l}{\pi} + \frac{\pi m_d r_d^2}{2l} & \frac{m_s l}{2\pi} - \frac{\pi m_d r_d^2}{l} & 0 & 0 & 0 \\
-\frac{m_s l}{\pi} + \frac{\pi m_d r_d^2}{2l} & \left(\frac{m_s}{2} + \frac{\pi^2 m_s r^2}{2l^2} + \frac{\pi^2 m_d r_d^2}{2l^2}\right) & -\frac{\pi^2 m_d r_d^2}{l^2} & 0 & 0 & 0 \\
\frac{m_s l}{2\pi} - \frac{\pi m_d r_d^2}{l} & -\frac{\pi^2 m_d r_d^2}{l^2} & \left(\frac{m_s}{2} + \frac{2\pi^2 m_s r^2}{l^2} + \frac{2\pi^2 m_d r_d^2}{l^2}\right) & 0 & 0 & 0 \\
0 & 0 & 0 & \left(\frac{m_s l^2}{3} + m_d l^2 + m_s r^2 + m_d r_d^2\right) & \frac{m_s l}{\pi} - \frac{\pi m_d r_d^2}{2l} & -\frac{m_s l}{2\pi} + \frac{\pi m_d r_d^2}{l} \\
0 & 0 & 0 & \frac{m_s l}{\pi} - \frac{\pi m_d r_d^2}{2l} & \left(\frac{m_s}{2} + \frac{\pi^2 m_s r^2}{2l^2} + \frac{\pi^2 m_d r_d^2}{2l^2}\right) & -\frac{\pi^2 m_d r_d^2}{l^2} \\
0 & 0 & 0 & -\frac{m_s l}{2\pi} + \frac{\pi m_d r_d^2}{l} & -\frac{\pi^2 m_d r_d^2}{l^2} & \left(\frac{m_s}{2} + \frac{2\pi^2 m_s r^2}{l^2} + \frac{2\pi^2 m_d r_d^2}{l^2}\right)
\end{bmatrix}$$

The damping matrix **C** is

$$\begin{bmatrix} \frac{9}{16}C_x l^2 & -0.53C_x l & -0.75C_x l & -\left(m_s r^2\omega + m_d r_d^2\omega\right) & 0 & 0 \\ -0.53C_x l & 0.5C_x & 0.707C_x & 0 & \frac{\pi^2 m_s r^2 \omega}{2l^2} & 0 \\ -0.75C_x l & 0.707C_x & C_x & 0 & 0 & 2\frac{\pi^2 m_s r^2 \omega}{l^2} \\ \left(m_d r_d^2\omega + m_s r^2\omega\right) & 0 & 0 & \frac{9}{16}C_y l^2 & 0.53C_y l & 0.75C_y l \\ 0 & -\frac{\pi^2 m_s r^2 \omega}{2l^2} & 0 & 0.53C_y l & 0.5C_y & 0.707C_y \\ 0 & 0 & -2\frac{\pi^2 m_s r^2 \omega}{l^2} & 0.75C_y l & 0.707C_y & C_y \end{bmatrix}$$

and the corresponding stiffness matrix **K** is

$$\begin{bmatrix} \begin{pmatrix} m_s g\frac{l}{2} + m_d g l \\ +\frac{9}{16}l^2 k_x \\ -m_d r_d^2\omega^2 - m_s r^2\omega^2 \end{pmatrix} & -0.53lk_x & -0.75lk_x & 0 & 0 & 0 \\ -0.53lk_x & \begin{pmatrix} \frac{\pi^4 EI}{2l^3} + 0.5k_x \\ -\frac{\pi^2 m_s r^2\omega^2}{2l^2} \end{pmatrix} & 0.707k_x & 0 & 0 & 0 \\ -0.75lk_x & 0.707k_x & \begin{pmatrix} \frac{8\pi^4 EI}{l^3} + k_x \\ -\frac{2\pi^2 m_s r^2\omega^2}{l^2} \end{pmatrix} & 0 & 0 & 0 \\ 0 & 0 & 0 & \begin{pmatrix} m_s g\frac{l}{2} + m_d g l + \frac{9}{16}l^2 k_y \\ -m_d r_d^2\omega^2 - m_s r^2\omega^2 \end{pmatrix} & 0.53lk_y & 0.75lk_y \\ 0 & 0 & 0 & 0.53lk_y & \begin{pmatrix} \frac{\pi^4 EI}{2l^3} + 0.5k_y \\ -\frac{\pi^2 m_s r^2\omega^2}{2l^2} \end{pmatrix} & 0.707k_y \\ 0 & 0 & 0 & 0.75lk_y & 0.707k_y & \begin{pmatrix} \frac{8\pi^4 EI}{l^3} + k_y \\ -\frac{2\pi^2 m_s r^2\omega^2}{l^2} \end{pmatrix} \end{bmatrix}$$

After

substituting the Mass (**M**), Damping (**C**) and Stiffness (**K**) matrices, the Eqs.2 were solved in MATLAB to determine the global motion of the system and the radial displacement of the rotor was monitored to avoid rubbing with the outer casing.

Results and Discussion

Results are presented to illustrate the response of the system under gyroscopic effect. Some general patterns are noted from these results in relation to the effects of rotating speed, damping, stiffness and mass imbalance. These results can not be compared directly with the past references due to different configurations of physical models used by different researchers. The developed mathematical model

represented by Eq.1 is first used to determine the natural frequencies of the system at zero rotor speed which are: $\omega_1 = 25.64$ rad/sec, $\omega_2 = 163.77$ rad/sec, $\omega_3 = 926.14$ rad/sec, $\omega_4 = 25.64$ rad/sec, $\omega_5 = 163.77$ rad/sec and $\omega_6 = 926.14$ rad/sec. To confirm the gyroscopic effect , the response of the system was obtained at rotating speeds ranging from 0 to 100 rad/sec with and without inclusion of $\mathbf{C}^G$ in the mathematical model keeping $Kx = K_y = 5000$ N/m, $Cx = C_y = 10$ N-sec/m and imbalance me = 87 gm-mm. It is shown in Figure-3 that at rotating speed of 25.64 rad/sec, i.e., at resonance, the radial displacement of rotor is 10 mm which is equal to the initial gap between the disk and the outer casing, whereas this displacement is about 6.5 mm in the absence of gyroscopic effect as indicated in Figure-4.

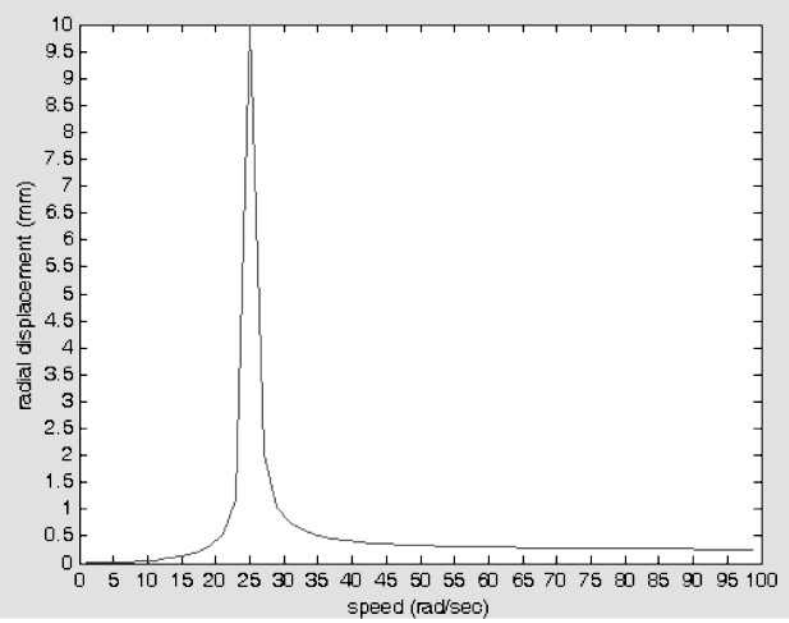

Figure 3: System response with gyroscopic effect

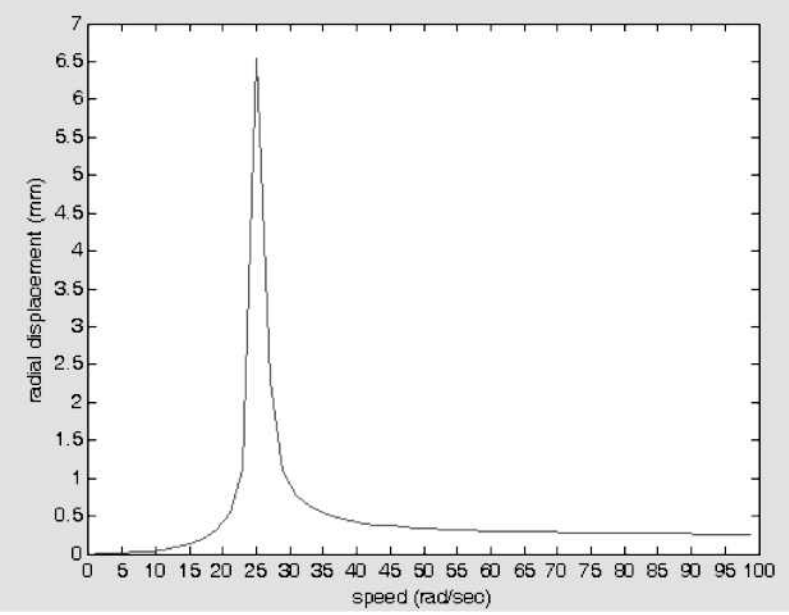

Figure 4: System response without gyroscopic effect

The corresponding motion orbits are shown in Figures- 5 and 6.It can be concluded that it is the gyroscopic effect which ensures the full rubbing of the rotor-disk system with the outer casing. Hence the effects of some other parameters on system's response were studied by incorporating CG in the mathematical model.

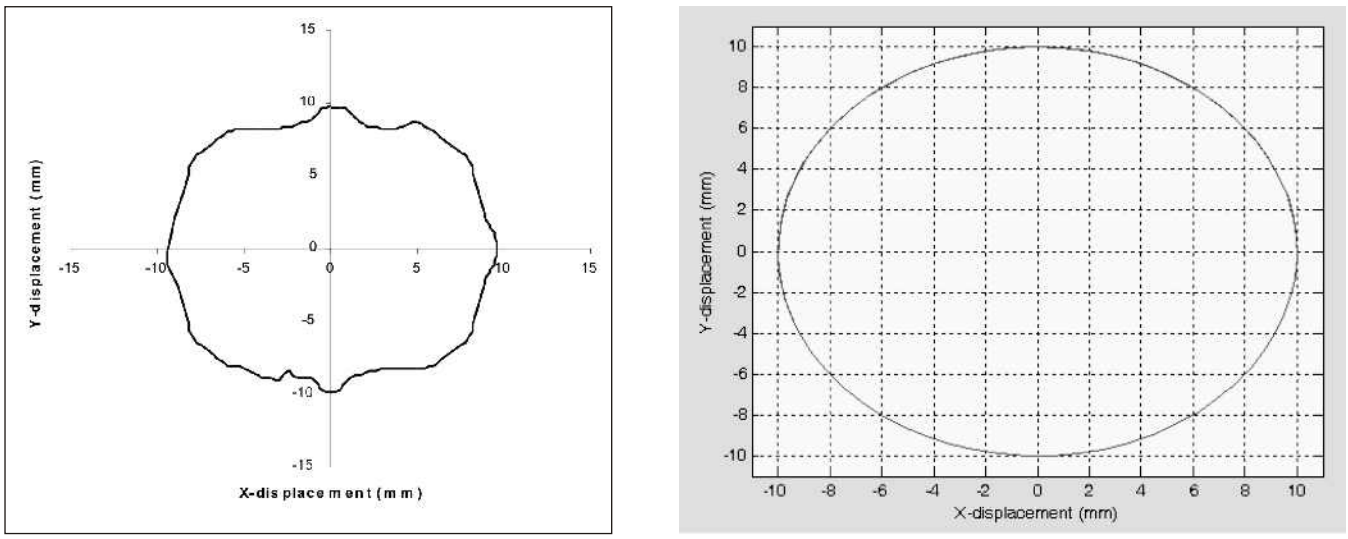

(a) Experimental (b) Computer predicted

Figure 5: Motion orbit with gyroscopic effect

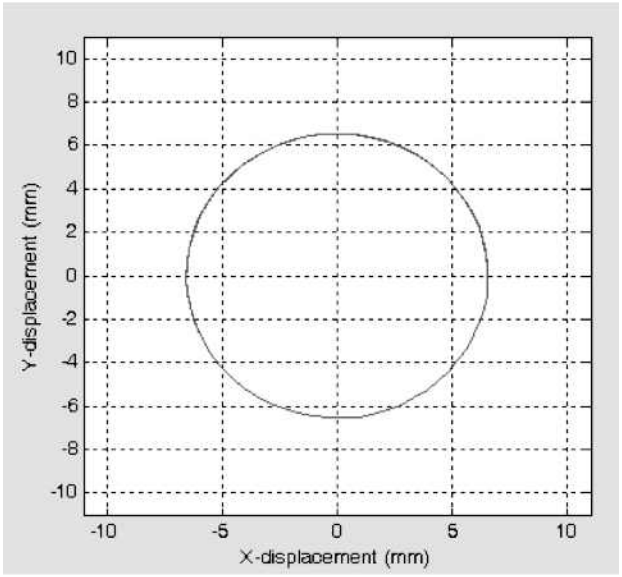

Figure 6: Computer predicted Motion orbit without gyroscopic effect

Rotating speed is an important parameter affecting the vibration response of rotor/casing system. It is noted from Figures- 7 and 8 that full rubbing is not possible at $\omega = 24$ rad/sec and $\omega = 30$ rad/sec.

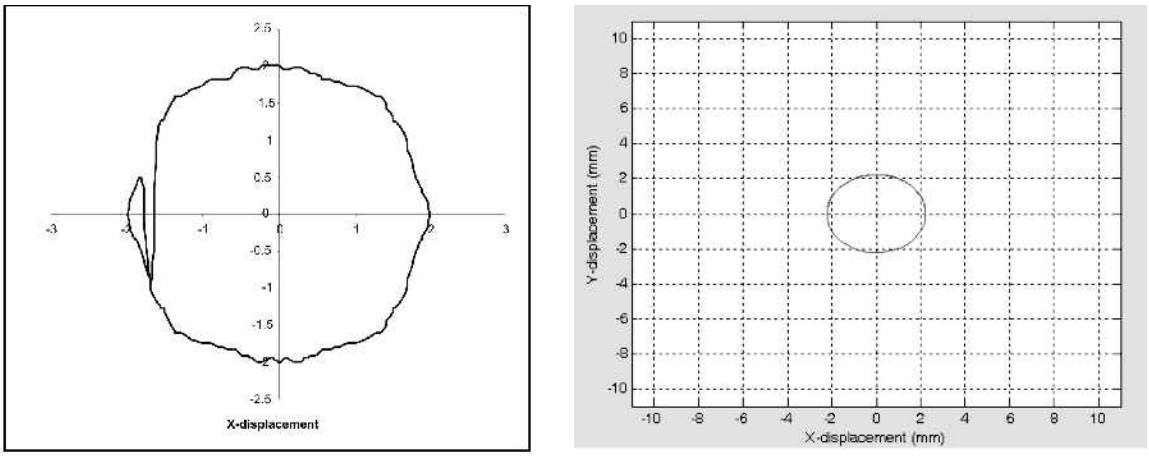

(a) Experimental (b) Computer predicted

Figure 7: Steady state response at ω = 24 rad/sec

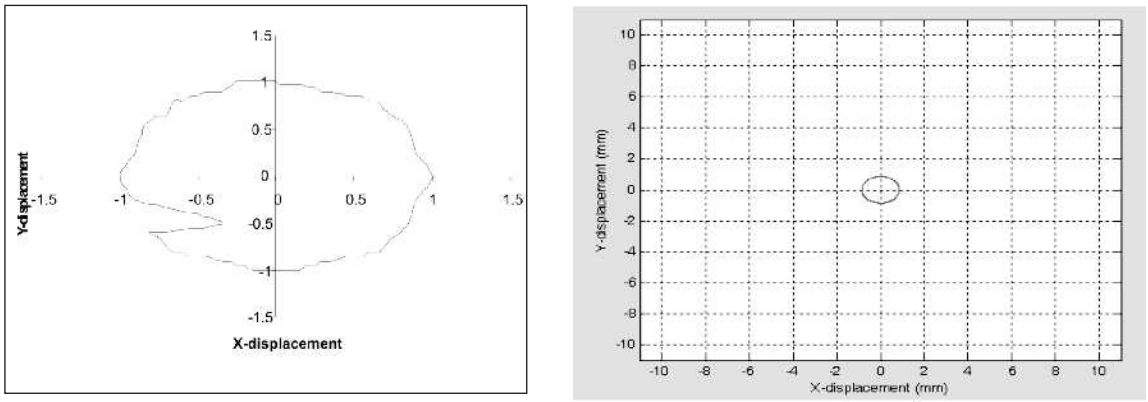

(a) Experimental (b) Computer predicted

Figure 8: Steady state response at ω = 30 rad/sec

With the increase in speed from zero to a value equal to 1st natural frequency of the system, the rotor starts rubbing against the casing. With further increase in speed, the contact breaks. With the introduction of damping, the amplitude of vibration may be suppressed as shown in Figures-9 and 10. i.e., as an example, at ω = 25.64 rad/sec and Cx = Cy = 20 N-sec/m, full rubbing is not possible.

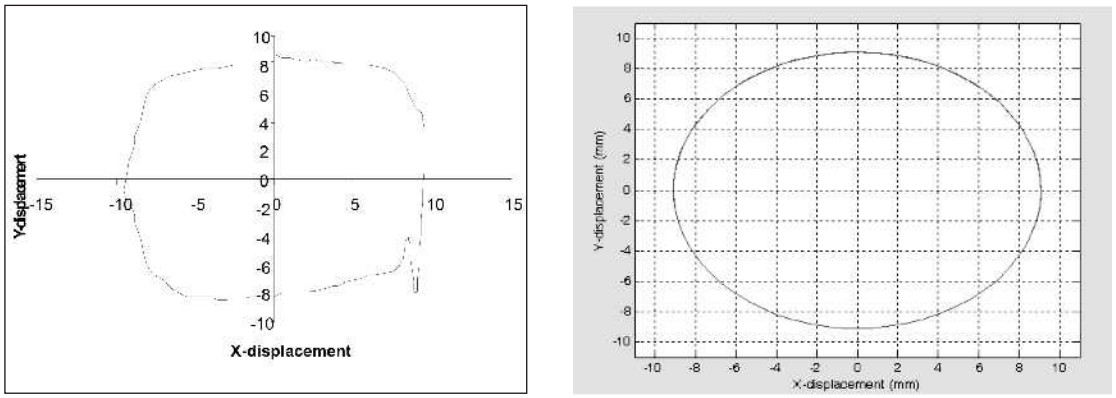

(a) Experimental (b) Computer predicted

Figure 9. Steady state response at ω = 25.64 rad/sec , C = 20 N-sec/m

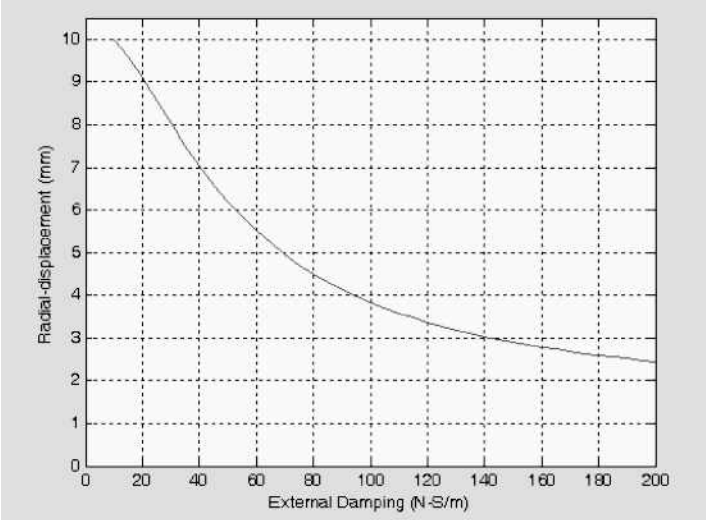

Figure 10: Effect of External Damping

To investigate the effect of stiffness on the dynamic response, the response was plotted for various stiffness values at constant angular speed in Figure-12, keeping all the other parameters fixed. As an example in Figure-11, rubbing is not observed for stiffness equal to 5100 N/m. By increasing the stiffness parameter, rubbing is avoided.

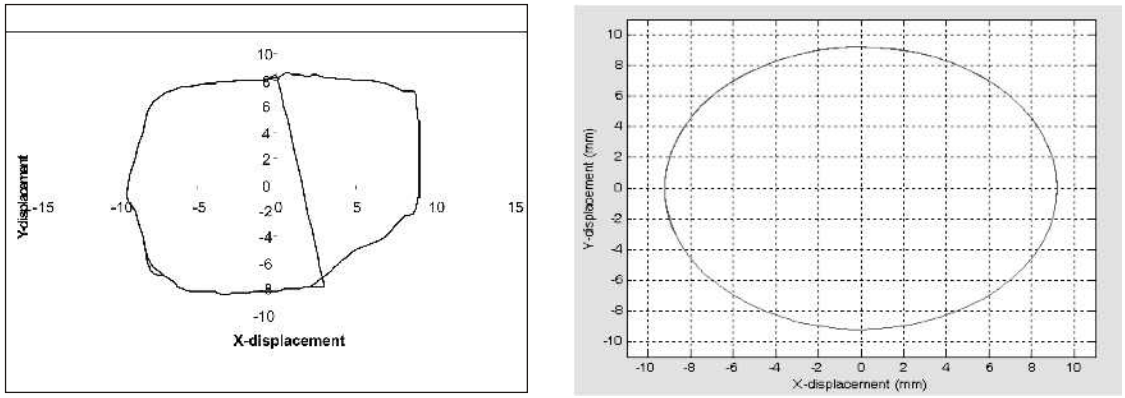

(a) Experimental (b) Computer predicted

Figure 11. Steady state response for $K_x = K_y = 5100$ N/m

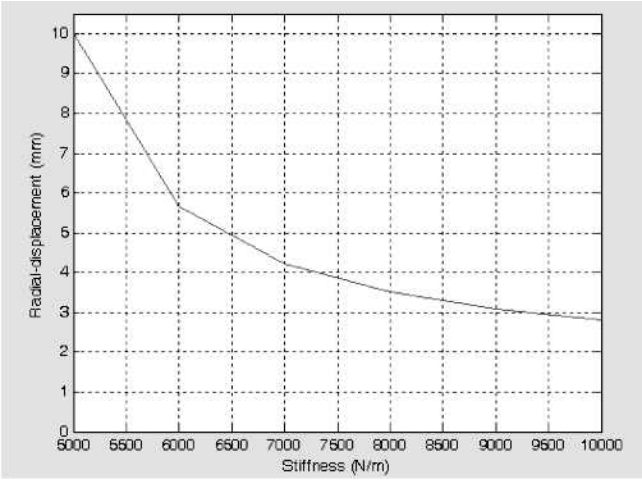

Figure 12: Effect of stiffness

Rotor imbalance is another important parameter affecting the dynamic behavior of the system. In the case of 80 gm-mm un-balance, the rotor did not make contact with the casing at rotating speed of 25.64 rad/sec as given in Figure-13. At the same rotating speed, Figure-14 shows the motion orbit of the rotor with rubbing in the case of imbalance equal to 87 gm-mm. It has been observed that this value of imbalance causes the largest response keeping the rotating speed constant, i.e., for causing rubbing between rotor and casing, the amplitude of imbalance must exceed a certain value known as the critical rubbing excitation.

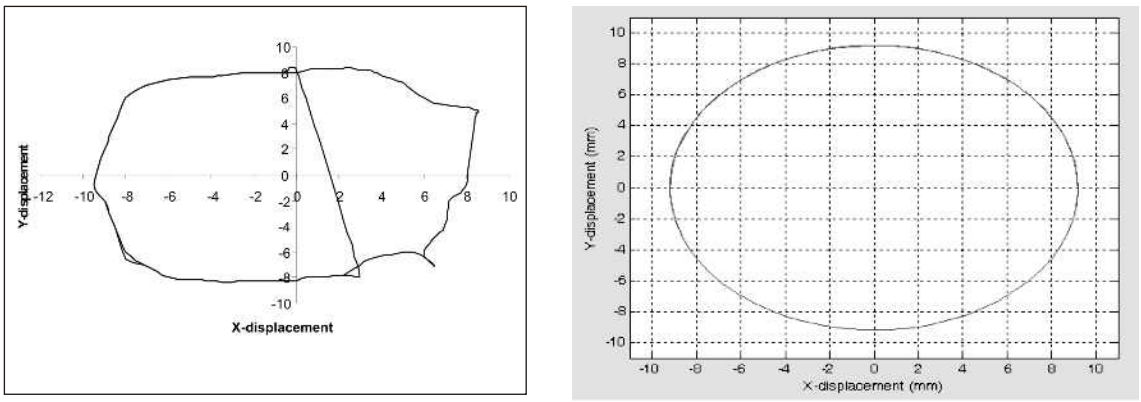

(a) Experimental (b) Computer predicted

Figure 13: Steady state response at me = 80 gm-mm

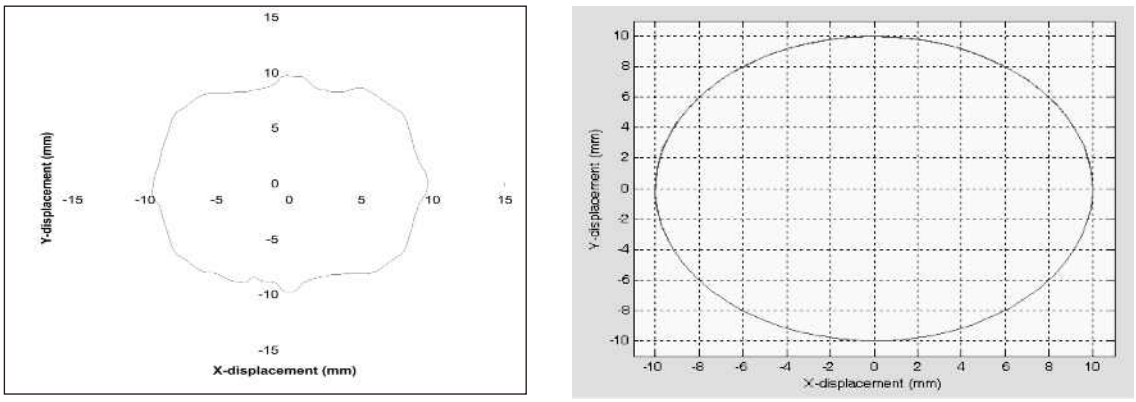

(a) Experimental (b) Computer predicted

Figure 14: Steady state response at me = 87 gm-mm

Conclusion

The dynamic vibration response of a flexible rotor/casing system before its interaction with the outer casing is obtained taking into account the gyroscopic effect. The simulation is carried out in MATLAB under variations in system's parameters .The conclusions are summarized as follows:

1. The inclusion of gyroscopic effect in the vibration model is useful in revealing the nature of vibration response.
2. The results demonstrate the dependence of the motion on system's parameters like imbalance, speed of rotation, stiffness, damping etc.
3. It is shown that by selecting the optimal system's parameters, the harmful heavy rubbing between the rotating and stationery parts can be avoided.

APPENDIX

Nomenclature with Numerical Model Physical Parameters

E = Young's Modulus of Elasticity = 71.7 GN/m2

ρ = Mass density = 2810 kg/m3

l = Length of the shaft = 0.6 m

d= Diameter of shaft = 0.01 m

r = Radius of the shaft = 0.005 m

rd = Radius of disk = 0.075 m

h = Thickness of disk = 0.01 m

Xs1 = Linear displacement of shaft in X-direction in 1st bending mode

Xs2 = Linear displacement of shaft in X-direction in 2nd bending mode

Ys1 = Linear displacement of shaft in Y-direction in 1st bending mode

Ys2 = Linear displacement of shaft in Y-direction in 2nd bending mode

θx = Angular displacement of shaft in X-direction

θy = Angular displacement of shaft in Y-direction

θz = Angular displacement of shaft about Z-axis

ω = Angular speed of shaft-disk system (rad/sec)

ms = Mass of the shaft in kg.

md = Mass of the disk in kg.

Cx , Cy = Damping coefficient in X- and Y-directions respectively.

References

[1] Bazan, E., Bielak J., and Griffin, J. H., 1986 "An Efficient Method for Predicting the Vibratory Response of Linear Structures with Friction Interfaces", Journal of Engineering for Gas Turbines and Power, Volume 94, pp 117-125.

[2] Currami, A., Pizzigoni, B. and Yania, A.1986, "On the Rubbing Phenomenon in TurboMachinery", Proceedings of the Fourth IFToMM International Conference on Rotordynamics, Tokyo, Japan 1986.pp.481-486.

[3] Choy, F. K and Padovan, J,1987, " Non-Linear Transient Analysis of Rotor-Casing Rub Events", Journal of Sounds and Vibrations, 113(3),pp 529-545.

[4] Zhang, W.,1988 "Dynamic Instability of Multi-Degree-of-Freedom Flexible Rotor System due to Full Annular Rub". Institute of Mechanical Engineering , C 252/88. pp 305-30,.

[5] Choy, F. K., Padovan, J., Batur, C., 1989 "Rub Interactions of Flexible Casing Rotor System"., ASME Journal of Engineering for Gas Turbines and Power, Vol.111, pp 652-658.

[6] Crandall. S., 1990 "From Whirl to Whip in Rotordynamics", IFToMM Third International Conference on Rotordynamics, Lyon, France, pp. 19-26.

[7] Childs D., "Turbomachinery Rotordynamics: Phenomena Modeling and Analysis", John Wiley and Sons, New York.1993.

[8] Wu, F., Flowers, G. T.,1993, "An Experimental Study of the Influence of Disk Flexibility and

Rubbing on Rotor Dynamics", DE-Vol.60 , Vibrations of Rotating Systems, ASME, DE-Vol.60, pp.19-26, 1993.

[9] Goldman, P., Muszynska, A.1995, " Rotor-to-Stator, Rub-related Thermal/Mech. Effects in Rotating Machinery ", Chaos Solitons & Fractals, Vol 5, No.9 pp.1579-1601.

[10] Chu, F., Lu, W., "Determination of Rubbing Location in a Multi-Disk Rotor System by Means of Dynamic Stiffness Identification", 2001 Journal of Sound and Vibration, 248(2), pp 235-246,

[11] Feng, Z. C., and Zhang, X.Z., 2002, "Rubbing Phenomenon in Rotor-Stator Contact", Chaos, Solitons and Fractals, Vol:14, Issue 2, pp 257-267.

[12] Karpenko, E. V., Wiercigroch, M., and Pavlovskia, E. E., 2003 " Bifurcation Analysis of a Preloaded Jeffcott Rotor", Chaos, Solitons & Fractals, Volume 15, pp. 407-416,.

[13] Qin, W., Chen, G., Meng, G., 2004 " Non-linear Responses of a Rub-impact Overhung Rotor", Chaos, Solitons & Fractals, Volume 19, pp. 1161-1172,.

[14] Jiang, J. and Ulbrich, H. 2005, "The Physical Reason and The Analytical Condition for The Onset of Dry Whip in Rotor-to-Stator Contact Systems", ASME Journal of Vibration and Acoustics., Vol.127, pp. 594-603.

[15] Jiang, J., 2007, " The Analytical Solution and the Existence Condition of Dry Friction Backward Whirl in Rotor-to-Stator Contact Systems" , ASME Journal of Vibration and Acoustics., Vol.129, April 2007, pp. 260-264

[16] Jiang J.2008, " Determination of the Global Responses Characteristics of a Piecewise Smooth Dynamical System With Contact" Nonlinear Dynamics, DOI 10.1007/s11071-008-9446-z (Springer) Published online: 20 Nov.

Performance Evaluation of H.264/avc Fidelity Range Extensions

Aliya Mazhar, Shaista Jabeen, Sadia Nisar and Gulistan Raja[1]

Abstract

The latest video compression standard, H.264/AVC standard has introduced Fidelity Range Extensions (FREXt) as coding tools to increase the applications areas towards high definition video storage and transmission in an efficient manner. This paper describes performance analysis of Fidelity Range Extensions of this standard. The three profiles High, High10 and Baseline are compared by using reference software JM 15.1. Test video sequences of different environment at various bit rates are used to evaluate performance of FREXt. The objective and subjective simulation results show that high profiles of FREXt are more efficient in coding performance as compared to baseline H.264/AVC standard.

Keywords: H.264/AVC, FREXt, Coding performance

Introduction

H.264 is the latest entry of international video coding standard as product of a combined effort by the Joint Video Team (JVT) [1]. H.264 has demonstrated improved coding efficiency, increased flexibility, reducing complexity design, enhancing error robustness to make it more efficient and more compatible with much more applications as compared to the previous standards [2-3]. However, H.264/AVC standard targeted on such applications which require low video resolutions i.e. video supporting 8 bits per sample and 4:2:0 sampling of chrominance components. Therefore extensions have been proposed in H.264/AVC known as Fidelity Range Extensions, FREXt which supports higher video resolutions [4-5]. The development committee has reported substantial gains by performing coding simulations but much research is still required for better assessment. With this idea, our research work shows comparison of latest H.264 FREXt (High and High10 profiles) and H.264 Baseline standard. Also usage of 4x4, 8x8 and adaptive transform within the High profiles has been evaluated. Section 2 depicts overview of H.264/AVC FREXt and its innovation. Section 3 illustrates performance analysis and simulation results of H.264/AVC FREXt while section 4 concludes the paper.

Overview of H.264/AVC FREXt

The main purpose of FREXt is to focus on the most demanding application areas like post processing, content contribution, studio editing and content distribution [5-6]. The FREXt of H.264/AVC was previously known as "professional" Extensions. The various profiles on H.264/AVC FREXt are shown in Figure1.

As depicted in Figure1, H.264/AVC FREXt specifies four additional profiles having interleaved qualities which are basically extended form of Main profile. Four profiles are High profile (HP) 4:2:0 8 bit/sample, High 10 profile (Hi10P) 4:2:0 up to 10 bit/sample, High 4:2:2 profile (H422P) up to 10 bit/sample, High 4:4:4 profile (H444P) up to 12 bit/sample. High 4:4:4 include support for predictive lossless coding and residual colour transforms. Each High profile supports all capabilities of its nested profile. High10, High 4:2:2 and High 4:4:4 profiles enhance the capabilities of previous profiles including more demanding applications which need higher chrominance precision, higher bit depths and higher sample precision. All new profiles support all features of main profile adding adaptive block switching between 8x8 and 4x4 transform (the main distinguishing feature from all the Non-FREXt profiles), perceptual quantization matrices and specific control of quantization parameter. Organizations which have adopted FREXt as their video compression standard are HD-DVD specification of the DVD Forum, BD-ROM Video specification of the Blue ray Disc Association, and DVB (digital video broadcast) standards for European broadcast of the Blue ray Disc Association, and DVB (digital video broadcast) standards for European broadcast television. The summary of comparison of applications of H.264/AVC baseline and FREXt is shown in Table 1.

[1] Electrical Engineering Dept., University of Engineering & Technology, Taxila.

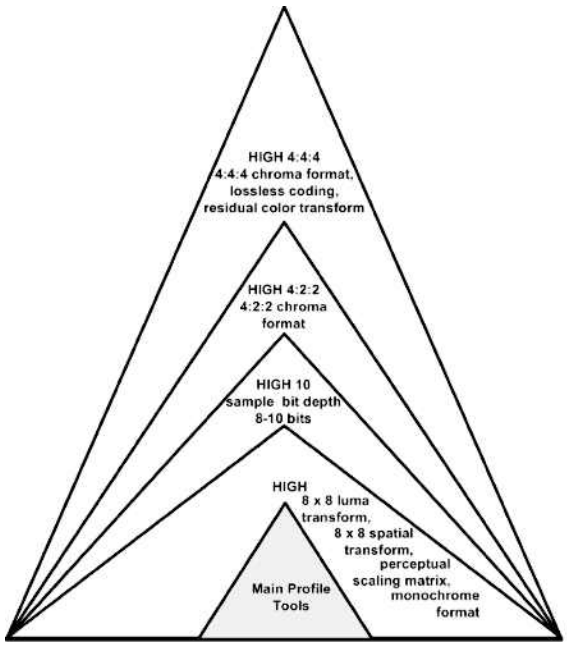

Figure 1: Interleaved high profiles of H.264/AVC FRExt

Performance Evaluation of H.264/AVC FRExt

To analyze the performance of FRExt, different input video sequences were encoded using JM FRExt 15.1 [7]. We have analyzed the performance of FRExt for mobile video applications such as video conferencing, video on internet, mobile TV, PDA's, hand held devices. CIF (Common Intermediate Format) and QCIF (Quarter Common Intermediate Format) video formats are therefore used in this analysis as these are supported by above mentioned applications. All video sequences are YUV (4:2:0) namely "Foreman", "Coastguard", "Mother Daughter", "Silent" and "Hall" [8]. The test environment is summarized in the given Table 2.

A comparison of luminance PSNR (Peak Signal to Noise Ratio) vs. bit rate was made among different sequences of high, high10 profiles of FRExt and Baseline profile of H.264/AVC. Bit rates were selected according to the standards specified internationally for each video format.

Table 1: Applications of H.264 baseline and FRExt

H.264 Baseline	▪ Video Conferencing ▪ Videophone ▪ Video-on-Demand ▪ Multimedia streaming services over ISDN, cable modem, DSL, LAN, wireless networks etc.
FRExt Profiles	▪ Content contribution ▪ Content distribution ▪ Studio editing ▪ Post processing ▪ HD-DVD specification ▪ DVB (digital video broadcast) ▪ BD-ROM (Video specification of the Blue-ray Disc Association)

Table 2: Test environment

Profile IDC	FRExt (high(100), high10(110)) , Baseline(66)
Deblocking filter	Off
Format	QCIF(176X144), CIF(352X288)
RD optimization	Enabled
LEVEL IDC	20 ,40
Q-Matrix (Scaling matrix)	Disabled
CAVLC	Enabled (Baseline)
Rate Control Enable	Enabled
CABAC	Enabled (High and High10)
Transform	4x4, adaptive, 8x8
Frames encoded	50
YUV Format	4:2:0
Frame Rate	30 frames per second

Table 3 and 4 summarizes the statistics of CIF High profile Vs. Baseline profile and QCIF High profile Vs. Baseline profile respectively. For High profile, CIF sequences were encoded at bit rates of 0.5 Mbps to 2.5Mbps while QCIF at 30Kbps to 600Kbps. High10 profile was used at bit rates of 0.2 Mbps to 6Mbps for CIF and at 20 Kbps to 600Kbps for QCIF format.

Table 3: Rate PSNR comparison between high and baseline profiles for QCIF sequences

Sequence	*Bit rate (kbps)*	*Y PSNR (dB)*						
		H.264 Base-line	*FRExt High Profiles*					
			High			*High 10*		
			4x4	*8x8*	*Adaptive*	*4x4*	*8x8*	*Adaptive*
QCIF Foreman	28	28.97	29.07	28.72	29.53	30.74	30.72	31.01
	62	32.39	33.71	33.44	33.81	33.86	33.64	34.09
	103	35.64	36.90	36.31	36.85	37.18	36.64	37.27
	129	36.82	37.99	37.41	38.08	38.27	37.84	38.44
	154	37.72	38.83	38.29	38.94	39.22	38.67	39.24
QCIF Coastguard	46	28.09	30.04	30.12	30.23	30.16	30.19	30.33
	90	29.32	32.41	32.43	32.59	32.53	32.40	32.70
	192	32.78	35.31	35.13	35.39	35.46	35.21	35.54
	280	33.62	37.31	37.08	37.33	37.48	37.30	37.59
	390	33.62	38.87	38.60	38.90	38.92	38.78	39.19
QCIF Mother Daughter	48	37.74	38.65	38.35	38.82	39.09	39.03	39.42
	92	37.91	42.97	42.68	42.79	43.80	43.36	43.98
	146	41.76	44.40	43.75	44.28	45.70	45.19	45.78
	195	43.37	45.04	44.47	44.99	46.88	46.45	47.05
	523	44.25	50.67	50.11	50.84	51.98	51.73	52.02

Table 4: Rate-PSNR comparison between high and baseline profiles for CIF Sequences

Sequence	Bit rate (Mbps)	Y PSNR (dB)						
		H.264 Baseline	FREXt High Profiles					
			High			High 10		
			4x4	8x8	Adaptive	4x4	8x8	Adaptive
CIF Foreman	0.5	33.80	38.59	38.13	38.64	35.16	34.87	35.25
	1.0	40.81	41.54	41.12	41.56	41.49	40.99	41.53
	1.5	42.34	42.99	42.49	43.04	43.64	43.17	43.66
	2.0	43.63	44.25	43.76	44.32	45.35	44.93	45.41
	5.0	44.55	50.50	50.04	50.58	46.64	46.29	46.88
CIF Coast-guard	0.5	28.09	31.7	34.2	31.86	35.77	36.29	36.41
	1.0	29.32	34.83	35.03	35.09	41.65	41.51	41.57
	1.5	31.45	36.90	37.03	37.11	43.92	43.93	44.01
	2.0	32.78	38.49	38.62	38.87	45.72	45.87	45.97
	5.0	33.62	46.71	46.33	47.05	52.10	52.08	52.36
CIF Mother Daughter	0.5	37.74	43.42	43.31	43.42	41.56	41.80	48.67
	1.0	37.91	45.92	45.77	45.94	49.81	47.34	47.11
	1.5	41.76	46.82	46.70	46.87	50.06	50.14	50.24
	2.0	43.37	47.99	47.86	47.98	51.73	51.80	51.91
	4.4	44.25	52.61	52.01	52.66	56.10	53.78	52.66

Subjective comparison for Mother Daughter sequence between FREXt adaptive, 8 x8, 4x4 and baseline H.264 is shown in Figure 2.

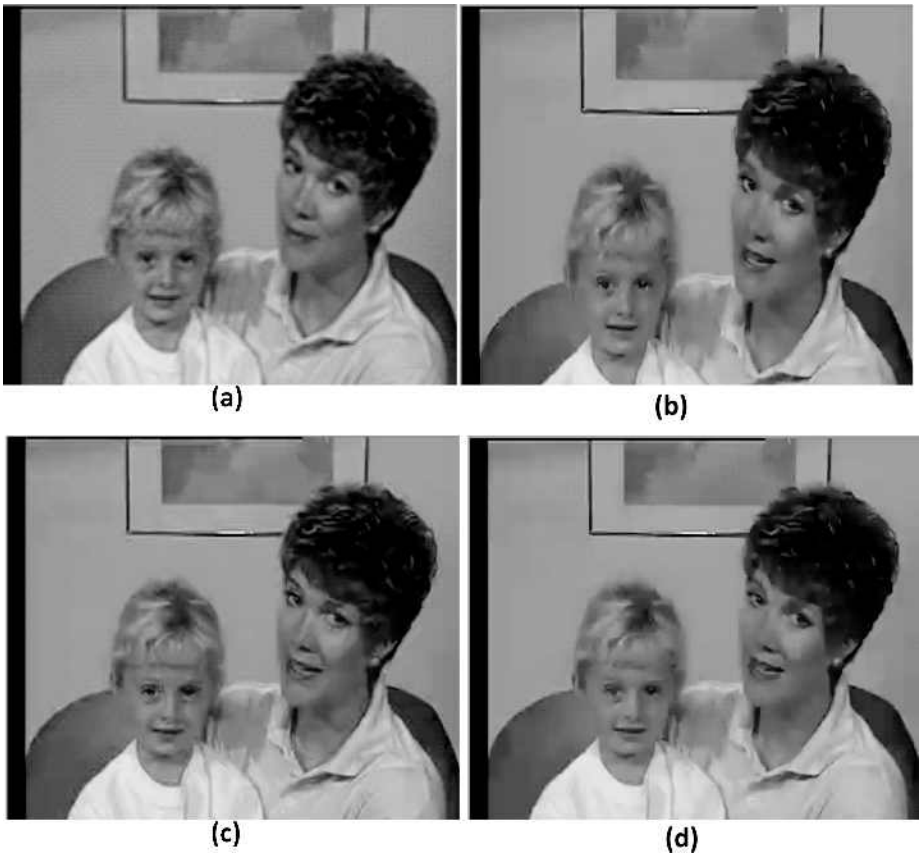

Figure 2: Frame 5 of Mother Daughter Sequence encoded at 200 Kbps
(a) FREXt Adaptive (b) FREXt 4x4 (c) FREXt 8x8 (d) H.264 Baseline

Figure 3 show comparison of PSNR at various bit rates between FRExt High10 profile and baseline H.264 for QCIF Coastguard and CIF foreman respectively.

These graphs clearly show that FRExt profiles have much better PSNR than Baseline profile and also among FRExt profiles, 4x4 and adaptive exceed in PSNR values from 8x8 transform mode.

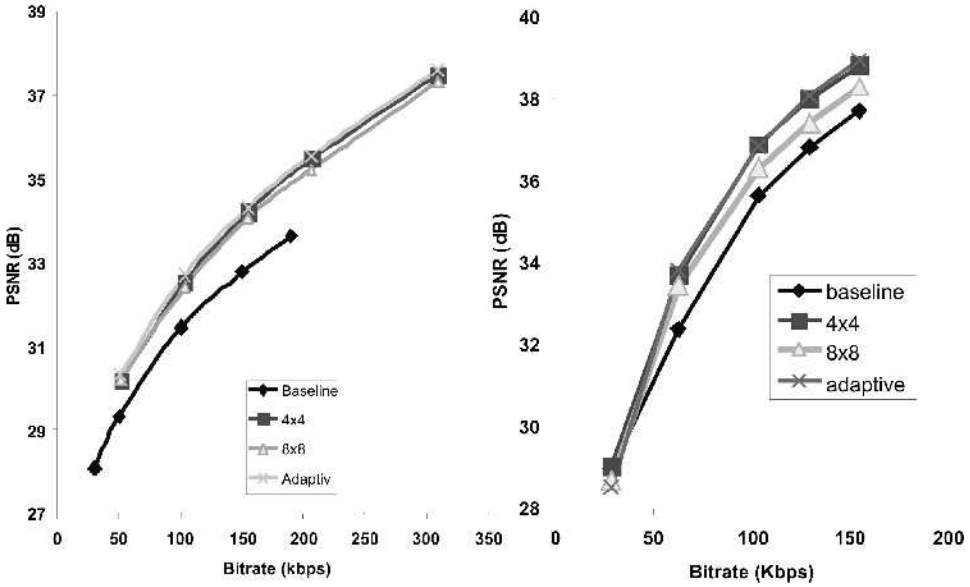

Conclusion

An in-depth performance analysis of H.264/AVC FRExt is performed. The results have shown that the FRExt profile far exceeds in efficiency and robustness than other profiles like baseline. The study also revealed that 4x4 and adaptive transform have higher coding gains than 8x8 transform. Because of these reason FRExt is becoming the preferable choice for video compression experts.

References

[1] T. Weigand, G. J. Sullivan, G. Bjontegaard, and A. Luthra 2003, Overview of H.264/AVC Video Coding Standard, IEEE Transactions on Circuits and Systems for Video Technology, Vol. 13 (7), pp. 560–576.

[2] Gulistan RAJA and Muhammad J. MIRZA, 2004 Performance Comparison of Advanced Video Coding H.264 Standard with Baseline H.263 and H.263+ Standards, International Symposium on Communications and Information Technologies, Sapporo, Japan, pp. 743-746.

[3] D. Marpe, T. Weignad and G. J. Sullivan, 2006 The H.264/AVC Advanced Video Coding and Its Applications, IEEE Communications Magazine, Vol. 44 (8), pp. 134-143.

[4] G. J. Sullivan, P. Topiwala and A. Luthra, 2004 The H.264/AVC Advanced Video Coding: Overview and Introduction to the Fidelity Range Extensions, SPIE Apps. Conf. of Digital Image Processing XXVII, Special Session on Advances in the New Emerging Standard H.264/AVC.

[5] ITU-T Recommendation H.264 & ISO/IEC 14496-10 (MPEG-4) AVC, 2005 Advanced Video Coding for Generic Audiovisual Services.

[6] D. Marpe,.T. Wiegand, and S.Gordon 2005, H.264/MPEG4-AVC Fidelity Range Extensions: Tools, Profiles, Performance, and Application Areas, IEEE International Conference on Image Processing, Vol. 1, pp. I - 593-6.

[7] H.264 Reference Software Mar 2009 http://iphome.hhi.de/suehring/tml/download/FRExt/.

[8] Test Video Sequences Mar 2009 at http://trace.eas.asu.edu/yuv/.

Optimized Embedding of Perceptual Hash for Image Authentication in Digital Cameras

Sami-ud-Din[1]

Abstract

Combination of watermark and cryptographic hash function has been used in prevailing research for the authentication, tamper proofing and copy right protection of digital images. The key elements in such schemes are the robustness of watermark, reliability of authentication mechanism and the quality of the watermarked image. Most of the algorithms proposed compromise on one of above factors. This paper attempts to optimize the balance between these three factors by first quantifying these qualitative factors and then using optimization technique to find an efficient balance between these key factors. The perceptual hash function is utilized to enhance the security and reliability of digital images. This algorithm has been tested on a large database of images and the results are shown.

Keywords: Optimal Wavelets, Image Security, Perceptual Hash, Watermarking, Multiresolution Analysis.

Introduction

The rapid growth and popularity in the field of digital photography and the use of communication networks for distribution of digital media has prompted the imminent need of copyright and ownership authentication [1],[2]. Digital watermarking, steganography and data hiding are promising methods for protection against piracy and malicious manipulations of original media contents [3]. Robust, fragile and semi-fragile authentication schemes are commonly used depending upon the nature of the applications. Small changes in digital contents due to lossy compression and image manipulations which do not survive in fragile watermarking are well tolerated in semi fragile schemes [4].

A typical state of the art digital image authentication system utilizes an embedded hash function [5] which is calculated over the image contents by utilizing a secret key [6]. Many different algorithms have been used for calculation of hash function. However, perceptual hash function [7] provides a promising and much more robust way of authentication of digital images. The perceptual hash function of an image is a short vector with random values and is indexed by using another vector i.e. secret key K and the resultant vector/hash is a function of this secret key. The key benefit of perceptual hash is that the numerical contents of image change due to compression, storage and transmission but its perceptual contents to human observer remains the same. Hence a perceptual hash is more resilient to compression and other attacks on the contents. The perceptual hash calculated by this hash algorithm is embedded in image itself in a transparent manner so that it remains invisible to normal storage, compression, communication and display systems. However, a compatible decoding system is capable of extracting the embedded hash and also generating the same hash if the encoding-decoding pair is known. If the hash calculated by the decoding system is the same as the hash embedded in the image, the authentications of contents of the digital image are verified.

Since the watermarking process distorts the image to some extent. It is important to quantify the distortion based on Human Visual System (HVS) with perceptual quality measures. Many techniques in literature [8] include Mean Squared Error (MSE), Peak Signal to Noise Ratio (PSNR), Root Mean Squared Error (RMSE), Mean Absolute Error (MAE) and Signal to Noise Ratio (SNR). The other techniques based on Human Visual System (HVS) with perceptual quality measure. The algorithm proposed by Z. Wang and A. C. Bovik in their research publication [9] for Universal Image Quality Index (UQI) is used to compute the UQI of the watermarked and the host images. This technique for image quality measurement does not depend on the viewing conditions of the scene and the individual observer. This technique provides useful quality measure for digital images after manipulations of image processing applications e.g. insecure transmission, storage media, compression and change of image format.

Watermarking using Fourier Transform and Wavelet Transform [12] provide a reliable means of embedding data into the host image [10]. Different flavors of Discrete Wavelet Transform (DWT) based watermarking

[1] Electrical Engineering Dept., University of Engineering & Technology, Taxila.

schemes are known [10]. We propose the use of Quantization Index Modulation (QIM) [11] on wavelet coefficients for embedding of perceptual hash in the digital images.

The robustness of watermark implies the ability to correctly extract watermark in the presence of image distortion due to compression, noise, basic image manipulations (intensity and contrast adjustment) and cropping etc. The adjustments of embedding parameters to increase the robustness of the watermark usually result in increase imperceptible distortion and hence decrease in quality index. The embedding process hence encounters a compromise between the reliability of the embedding and the perceptual quality of the image. An unreliable/ non-robust embedding of hash function may generate positive alarms in the forgery and false tamper detection process. Hence an optimized balance between the robustness and the image quality is desirable. This research aims at designing a suitable objective function, appropriate parameters for this optimization process. The advantage of this scheme is that it does not rely upon the fragility of the watermark as proposed by many research methodologies rather it aims at making the watermarking process as robust as possible while the reliability of the authentication mechanism comes from the use of perceptual hash function [7]. Any modification in the image will distort the perceptual hash function and the image will not be authenticated at the point of use.

A pre-stored key in the digital camera is used to generate the perceptual hash from the acquired image. The bits of this hash algorithm are embedded in the same image using watermarking in image. This watermarked image being optimized for both robustness and perceptual quality does not appear degraded to the user and can be used just like a normal digital image. However, if a deciding algorithm is used on this image with same secret key (compatible if private/ public key is used) then the perceptual hash can be recalculated and computed with the embedded perceptual hash function. For an un-tampered image the values of the two hash functions will be same.

This paper is organized in six sections; Section 1 gives an overview of digital image authentication scheme and its allied technologies. In section 2 embedding of watermark is explained. In section 3 we suggested methodology for optimization. In section 4 the methodology for image authentication mechanism is elaborated and finally sections 5 and 6 are dedicated for experimental results and conclusion respectively.

Embedding of Perceptual Hash

The perceptual hash function H(K,I) is embedded into wavelet coefficients of Discrete Wavelet Transform (DWT) of digital image I(x,y). The DWT provides a simple hierarchical framework for interpretation of the image/signal information [14]. The detail of an image in general characterizes different physical structure at different resolutions. The coarse resolution/ approximation correspond to the larger structure in the scene. It is, therefore natural to analyze the image initially at coarse level and then resolution gradually be increased from coarse-to-fine for particular application [14]. The DWT of an image provides the sub-bands of an image as LL, LH, HL and HH. The sub-band selection parameter is , = 0 for LL, = 1 for LH, = 2 for HL and = 3 for HH. The distribution is shown in Fig. 1.

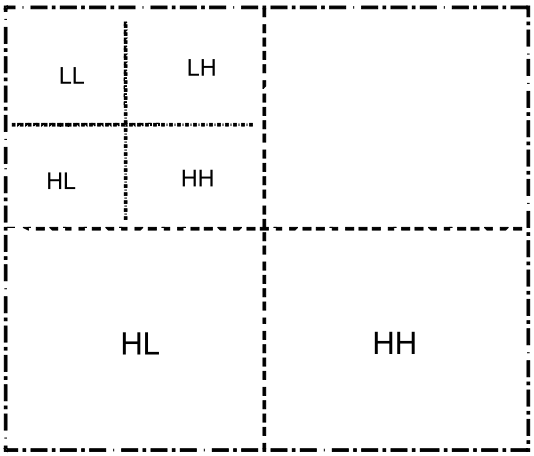

Figure 1: DWT Transform of an image into sub-images

The selection of sub-band is carried out by Genetic Algorithms between β = 1 or 2 for higher payload to embed maximum data as characterized by the distribution of the contents of the digital images, whereas sub-band β = 3 is used to embed optimizing parameters. The perceptual hash is embedded in wavelet coefficients of the selected sub-band using dither Quantization–Index Modulation (QIM) codes [11]. The scalar uniform quantizer $Q(s)$ of the original signal with the step size γ is given by

$$Q(s) = \gamma \left\lfloor \frac{s}{\gamma} \right\rfloor \quad (1)$$

The function $Q(s)$ is used to generate two new dithered quantizers as given below

$$Q_{0(x)} = \gamma \left\lfloor \frac{\left(s - \frac{\gamma}{4} \right)}{\gamma} \right\rfloor - \frac{\gamma}{4} \quad (2)$$

$$Q_{1(x)} = \gamma \left\lfloor \frac{\left(s + \frac{\gamma}{4} \right)}{\gamma} \right\rfloor + \frac{\gamma}{4} \quad (3)$$

Where *s* is the original signal. These dithered quantizers are used to quantize and embed bit *m* of the hash function into the wavelet coefficients $w^{\beta}(x,y)$ as follows

$$w^{\beta}(x,y) = Q_i(w^{\beta}(x,y)) \text{ for } \begin{cases} i=0 \text{ for bit } m=0 \\ i=1 \text{ for bit } m=1 \end{cases} \quad (4)$$

The graphical representation is depicted in Fig. 2 below.

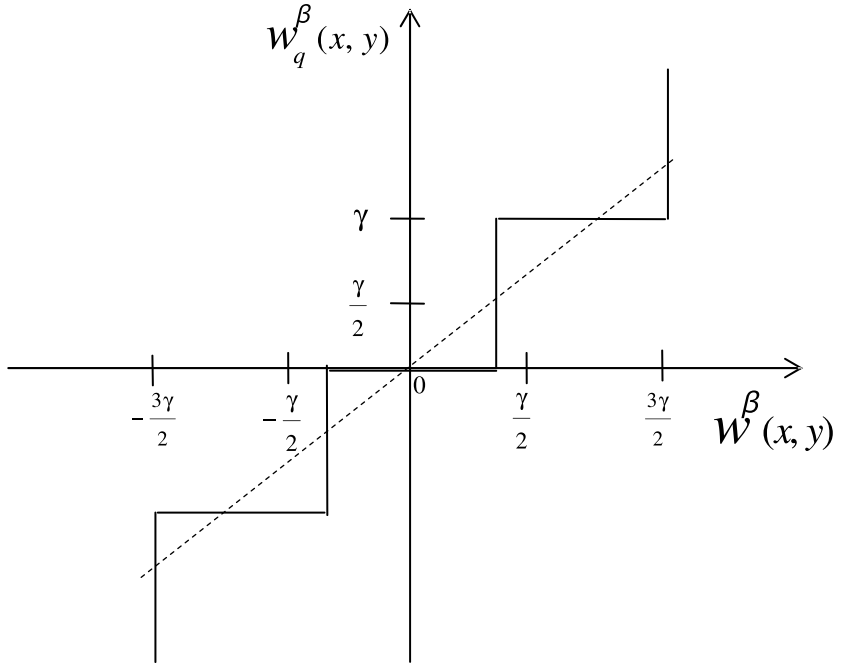

Figure 2: Selection of quantized sample for given sample using original QIM.

This Scalar QIM embedding scheme is modified to reduce the quantization noise in wavelet coefficients of the host image *s*, therefore quantization step γ is to be optimized. An additional parameter α is introduced to upgrade these quantizers to distortion-compensated QIM.

$$w_q^{\beta}(x,y) = Q_i(\alpha w^{\beta}(x,y)) + (1-\alpha)w^{\beta}(x,y) \quad (5)$$

where $\alpha \in (0,1]$ and $\begin{Bmatrix} i=0 & for & bit\ m=0 \\ i=1 & for & bit\ m=1 \end{Bmatrix}$ (6)

The graphical representation of distortion-compensation is shown in Fig. 3.

For $\alpha = 1$ the results are the same as Scalar QIM and for $\alpha = 0$ the results are $w_q^{\beta}(x,y) = w^{\beta}(x,y)$ indicating that nothing is embedded hence no distortion is introduced. The distortion introduced by the quantizer can be compensated by the adjustment of value of $\alpha \in (0,1]$. This distortion compensated technique is selected for achieving the objectives of distortion less embedding and error free retrieval of the embedded/hidden message.

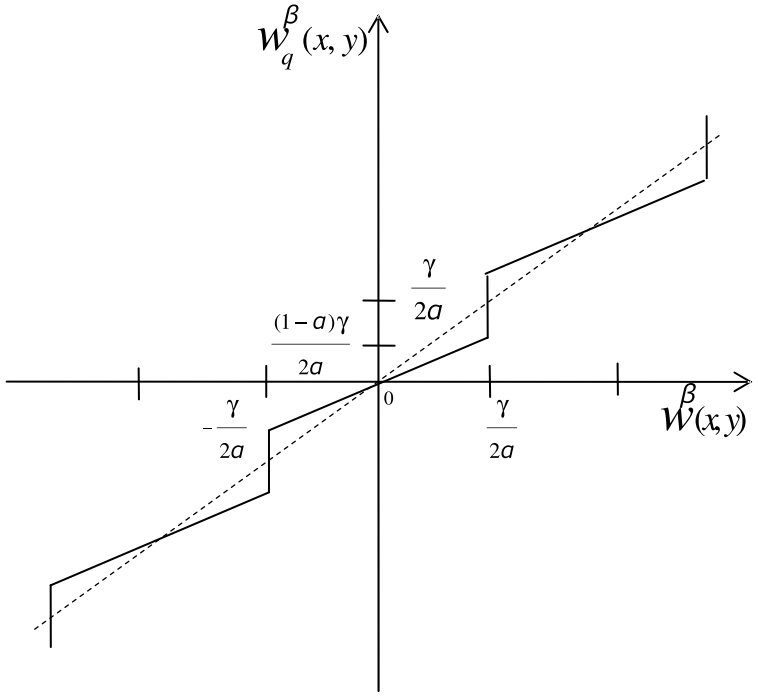

Figure 3: Selection of quantized sample for given sample using distortion compensated QIM.

Optimization of Embedding Parameters

The key factors in the process of embedding of watermark in digital images are Quality of image, robustness of watermark and security/reliability of the authentication process. These all parameters have conflicting properties and are interdependent and hence it is necessary to attain compromise between these factors. The parameters which are optimized in this algorithm are the distortion compensation factor of embedding process α, the choice of wavelet sub-band β and the quantization step γ. All of these factors have been introduced above. The optimization process tunes these parameters according to the objective function ***J*** described later.

- **Tuning process of** α – As the value of α increases the distortion-compensation in the embedding process decreases and hence the quality of image degrades. As mentioned above the extreme case is $\alpha = 1$ where the distortion-compensation Quantizer-Index Modulation becomes Scalar Quantizer-Index Modulation. On the other hand when α is lowered the distortion compensation improves but the embedding capacity decreases and hence the watermark goes from robust to fragile. The extreme case is $\alpha = 0$ where the quantization step becomes a straight line and no embedding can take place. This is degenerate case and hence $\alpha = 0$ is not included in the valid range of α.
- **Choice of** β - The choice of 'β' is translated into the objective function in such a way that a sub-band with higher absolute values of wavelet coefficients is chosen because higher values of wavelet coefficient ensure greater embedding capacity and hence robustness and also the better perceptual quality because of lower percentage of distortion.
- **Selection of** γ **-** A higher value of γ results in larger quantization bands and hence more robust watermark. Unfortunately larger γ result in greater distortion and visual quality becomes poor. On the other hand if we degrade the robustness it eventually improves the quality of the image (UQI).

In view of the above discussion the robustness of the watermark is defined as

$$R(\alpha, \beta, \gamma) = \frac{\gamma}{\alpha N} \sum_{n=0}^{N-1} \left| w^{\beta}(x, y) \right| \qquad (7)$$

Where *N* is total number of wavelet coefficient in the sub-band and $\alpha \in (0, 1]$ for β = 1 or 2

- **Objective Function Evaluation -** The objective function *J*, $J = \max_{\alpha,\beta,\gamma}(w_1 R + w_2 Q_{I,I_w})$

I and I_w are host and watermarked images respectively. Subject to the constrains

$$w_1 + w_2 = 1 ; \quad \alpha \in (0, 1] \quad \beta = 1 \text{ or } 2, \quad \gamma = (0, L) \qquad (8)$$

L is maximum absolute value of the wavelet coefficient. The distortion measure parameters w_1 and w_2 are empirically related with the condition, however $w_1 \neq 0$ and $w_2 \neq 0$. For this experiment we select both the factors of equal importance *i.e.* $w_1 = 0.5$ and $w_2 = 0.5$.

- **Genetic Algorithm-** The optimizing parameters (α, β, γ) for embedding of hash function are searched using Genetic Algorithms (GA). Genetic Algorithms are very efficient and stable for searching optimum solutions [15]. The GA uses the group of chromosomes for representation of the solution. The chromosomes and the problem solution are inter-transformed. The fitness function is evaluated for objective function for the fitness of each chromosome. The particular fittest chromosomes are chosen to be parents. The crossover and mutation are used to generate offspring from the parents. The fitness of offspring is evaluated and replacement of the selected chromosome is performed and the cycle is repeated until desired criterion is achieved.

4 Image Authentication Mechanism

The complete architecture of an image authentication mechanism is depicted in Fig. 4. This mainly consists of two processes entitled as watermark encoding and decoding process. The detail of both these processes is given as follows:

Encoding Process

The inputs of encoding process of the image authentication mechanism are digital image **I(x,y)** and the secret key **K**. The digital image **I(x,y)** is the data extracted by the image sensor such that $\mathbf{I(x, y) \in I}$ where **I** is set of all possible images of same size. The perceptual hash of the image **I(x,y)** is computed through perceptual hash algorithm as function of secret key **H(K,I).** The secret key is unique for each media device and hence the perceptual hash computed for the same image with different devices will be different. Similarly, the perceptual hash is different if image has gone through certain malicious manipulations. The bit stream of perceptual hash function is embedded into image in DWT domain by quantizing the wavelet coefficients of the selected sub-band. The value of β *i.e.* the sub-band is calculated as one of the output parameter of the optimization process. This selection of sub-band is done for embedding of perceptual hash function. The optimization function aims at enhancing the robustness of the embedding process through proper selection of β =1 or 2 as described in section 3. The quantization step size for amplitude quantization of wavelet coefficients is another parameter γ computed by optimizing process utilizing Genetic Algorithms [14]. The Inverse Discrete Wavelet Transform of the watermarked image is computed after embedding of the perceptual hash and the image is watermarked but visually undistorted.

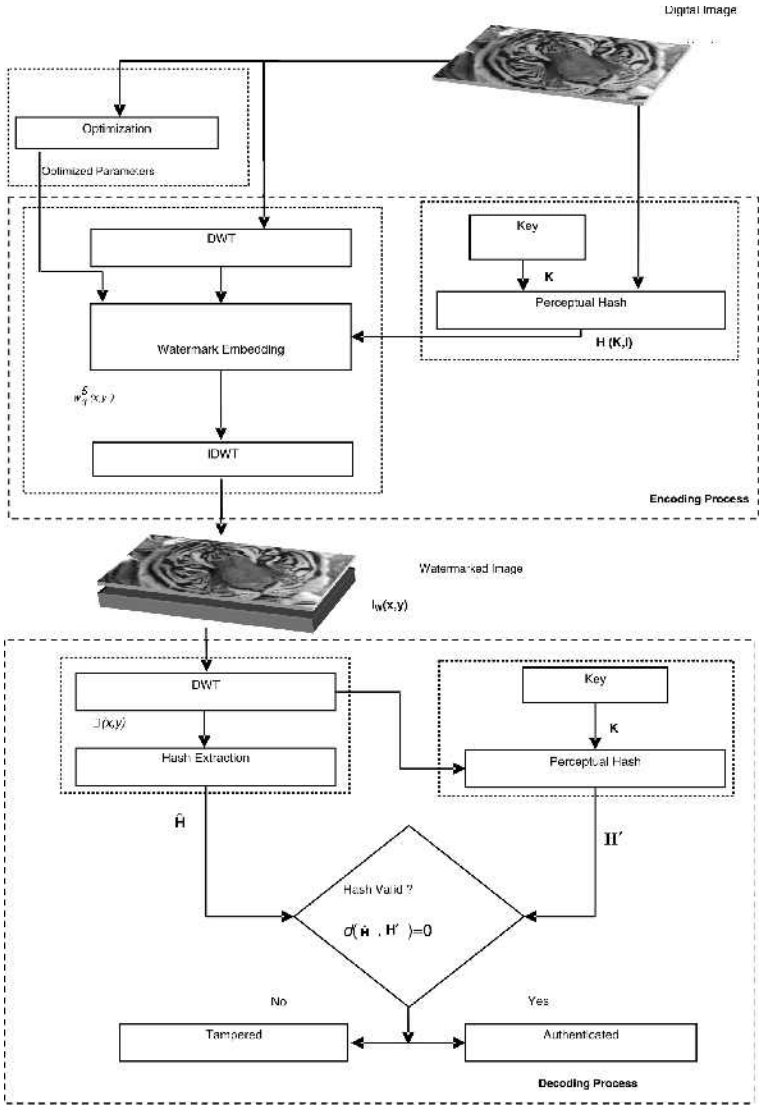

Figure 4: Algorithm for image authentication aided with perceptual hash of the host image.

Decoding Process

The decoding process starts first of all by taking Discrete Wavelet Transform of the watermarked image $\mathbf{I_w(x,y)}$. The perceptual hash $\hat{\mathbf{H}}$ [7] of the watermarked image $\mathbf{I_w(x,y)}$ is computed with the same secret key **K** utilized at the encoding end for computing perceptual hash **H(K,I).** Similarly, perceptual hash $\mathbf{H}'$ of watermarked image $\mathbf{I_w(x,y)}$ is also computed [7]. The perceptual hashes $\hat{\mathbf{H}}$ and $\mathbf{H}'$ computed are compared and the absolute error is tested for a certain threshold ε as given

$$| \mathbf{H}' - \hat{\mathbf{H}} | < \boldsymbol{\varepsilon} \qquad (9)$$

Where ε is the expected error due to different image/signal processing application through which the image is passed. The image authenticity is verified if absolute error is less than ε and otherwise image is declared as tampered.

Experimental Results

The algorithm is tested over a large data base of images and reliable results are observed indicating the effectiveness of proposed watermarking scheme. In this scheme original image is not required whereas secret key and the optimized parameters from Genetic Algorithm are required, which are embedded in sub-band β = 3 i.e. HH. We selected four images for which the computed optimized parameters, α, β, γ are tabulated in table I. High contrast images give large variation in amplitude of wavelet coefficients as compare to low contrast images and hence results in large quantization step size γ . Similarly, sub-band selection depends on the total number of wavelet coefficients in the sub-band. We observe β =1 for image (d) in Fig. 5 as image has high vertical frequencies thus more coefficients in LH sub-band. We selected a set of ten images and pass these images through a variety of attacks from StirMarks software [16] after embedding watermark and then evaluate the algorithm for tamper detection and achieve significantly reliable results. We measure/ observe the robustness and imperceptibility of the watermark by content authentication and UQI of I and Iw respectively. The results of watermark survivability of the selected images at different compression levels by JPEG are shown in Fig. 6. The height of bars show the compressing ratio at which the watermark fails. We computed the quality of watermark image by computing UQI. The resulted UQIs for selected test images after embedding of watermark are shown Fig.7. The results obtained are then compared with other proposed watermarking techniques with and without hash function embedding and the results are found significantly reliable for tamper detection.

(a) (b) (c) (d)

Figure 5. Different type of images for the verification of optimization factors:
(a) High contrast image, (b) Low contrast image, (c) Image with vertical details and (d) image with vertical frequencies.

Table 1: Optimized Parameters

Image	α	β	γ
Image (a)	0.60	2	15
Image (b)	0.53	2	11
Image (c)	0.31	2	05
Image (d)	0.59	1	14

We used Genetic Algorithm toolbox in MATLAB 7.1 environment with population size of 20 for 100,000 maximum generations with 100 stall generations (number of generations in which fitness value is unchanged) and two point crossover with mutation rate 0.01 for the design of desired parameters.

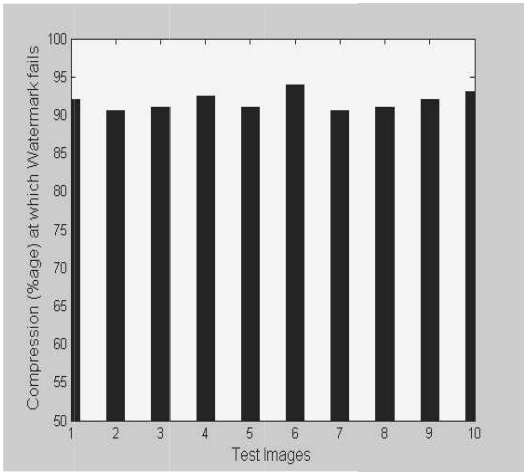

Figure 6: Watermark survivability for ten different images at different compression levels by JPEG compression

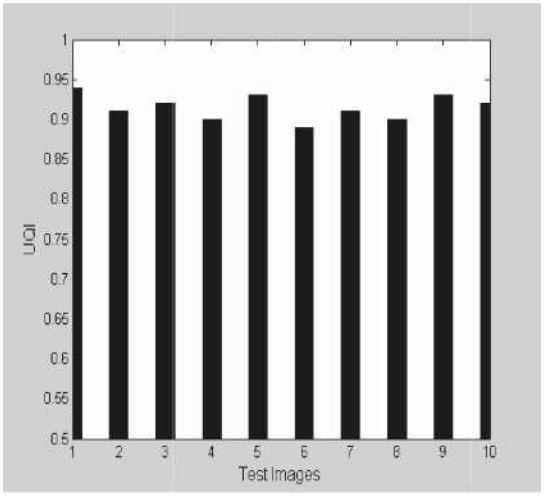

Figure 7: The Universal Quality Index of ten different watermarked images

Conclusion

In this paper, we propose the optimized image authentication perceptual hash function indexed with secret key of digital camera as watermark. The experimental results show that proposed methodology improves the quality of the watermarked image while giving extremely good robustness and security. The proposed authentication mechanism is resilient to compression transformations and common geometric operations because of embedding of perceptual hash rather than numerical hash. The key benefit of perceptual hash is exploited as the numerical contents of image change due to compression, storage and transmission but its perceptual contents to human observer remain the same. Hence a perceptual hash is more resilient to compression and other attacks on the contents. Furthermore algorithms for perceptual hash computation are highly secure and reliable as compare to randomly chosen regions which provides unpredictable results for different intermediate hashes.

References

[1] G. L. Friedman, 1993 “The trustworthy digital camera: Restoring credibility to the photographic images,” IEEE Trans. Consumer Electronics, vol. 39, no.4, pp 905-910, Nov.

[2] L. Xie and G. R. Arce, July 1999 “A class of authentication digital watermarks for secure multimedia communication,” IEEE Trans. Image Processing, vol. 10, no. 11, pp. 1754-1764, Nov 2001.

[3] F. Hartung and M. Kutter, “Multimedia watermarking techniques,” Proc. IEEE, vol. 87, no. 7, pp. 1079-1107.

[4] E. Martinian, G. W. Wornell and B. Chen, July 2005 “Authentication with Distortion criteria,” IEEE Trans. on Information. Theory, vol. 51, no. 7, pp.2523-2542.

[5] J. Cannons and P. Moulin, Oct. 2004 “Design and Statistical Aalysis of a Hash-Aidd Image Watermarkin System,” IEEE Trans. on Image Processing, vol. 13, no. 10, pp. 1393-1408.

[6] M. S. Hawang, C. Chang and K. Hwang, May 1999 “A Watermarking Technique Based on One-Way Hash Functions,” IEEE Trans. on Consumer Electronics, vol. 45, no. 2, pp. 286-294.

[7] V. Monga and B. L. Evans, Nov. 2006. “Perceptual Image Hashing Via Feature Points: Performance Evaluation and Tradeoffs,” IEEE Trans. on Image Processing, vol. 15, no. 11, pp3453-3466, T. N. Pappas and R. J. Safranek, “Perceptual criteria for image quality evaluation,” in Handbook of Image and Video Processing, A. C. Bovik, Ed. New York: Academic, May 2000.

[8] Z. Wang and A. C. Bovik, March 2002 “A Universal Image Quality Index,” IEEE Signal Processing Letters, vol. 9, no. 3, pp. 81-84.

[9] M. D. Swanson, M. Kobayashi, and A. H. Tewfik,“ Multimedia data-embedding and watermarking technologies,” Proc. IEEE, vol. 86, pp. 1064-1087.

[10] B. Chen and G. W. Wornell, June 1998Quantization index modulation: A class of provably good methods for digital watermarking and information embedding,” IEEE Trans. Information Theory, vol. 47, no. 4, pp.1423-1443, May 2001.

[11] W. Zhu, Z. Xiong, and Y. Q. Zhang, 1998 “Multiresolution Watermarking for images and video: a unified approach,” in Proc. Int. Conf. on Image Processing (ICIP), Chicago, IL.

[12] S. G. Mallat, July 1989 “A Theory for Multiresulation Signal Decomposition: The Wavelet Representation,” IEEE Trans Pattern Analysis and Machine Intelligence, vol. 11, no.7, pp. 674-693.

[13] P. Kumsawat, K. Attakitmongcol and A. Srikew, “A New Approach for Optimization in image Watermarking by Using Genetic Algorithms,” IEEE Trams. on Signal Processing, vol. 53, no. 12, pp. 4707-4719,.

[14] J. H. Holland, 1975 Adaptation in Natural and Artificial Systems. Ann Arbor, MI: University of Michigan Press.

[15] Fair Evalution Proceddures for Watermarking System, 2000[online]. Available http://www.petitocolas.net/fabien/watermarking/strimark.html.

Towards Energy Efficient High Performance Computing Perceptions, Hurdles & Solutions

Muhammad Zakarya[1], Izaz Ur Rahman[2]

Abstract

Global Warming (GW[1]) and Energy Crisis (EC[2]) have forced the researchers at teaching institutes, organization, research laboratories and other academia to study and minimize the power requirements of digital and electronic devices especially the huge amount of computers in the global village. With the rise of new computing era i.e. Green computing there is a need to reduce the power consumption in High Performance Computing (HPC[3]) like Clusters, Grids (GC[5]) and Clouds (CC[6]). This research work will study HPC and green computing (GC[4]) and will result in an integrative solution to reduce the energy consumed by processors in HPC. In recent times it is realized that there is a need for energy reduction in processors. And a lot of work has been done on minimizing the energy expenditures and use. When we reduce the energy consumption then the response time is increased. And it will degrade the performance of processor and the underlying real time systems. The same scenario is also applicable in HPC. The processors taking part in a cluster, grid or cloud environment are to be energy efficient without losing its peak performance. In our work we will try to study and propose some solutions that reduce the power consumption of a HPC, keeping its performance and response time to the best level [1].

Keywords: Global Warming, Energy Crisis, High Performance Computing, Green Computing, Grid Computing,Cloud Computing, Static Power Management, Dynamic Power Management.

Introduction & Concepts

The reliability of distributed systems is superior to monolithic single processor machines, which makes distributed systems a most widely usable technology. In such systems single failure of one network node does not prevent the whole process from completion as it happens in single CPU resource. Distributed computing prototype knot jointly the power of huge number of resources dispersed across a network. Millions of processors linked across the Internet are frequently unused and can become a part of cooperative computing. A distributed system has the capability to answer the problem alternatively. The chief endeavor of Cluster Computing is to propose a competent hardware media, networks, and software to develop and improve the performance and accessibility of computing platform that uses a collection of commodity computer resources integrated through some a single computer resource. The concept of Grid Computing is based on using the high speed connection network i.e. Internet as a medium for the wide spread availability of powerful computing resources as low-cost commodity components [8]. Cloud Computing describes a new supplement, consumption, and delivery model for IT services based on the Internet, and it typically involves over-the-Internet provision of dynamically scalable and often virtualized resources [2]. One of the major issues in computer system is reducing the energy consumption. The energy consumption should be reduced due to the operational cost. For example about 25% of the operational cost is spent on air conditions, backup cooling and power release systems. The entire power dissipation for desktop system is 160MW in 1992, and in 2001 it is increased to 9000MW [13].

When the power consumption of the system is increased, then it would produce a lot of heat and according to the data from two popular vendors the rate of failure would be doubled, when there as an increase of 10^0C [14] and the cost of the system would also be increased, because we need a complex cooling system to deal with it according to the data from Intel Corporation when the power dissipation is more than 35-40W, then it would need more than 1W per CPU chip [15]. For battery powered, advanced Personal Digital Assistants (PDAs), cell phones, laptops and pocket PC's, when the system is exactly more than 500MIPS then the power consumption should be best if it is kept at or below 500MW [16].

One solution to this problem would be to increase the battery capacity but it would not work because the battery capacity is increasing only 5-10% annually while the power required by the system is increasing day

[1] Computer Science Dept., Abdul Wali Khan University (AWKU), Mardan (KPK),
[2] Computing and Mathematics Dept.,Brunel International University, London, UK

by day. Much slower than what is needed to support ever increasing processor power [17]. Therefore the solution of the problem would be to decrease the energy consumption by using some energy efficient techniques. Techniques that are used for the reduction in energy consumption are the same as that are used to increase the battery capacity.

The energy expenditure & utilization can be diminished either by hardware or through the software perception. Through the hardware viewpoint, numerous power states are incorporated into the micro-architect, circuit land, and device level. Many engineering standards are made, such as ACPI[3] and the APM[4] specification, from the software point of view, the power shutdown procedures can be used that makes the system sleep or stop the carrying out of task when the system is idle. But still this software and wakeup operation has a high overhead, so it cannot be used in many situations. When the system goes to sleep mode then the response time of the system would be slower. When the system does not have continuous idle time, then this technique cannot be used. Then some other sophisticated approaches are used such as DVS[5].

The internet and open nature of the CC makes it vulnerable to security issues. Table 1 summarizes some common features of three major HPC systems. One of the most important dissimilarity between CC and cluster computing is that clouds frequently take the shape of web-based applications that can be accessed using internet browser [3].

The rest of the paper is structured as follows. Section I introduced HPC i.e. Cluster Computing, GC and CC. We conclude in section VIII, with some future directions and work in subsequent section IX.

Table 1: Cluster, Grid and Cloud Systems [2]

Feature	Cluster	Grid	Cloud
Size	Small	Large	Small to large
Network	LAN	WAN	WAN
System cost	Very High	High	Very Low
Network Type	Private	Private	Public
Resource Support	Homogeneous	Heterogeneous	Heterogeneous
Security	Medium	High	Low
Initial Infrastructure Cost	Very high	High	Low
Administrative Domain	Single	Multi	Both
QoS	Excellent	Good	Moderate
Availability	Very High	High	High
Reliability	High	Moderate	Low
Fault Tolerance	High	Good	Good

Related Work

In [3] the authors divide power management into two diverse mechanisms: (a) SPM[1] technique with the intention of utilization low-power apparatus to save power and (b) DPM[2] technique which utilize software and power-scalable apparatus to save power.

Energy efficiency can assist to improve HPC reliability by diminishing heat quantity in the system. We know that computing at higher temperature is more erroneous and result in less reliability. According to Arrhenius equation (Eq. 1) components failure ratio doubles with every 18° F increase in temperature [5].

$$k = A * e^{-\frac{E_a}{R \cdot T}} \qquad (1)$$

Where k is the rate constant, ***A*** is the pre-exponential factor, ***Ea*** is the activation energy, ***R*** is the gas constant, and ***T*** is the absolute temperature. The quantity of energy (E) consumed in HPC system over a time period (T) is equivalent to the product of the time period T and the average system power (P) consumed over the time interval T. The relation between power and energy is shown in equation (Eq. 2).

$$E = P * T. \quad (2)$$

It is clear from Eq. 2, if we reduce power P or time interval T, then overall energy consumed is also diminished. The prospective hazard of existing SPM mechanisms is that humanizing energy efficiency via low-power components is expensive.

On the other hand DPM mechanisms have revealed swear for civilizing energy efficiency; yet, scheming power-aware schedulers is not slight. Energy savings diverge considerably with applications, workload, and scheduling tactic *[6]*.

In *[7]* the authors proposed an approach that implements DVFS[3] to safeguard processor power expenditure during communication, and uses load balancing mechanism to on-line and off-line memory reducing power consumption.

HPC are multiprocessor that can be defined as a computer system having more than one processor, each one sharing system main memory & some peripherals, to concurrently process and execute programs. A lot of work on energy efficiency is related to the tasks scheduling algorithms. The concept behind the scheduling mechanism is to assign tasks and processes to processors based on their execution speed and other properties. It enables some processor in idle mode and hence results in energy saving. The scheduling algorithms optimal on uniprocessor machines are not subject to be optimal on multiprocessor machines. So for multiprocessors are concerned, we use different scheduling algorithms like DM[4], RM[5], and EDF[6]. In *[9]* the authors reduced the response time using concept of aperiodic server.

The periodic server or total bandwidth server services aperiodic requests as soon as possible. The aperiodic server is consisting of a period and fixed execution time called server capacity and is scheduled with the same algorithm that is used for the periodic tasks. There are two types of scheduling techniques for multiprocessors i.e. HPC. In partitioned scheduling, each task is assigned to a specific processor and then it is executed on that processor without migration. These processors are then scheduled independently and separately.

This reduces the multiprocessor scheduling into a set of uniprocessor scheduling. With this scheduling we can use an optimal uniprocessor scheduling algorithm for multiprocessor systems. The alternative is the global scheduling, in which all the tasks are stored in a single priority queue. The scheduler selects the task having the high priority for execution. In global scheduling the tasks are not fasten to a particular processor and it can be executed on any processor.

In *[10]* the authors proposed DVS. They claim that for energy reduction we can use the DVS in latest processors. It means that power is a linear function of frequency i.e. f and a quadratic function of the voltage i.e. V given by

$$p \propto fV^2 \quad (3)$$

The voltage adjustment at an instant of time is called DVS, which is an effective way for power saving in current HPC systems. In recent processors the relationship between frequency f and power p gives foundation to Dynamic Voltage Scaling explained in equation 4.

$$EPt \quad (4)$$

Where E is energy consumed, t is time taken and P is power consumed. We can achieve the low performance by simply reducing the operating frequency of the processor when the peak speed is not required. As a result DVS scales the operating voltage of the processor along with the frequency. DVS is a standard for managing the power consumption of a system. It is based on the fact that the dynamic (switching) power P of CMOS circuits is strongly dependent on the core voltage V and the clock frequency f. It is shown that the execution time is inversely proportional to the frequency and thus, the total energy E for the computation is then proportional to the square of the voltage.

$$E = v^2 \quad (5)$$

The average power dissipation in processor is:

$$P_{avg} = P_{capt} + P_l + P_{stdby} + P_{sc} \quad (6)$$

Where P_{capt}, P_l, P_{stdby}, and P_{sc} is capacitance, leakage, standby and short circuit power. The P_l, P_{stdby} and P_{sc} are important but they are least important as compared to P_{capt}. So we will not consider P_l, P_{stdby}, and P_{sc}. So the P_{capt} is equal to:

$$P_{capt} = \alpha C V_d^2 f \quad (7)$$

Where α is the transition activity dependant parameter, C, V_d and f is switched capacitance, supply voltage, and clock frequency. Equation (3) shows that the supply voltage V_d is quadratic as compared to clock frequency f; furthermore it also shows that lowering the supply voltage would be the most efficient way to reduce the power consumption. But when V_d is reduced then the circuit delay t_d would be increased:

$$t_d = \frac{m V_d}{(V_d - V_{tv})^2} \quad (8)$$

Where t_{delay} threshold voltage and m is is a constant which will depend on gate size and capacitance. As from equation (8) the f and t_d are inversely proportional, so it would mean that the energy expenditure would be reduced in CMOS devices at the expense of performance delay.

The frequency f is:

$$f = \frac{(V_d - V_{tv})^2}{k V_d} \quad (9)$$

Equation (9) shows that the clock frequency is directly proportional to supply voltage. If we would consider $P = P_{capt}$, then equation (7) can be written as:

$$P = \alpha C V^2 f \quad (10)$$

Equation (10) shows that when the clock speed f and voltage is changed then it would affect power consumption linearly and quadratically, respectively.

Problem Statement

HPC is a great source for today's communication. HPC has altered the face of computing and presented rapid and clear-cut solutions for a diversity of complex issues & problems for diverse disciplines and fields. With the rise of new computing era distributed systems like Cluster, Grid, Cloud systems, there is a need to implement cloud computing over the sheer amount of data in bioinformatics. Researchers are trying to implement HPC over huge amount of data, making the data easily accessible, thus increasing the HA. But still its implementation gives birth to other problems like heat and cooling cost. We need some mechanisms to reduce the amount of heat that is produced during operation i.e. OPEx and cooling cost. The area is still in infancy and needs researcher's attention.

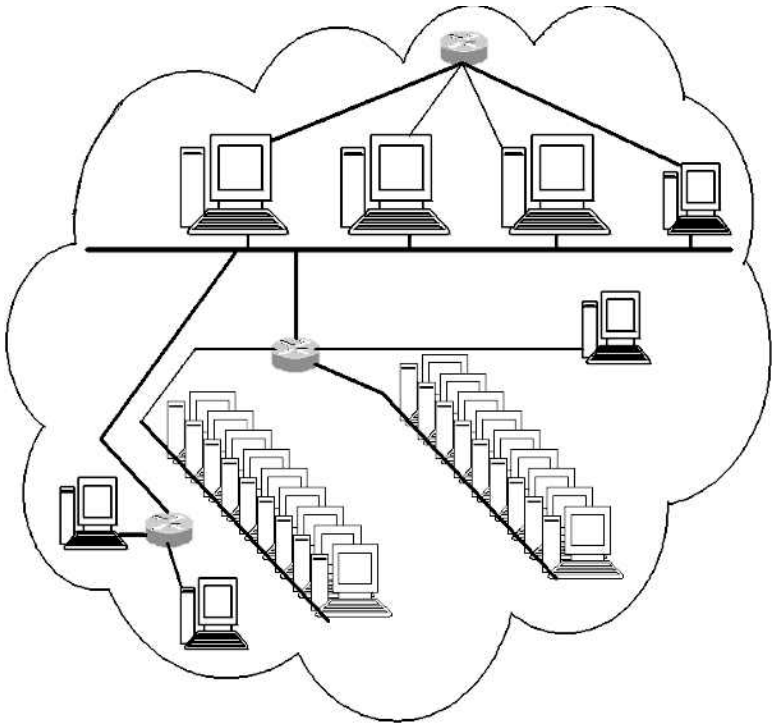

Figure 1: High Performance Computing

In *[30]* the authors have sketched an overview of existing mechanism for energy and power reduction in cloud data centers. According to them techniques like Power-aware scheduling of virtual machines in DVFS-enabled clusters, Energy-efficient management of data centre resources for cloud computing: a vision, architectural elements, and open challenges *[31]*, Machine learning, Green scheduling algorithm for energy savings in Cloud computing, Green Cloud: a new architecture for green data center *[32]*, Performance and energy-aware cluster level scheduling of compute-intensive jobs with unknown service times, Allocation and migration policies considering workload types and behaviors, Dynamic selection of physical nodes in heterogeneous environments, Prediction mechanisms for a smart workload distribution, Improved resource monitoring and Live migration's overhead reduction mechanisms are subject to energy reduction but have not mainly focused on performance and QoS. Some approaches have arisen frustrating to diminish energy spending at cloud computing data centers. On the other hand, cloud providers are in want of mechanisms and techniques not only for sinking energy eating to support the offered prices and demand but also for accomplishing with the required QoS to guarantee the customer happiness. From their analysis it is probable to wind up that there still stay alive some gaps that must be sheltered to attain the energy-performance stability that is essential in cloud computing environments and other HPC.

Discussion

Climate change and environmental damage due to emission of CO_2, cost savings, rising energy costs, reliability of power, power crisis, and heat produced by HPC and datacenter are major issues that have forced researchers at academia and research laboratories to study and propose power diminishing mechanisms *[22]*. In *[22]* the author has proposed some mechanism to reduce the power requirements. Energy efficient processors, multi-core processors, virtualization, storage area network (SAN) and some proper planning like performance, capacity, reliability considerations, cooling considerations, maximization of available resources and designing planning are the major solutions that are proposed to make the systems energy efficient. Code and data migration has been one of the most challenging criteria in the filed of distributed systems.

In *[18]* the authors have discussed advantages of migration including load sharing, load balancing, communication performance, availability, fault tolerance, and utilizing special capabilities. In a distributed system network i.e. HPC, Cluster, Grid, Cloud, the procedures usually communicate with each other by means of remote procedure calls (RPC). As a result, the consumed energy by message passing can be outstandingly condensed with the help of code and data migration that is to say putting more communicating codes in close proximity to each other. In *[18]* the authors implemented data migration technique to wireless ad-hoc sensor networks.

We observed that the same mechanism can also be implemented in HPC like Cluster, Grid or Cloud systems. In this way the energy consumed in the network channels i.e. media can be diminished to some limit.

The total energy consumed is given by Eq 11 where ds is the distance among two HPC systems.

$$EC = \frac{1}{2}\sum_{u\in G}\sum_{v\in G} w_G(u,v).d_S(F(u),F(v)) \qquad (11)$$

The above equation can be written as Eq 12 where d represents the Euclidian distance among two points i.e. HPC systems. In order to reduce the value presented by Eq 11 derivative method is used.

$$EC = \frac{1}{2}\sum_{u\in G}\sum_{v\in G} w_G(u,v).d(F'(u),F'(v)) \qquad (12)$$

Using Euclid Formula for the distance of two points in the field we conclude:

$$EC = \frac{1}{2}\sum_{u\in G}\sum_{v\in G} w_G(u,v).\sqrt{(x_u - x_v)^2 + (y_u - y_v)^2} \qquad (13)$$

Where xu, yu, xv, yv, represents different dimensions of the points u, v respectively. The partial derivatives according to x, y are used to find the most favorable point of the function. Here the computation process for xu is presented.

$$\frac{\partial EC}{\partial x_u} = \frac{1}{2}\sum_{v\in G}\frac{w_G(u,v).(x_u - x_v)}{\sqrt{(x_u - x_v)^2 + (y_u - y_v)^2}} = 0 \qquad (14)$$

The coefficient a, is defined as follows:

$$a_{u,v} = \frac{w_G(u,v)}{\sqrt{(x_u - x_v)^2 + (y_u - y_v)^2}} \qquad (15)$$

Simplifying equation (14) with respect to definition of Eq (15), it could be deduced that the optimal energy consumption, EC, formulated in (12), can be reached by positioning the procedures at the solution points of the following system of equation:

$$x_u = \left(\sum_{v\in G} a_{u,v}.x_v\right) \Big/ \sum_{v\in G} a_{u,v} \qquad (16)$$

$$y_u = \left(\sum_{v\in G} a_{u,v}.y_v\right) \Big/ \sum_{v\in G} a_{u,v} \qquad (17)$$

It is worth noting that in this system of equations, for each unknown value x_u or y_u an equation exists. There exist diverse numerical methods for solving system of equations like (16) and (17). Jacobi and Gauss-Seidel are two well-known iterative techniques *[19, 20]* that are used to solve identical systems. Due to

above discussions, a simple algorithm can be wished-for to discover a placement for procedures that minimizes EC. In a distributed approach, the time is divided into equivalent sized divisions, called epochs. Then, at the start of each time division each node computes its destination coordinates with respect to formula (16), and (17) *[21]*. In other words, in each step, the procedure computes the weighted average of its incoming and outgoing remote procedure calls in the field, and starts moving toward there.

Conclusion

HPC is currently an area of great academic and industrial interest; the concept of being able to dynamically scale the amount of computational resources available to an organization on demand offers great benefits to individual companies and economic opportunities for high performance services providers. However, in order to reduce costs to all parties, it is necessary to reduce the power consumption overhead of a HPC *[11, 12]*. We can minimize the energy consumption at OSI layer with different mechanisms. For example at Hardware layer we can use power efficient circuits, smarter antennas and better batteries. At Link or Physical layer we must try to reduce the number of collisions and resends requests. At Network layer we must implement some energy conserving topology and / or energy conserving message transfer. Similarly at higher layers we have to modify transport and application layers according to our criterion.

Future Work

In HPC the main issue is heating and energy conservation. Our goal is to minimize the energy consumption so that the cooling cost will be reduced. Scheduling periodic and aperiodic tasks such that the load is balanced among different processors and the energy consumption is reduced, is a major concern and an active research topic. Runtime power reduction mechanisms can also reduce the energy expenditure to some extent. Some approaches have arisen frustrating to diminish energy spending at HPC but still HPC providers are in want of mechanisms and techniques not only for sinking energy eating but also for accomplishing with the required QoS to guarantee the customer happiness. There still stay alive some gaps that must be sheltered to attain the energy performance stability that is essential in HPC.

Acknowledgment

This work is fully supported by Abdul Wali Khan University, Mardan, Khyber Pakhtun Khwa (KPK), Pakistan. The author(s) of this article are greatly thankful to SAIMS i.e. Society for Advancement & Integration of Multiple Sciences for full guidance and major support. iFuture is also given a number of credits for arranging seminars on the subject matter. iFuture is a Research Group in the Department of Computer Science, Abdul Wali Khan University, Mardan.

Nomenclature

SPM Static Power Management
DPM Dynamic Power Management
ACPI Advanced Configuration & Power Interface
APM Advanced Power Management
DVS Dynamic Voltage Scaling
DVFS Dynamic Voltage & Frequency Scaling
DM Deadline Monotonic
RM Rate Monotonic
EDF Earliest Deadline First

References

[1] Muhammad Zakarya, Izaz Ur Rahman, Mukhtaj Khan, 2011 Cloud QoS, High Availability & Service Security Issues with Solutions, BUJICT.

[2] Hameed Hussain, Nasro Min-Allah, Samee Ullah Khan, A Survey on Resource Allocation in High Performance Distributed Computing Systems.

[3] Walter Lassonde, Samee Ullah Khan, Nasro Min-Allah, An Overview of Achieving Energy Efficiency in Cluster Computing Systems, NDSU.

[4] Dzmitry Kliazovich, Pascal Bouvry, Yury Audzevich, Samee Ullah Khan, GreenCloud. 2010 A Packet-level Simulator of Energy-aware Cloud Computing Data Centers, IEEE Globecom proceedings.

[5] K. W. Cameron, R. Ge, and X. Feng., High-performance, Power-aware Distributed Computing for Scientific Applications.

[6] R. Ge, X. Feng, and K. W. Cameron. 05, November 2005 "Performance Constrained Distributed DVS Scheduling for Scientific Applications on Power-Aware Clusters." In Supercomputing Conference .

[7] M. Y. Lim, V. W. Freeh, and D. K. Lowenthal. 2006 "Adaptive, Transparent Frequency and Voltage Scaling of Communication Phases in MPI Programs." In ACM/IEEE Supercomputing (SC06).

[8] Muhammad Zakarya, Ayaz Ali Khan, Hameed Hussain, 2010 “Grid High Availability & Service Security Issues with Solutions”, ICIIT, 978-1-4244-813 8-5/10 / $ 26.00 C 2010 IEEE.

[9] M. Spuri and G. Buttazzo, 1996 Scheduling Aperiodic Tasks in Dynamic Priority Systems, Journal of Real-Time Systems, 10(2):179-210.

[10] T. D. Burd., T.A. Pering, A. J. Stratakos, and R. W. Rodersen, 2000 Adynamic Voltage Scaled Microprocessor system. IEEE Journal of Solid State Circuits, Vol. 35, No. 11,pp. 1571-1580.

[11] D. Shin and J. Kim, 2006 Dynamic voltage scaling of mixed task sets in priority-driven systems. IEEE Transaction on CAD of Integrated Circuits and Systems 25(3): 438-453.

[12] Nasro Min-Allah, Asad-Raza Kazmi, Ishtiaq Al, Xing Jian-Sheng, Wang Yong-Ji, Minimizing Response Time Implication in DVS Scheduling for Low Power Embedded Systems.

[13] M. Spuri and G. Buttazzo, “Scheduling Aperiodic Tasks in Dynamic Priority Systems,” The Journal of Real-Time Systems.

[14] Wu chun Feng, Michael S. Warren, and Eric Weigle. 2002 The bladed beowulf: A coste _ective alternative to traditional beowulf. In IEEE International Conference on Cluster Computing (CLUSTER 2002), 23-26, Chicago, IL, USA.

[15] Vivek Tiwari, Deo Singh, Suresh Rajgopal, Gaurav Mehta, Rakesh Patel, and Franklin Baez. 1998.Reducing power in high-performance microprocessors. In DAC '98: Proceedings of the 35th annual conference on Design automation, pages 732-737, New York, NY, USA, ACM Press.

[16] K. Nowka, G. Carpenter, and B. Brock. September/November 2003 The design and application of the powerpc 405LP energy-e_cient system on chip. IBM Journal of Research and Development, 47(5/6).

[17] Kanishka Lahiri, Sujit Dey, Debashis Panigrahi, and Anand Raghunathan. Battery-driven system design: A new frontier in low power design. In ASPDAC.

[18] E. Jul, H. Levy, N. Hutchinson, A. Black, 1988 'Fine-Grained Mobility in the Emerald System", ACM Trans. Comput. Syst. 6(1): 109-133.

[19] John H. Mathews 1987. Numerical Methods for Computer Science, Engineering, and Mathematics, Prentice-Hall International, Inc.

[20] Dahlquist, Germund, and AkeBjork 1974. Numerical Methods, Prentice-Hall, Inc., Englewood Clifs, N. J.

[21] Aitkinson, Kendall 1978. An Introduction to Numerical Analysis, John Wiley & Sons, Inc., New York.

[22] Phillip Carinhas, PhD, Green Computing Guide, http://fortuitous.com

[23] Samee Ullah Khan, Sherali Zeadally, Pascal Bouvry, Naveen Chilamkurti, 09 June 2011 Green Networks, Springer

[24] Samee Ullah Khan, Pascal Bouvry, Thomas Engel, 12 October 2010 Energy-efficient high-performance parallel and distributed computing, Springer

[25] Giorgio Luigi Valentini, Walter Lassonde, Samee Ullah Khan, Nasro Min-Allah, Sajjad A. Madani, Juan Li, Limin Zhang, Lizhe Wang, Nasir Ghani, Joanna Kolodziej, Hongxiang Li, Albert Y. Zomaya, Cheng-Zhong Xu, Pavan Balaji, Abhinav Vishnu, Fredric Pinel, Johnatan E.Pecero, Dzmitry Kliazovich, Pascal Bouvry, 10 September 2011An overview of energy efficiency techniques in cluster computing systems, Springer

[26] Sherali Zeadally, Samee Ullah Khan, 31 May 2011 Energy-efficient networking: past, present, and future, Springer

[27] Dzmitry Kliazovich, Pascal Bouvry, Yury Audzevich, Samee Ullah Khan, GreenCloud, 2010. A Packet-level Simulator of Energy-aware Cloud Computing Data Centers, IEEE Globecom Proceedings

[28] Samee Ullah Khan, Nasro Min-Allah, 19 April 2011 A goal programming based energy efficient resource allocation in data centers, J Supercomput Springer

[29] NasroMin-Allah, Hameed Hussain, Samee Ullah Khan, Albert Y. Zomaya, 2011 Power efficient rate monotonic scheduling for multi-core systems, J. Parallel Distrib. Comput. ELSEVIER

[30] Ismael Solis Moreno, Jie Xu, Energy-Efficiency in Cloud Computing Environments: Towards Energy Savings without Performance Degradation, University of Leeds, UK

[31] Buyya, R., Beloglazov, A., & Abawajy, J. 2010, July 12-15. Energy-Efficient Management of Data Center Resources for Cloud Computing: A Vision, Architectural Elements, and Open Challenges. Paper presented at the Proc. of the 2010 International Conference on Parallel and Distributed Processing Techniques and Applications, Las Vegas, NV, USA.

[32] Liu, L., Wang, H., Liu, X., Jin, X., He, W. B., Wang, Q. B., et al. 2009. GreenCloud: a new architecture for green data center. Paper presented at the Proc. of the sixth International Conference on Autonomic Computing Barcelona, Spain.

Process Simulation of Ammonia Synthesis for Increasing Heat Recovery in a Thermal Storage Plant: A Review

Sadaf Siddiq[1], Shahab Khushnood [2], Zafar Ullah Koreshi [3], and M. Tasneem Shah [4]

Abstract

Thermal storage of solar energy can be achieved in solids and liquids, during solar insolence, for subsequent recovery to enable 24-hour base-load plant operation similar to conventional fossil-fueled and nuclear power plants. Liquid ammonia, due to its global availability and chemical suitability, has been considered for thermal energy storage in plants of the order of 10 MW(e). The energy is stored in chemical bonds of constituent gases arising from the endothermic dissociation of ammonia, and subsequently recovered in the well-known exothermic synthesis Haber-Bosch reaction.

The efficiency of such a solar plant depends on the process variables – temperature, pressure and flow-rate; which can be modeled with the thermo-fluid conservation equations incorporating the underlying thermodynamics and chemical reaction kinetics. This paper reviews the models, and the computational schemes, that have been used to simulate the industrial ammonia synthesis process. We have also reviewed the accuracy of the simulations reported in the literature.

Keywords: Solar Thermal Storage, Ammonia Synthesis, Solar Heat Recovery, Optimization of Synthesis Process.

Introduction

Solar energy currently accounts for an installed capacity of about 23 GWe, compared with geothermal (installed capacity 10.7 GW), and wind (160 GW) [1]. This is insignificant in the global scenario where in 2010, the total primary energy consumption was 12002.4MTOE**[1]consisting of oil (33.8%), coal (29.6%), natural gas (23.8%), hydroelectric (6.5%) and nuclear (5.6%). Even though renewable sources such as solar, geothermal and wind are not presently significant, they offer the promise of providing clean and sustainable energy by mitigating the effect of the carbon release from fossil fuels, in the form of greenhouse gases [1, 2]. Such reductions are necessary for the environment and are binding on states signatory to the Kyoto Protocol [46]. Emission of greenhouse gases (carbon dioxide, methane, nitrous oxide, hydrofluorocarbons, perfluorocarbons and sulphur hexafluoride) as well as toxic and pollutant gases, also have a harmful effect on people.

The Sun, as the primary source of energy for the solar system, supplies over 30,000 TWyr/yr which, compared with the global energy requirement of the order of 20 TWyr/yr may be considered to be virtually inexhaustible source. The issues which will ensure its place in the future energy scenario are its economic competitiveness in comparison with existing technologies. A key technological issue that lies at the core of economic competitiveness of solar energy is the operation of solar energy power plants. Presently, solar power plants, based on photovoltaic (PV) and concentrated solar power (CSP) technologies [16, 19], are capable of electricity generation during solar insolence only. Continuous, base-load operation will only be possible if such plants can generate electricity in the absence of solar insolence; and hence thermal storage mechanism becomes necessary.

The thermal energy storage technologies can be classified [29] by the mechanism of heat viz

1. sensible
2. latent
3. Sportive
4. chemical

[1&2] University of Engineering & Technology, Taxila, [3&4] Air University, Islamabad, Pakistan.

In the sensible heat storage systems, there is the possibility of liquid (water tank, aquifier, thermal oil) and solid systems (building mass, concrete, ground). In the latent heat storage systems, both organic (parrafins) and inorganic (hydrate salts) compounds can be used. In the sorptive, both absorption and adsorption systems can be used. Finally, in the chemical storage, energy can be stored in chemical bonds which can be broken endothermically and recovered in a synthesis exothermically. Storage materials and technology will also depend on the temperatures in the plant [27].

A base-load plant of 10 MW(e), assuming that a solar insolation of 1 kW/m^2 is available for 8 hours in a day (28.8 MJ/m^2, compared with 20 MJ/m^2 for Pakistan [57] would require 400 parabolic dishes, each of area 400 m^2 [41], with a synthesis plant of 1500 MeT per day.

The Synthesis Process

The Haber-Bosch process first demonstrated by Fritz Haber in 1909 and scaled up to an industrial process by Carl Bosch in 1913. Both Haber and Bosch were awarded Nobel Prizes for their inventions, and ammonia was used in Germany in the First World War for the manufacture of explosives.

Ammonia Industry

Global fertilizer industry produces about 170 million tones of fertilizer nutrients every year [18] for boosting agricultural output, of which more than 15 million tones was ammonia produced in 2009. Fertilizers are based on nitrogen, phosphorus or potassium. Nitrogen accounts for 78% of the earth's atmosphere. Since plants cannot breathe nitrogen, it must be converted to a suitable form such as ammonia. Its major uses are as fertilizer and for production of nitrogen containing compounds such as nitric acid. It is also used as a refrigerant and in textile processing. Ammonia (NH3) stays in the liquid form at temperatures higher than its melting point -77.73 oC and has a density of 681.9 kg/m3 at its boiling point -33.34°C; it must thus be kept at very low temperature or stored at very high pressure. Liquid ammonia was first produced on an industrial scale in Germany, during the First World War, by the Haber-Bosch Process. In industry, the Haber-Bosch process, involving the steam reforming of methane to produce hydrogen is used with nitrogen taken from the air, to produce ammonia. The typical size of urea plants is 1000 MeT per day with a capital cost of US$ 150 million. The total production of ammonia was 130 million tons in 2000, produced in 80 countries and 85% of which was used for nitrogen fertilizer production [39]. The largest chemical industry in the world is in the U.S. [40], with ammonia being the most important intermediate chemical compound produced in 41 plants. In Pakistan, there are eight urea fertilizer plants with a large ammonia plant capacity [9].

Ammonia Dissociation and Synthesis

The dissociation of ammonia (H = 66.9 kJ/mol) is an endothermic reaction that can be carried out by thermo-catalytic decomposition using catalysts: ruthenium, indium, nickel, Fe-Al-L, Fe-Cr. Typical temperatures are in the range of 850 – 1000 oC. Approximately 1.4 kW power per cubic meter of hydrogen is typically used. Conversely, the synthesis of ammonia from nitrogen and hydrogen reactant gases (H = -92.22 kJ/mol) is an exothermic reaction for which the pressure required is in the range 130 – 250 bar, and the temperature required is in the range 250 – 600 oC. High temperature gives higher reaction rate, but as reaction is exothermic, higher temperature according to Le Chatelier's principle causes the reaction to move in the reverse direction hence a reduction in product. Similarly, higher Temperature reduces the equilibrium constant and hence the amount of product

Ammonia Dissociation and Synthesis

The dissociation of ammonia $2NH_3 \Leftrightarrow N_2 + 3H_2$ (ΔH = 66.9 kJ/mol) is an endothermic reaction that can be carried out by thermo-catalytic decomposition using catalysts: ruthenium, indium, nickel, Fe-Al-L, Fe-Cr. Typical temperatures are in the range of 850 – 1000 °C. Approximately 1.4 kW power per cubic meter of hydrogen is typically used. Conversely, the synthesis of ammonia from nitrogen and hydrogen reactant gases $N_2 + 3H_2 \Leftrightarrow 2NH_3$ (ΔH = -92.22 kJ/mol) is an exothermic reaction for which the pressure required is in the range 130 – 250 bar, and the temperature required is in the range 250 – 600 °C. High temperature gives higher reaction rate, but as reaction is exothermic, higher temperature according to Le Chatelier's principle causes the reaction to move in the reverse direction hence a reduction in product. Similarly, higher

Temperature reduces the equilibrium constant and hence the amount of product decreases; this is the Van't Hoff equation: $\ln K = -\frac{\Delta H^{\circ}}{RT} + \frac{\Delta S^{\circ}}{R}$. An increase in pressure, however, causes a forward reaction and is thus favorable. Synthesis is achieved by using catalysts such as osmium, ruthenium, and iron-based catalysts.

causes a forward reaction and is thus favorable. Synthesis is achieved by using catalysts such as osmium, ruthenium, and iron-based catalysts.

Ammonia Synthesis Plant

The principle of circulating gas over the catalyst in a loop system, first appreciated by Haber in 1908, is still an important feature of modern ammonia plants. Over the past 50 years the typical operating pressures with available catalysts have been in the range 120 – 350 bar (1740 – 5075 psi). However during the last 20 years low pressure synthesis loops operating in the region of 80 - 120 bar (1160 - 1740 psi) have been an integral part of new technology. Figure 1 below shows a synthesis loop for a typical 1500 TPD plant operating at 200 bar (2900 psi) and using a three bed radial converter.

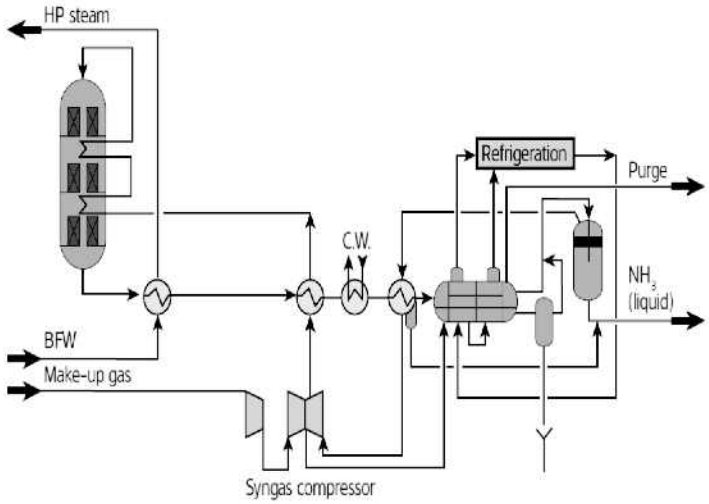

Figure 1: Ammonia loop for typical 1500 TPD plant

The ammonia synthesis technology is now mature, with the market dominated by five licensers-Haldor Topsøe, M.W. Kellogg, Uhde, ICI, and Brown & Root, of which Haldor Topsøe has a 50 per cent world market share as supplier of the technology [3, 4, 5, 6, 7,12, 13, 15, 39]. Figure 2 shows Udhe Dual Pressure Process, based on using a once-through converter to produce some ammonia before entering the conventional synthesis loop.

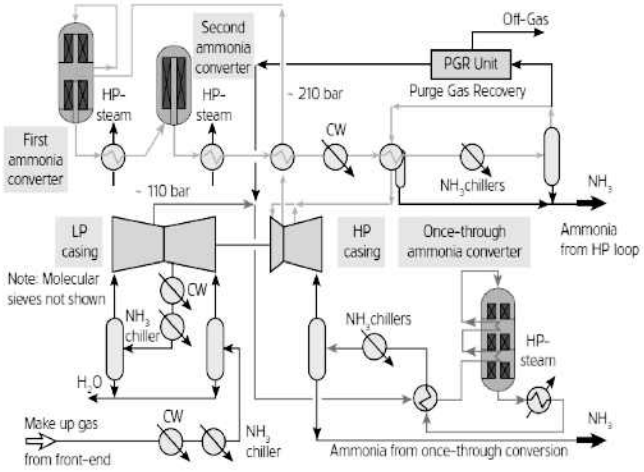

Figure 2: Uhde Dual Pressure Process – ammonia synthesis loop

A simplified Thermal Storage Plant (TSP) model [43] using such as reactor, shown in Figure 3, is considered as it includes the essential features of an ammonia synthesis plant. The input syn gas stream (ST1), consisting of nitrogen, hydrogen and small amounts of other gases, is taken from the day-cycle ammonia dissociation of the solar plant [42]. This feed-stream is compressed to the temperature and higher pressure required for synthesis, typically, of the order of 250 -600 oC and 130 - 250 bar. This stream is then mixed with the recycle stream (ST10) and fed into the catalyst-containing synthesis reactor where the synthesis reaction, in the forward direction, converts nitrogen and hydrogen into ammonia producing energy. The effluent stream passes through the recovery heat exchanger and liquid ammonia condenser E-1 and into the Knock-Out drum F-1, where the liquid ammonia is sent to the storage tank and stream ST6 is carried to the purging system for removing inert gases which are 'poisons' for the catalyst in the reactor. Another re-cycle compressor is required at this stage to restore the pressure to the required level till the stream (ST10) is mixed with the feed stream and enters as stream ST3.

A simplified Thermal Storage Plant (TSP) model [43] using such as reactor, shown in Figure 3, is considered as it includes the essential features of an ammonia synthesis plant. The input syn gas stream (ST1), consisting of nitrogen, hydrogen and small amounts of other gases, is taken from the day-cycle ammonia dissociation of the solar plant [42]. This feed-stream is compressed to the temperature and higher pressure required for synthesis, typically, of the order of 250 -600 ^{o}C and 130 - 250 bar. This stream is then mixed with the recycle stream (ST10) and fed into the catalyst-containing synthesis reactor where the synthesis reaction, $N_2 + 3H_2 \Leftrightarrow 2NH_3$ in the forward direction, converts nitrogen and hydrogen into ammonia producing energy. The effluent stream passes through the recovery heat exchanger and liquid ammonia condenser E-1 and into the Knock-Out drum F-1, where the liquid ammonia is sent to the storage tank and stream ST6 is carried to the purging system for removing inert gases which are 'poisons' for the catalyst in the reactor. Another re-cycle compressor is required at this stage to restore the pressure to the required level till the stream (ST10) is mixed with the feed stream and enters as stream ST3.

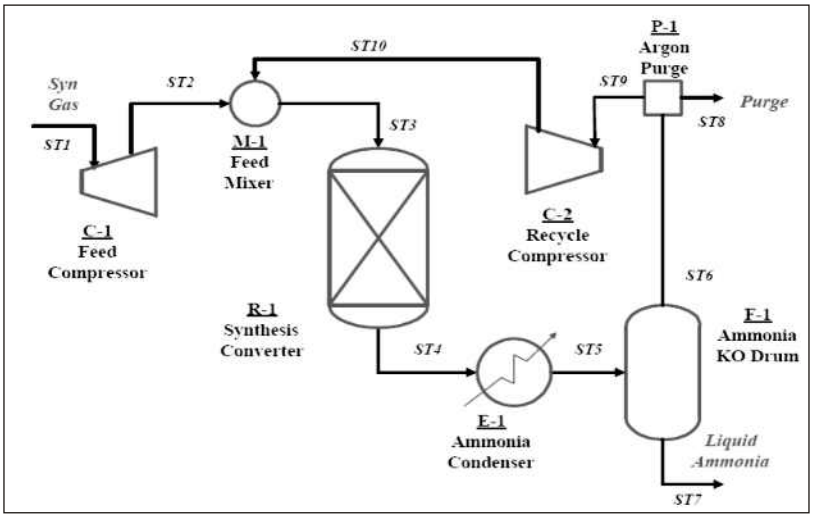

Figure 3: Ammonia synthesis energy recovery system for a Thermal Storage Plant.

Review of Mathematical Models

The synthesis of ammonia from the flow of syn gases in the convertor can be modeled using the laws of conservation of mass, momentum and energy for non-isothermal multi-component systems undergoing chemical reactions and mass transfer [35]. In the case of unsteady flow the governing equations are

Mass:

$$\frac{d}{dt}m_{tot} = \Sigma\omega_1 - \Sigma\omega_2 + \omega_0 = \Sigma\rho_2\langle\upsilon_2\rangle S_2 + \omega_0 \tag{1}$$

Mass of Species α:

$$\frac{d}{dt}m_{\alpha,tot} = \Sigma\omega_{\alpha 1} - \Sigma\omega_{\alpha 2} + \omega_{\alpha 0} + r_{\alpha,tot} \qquad \alpha = 1,2,3,.....N \tag{2}$$

Momentum:

$$\frac{d}{dt}P_{tot} = \Sigma(\frac{\langle\upsilon_1^2\rangle}{\langle\upsilon_1\rangle}\omega_1 + p_1S_1)u_1 - \Sigma(\frac{\langle\upsilon_2^2\rangle}{\langle\upsilon_2\rangle}\omega_2 + p_2S_2)u_2 + m_{tot}g + F_0 - F_{f\to s} \tag{3}$$

(Total) energy:

$$\frac{d}{dt}(K_{tot} + \Phi_{tot} + U_{tot}) = \Sigma(\frac{1}{2}\frac{\langle\upsilon_1^3\rangle}{\langle\upsilon_1\rangle} + gh_1 + \hat{H}_1)\omega_1 - \Sigma(\frac{1}{2}\frac{\langle\upsilon_2^3\rangle}{\langle\upsilon_2\rangle} + gh_2 + \hat{H}_2)\omega_2 + W_m + Q_0 - Q \tag{4}$$

where

m	mass	Φ	potential energy
ω	mass flow rate	U	internal energy
r	molar production	H	enthalpy per unit mass
P	linear momentum	Q	heat
υ	velocity vector	W	work
F	force (external, fluid to solid)	S	surface area
K	kinetic energy		

In terms of molar quantities, the continuity equation is expressed in terms of the molar concentration c, and the mole fractions x_i as

$$c\left(\frac{\partial x_\alpha}{\partial t} + (v^* \cdot \nabla x_\alpha)\right) = -(\nabla \cdot J_\alpha^*) + R_\alpha - x_\alpha\sum_{\beta=1}^{N} R_\beta \qquad \alpha = 1,2,3,.....N \tag{5}$$

Table 1: Equations of change of Multi-component Mixtures in terms of the Molecular Fluxes

Total mass:	$\frac{D\rho}{Dt} = -\rho(\nabla \cdot v)$
Species mass: (α=1,2,3,…..N)	$\rho\frac{D\omega_\alpha}{Dt} = -(\nabla \cdot j_\alpha) + r_\alpha$
Momentum:	$\rho\frac{Dv}{Dt} = -\nabla\rho - [\nabla \cdot \tau] + \rho g$
Energy:	$\rho\frac{D}{Dt}(\hat{U} + \frac{1}{2}v^2) = -(\nabla \cdot q) - (\nabla \cdot pv) - (\nabla \cdot [\tau \cdot v]) - (\rho v \cdot g)$

The above have been expressed by Dashti [25] as

$$\left\{\begin{array}{c} \dfrac{dz}{dx}=\dfrac{\eta r_{NH_3}}{2F^{o}_{N_2}/A} \\ \rho u C_p \dfrac{dT}{dx}+(-\Delta H_r)\eta r_{NH_3}=0 \\ \dfrac{dP}{dx}=-\mu\nabla^2 u=-150\dfrac{(1-\varepsilon)^z}{\varepsilon^3}\times\dfrac{\mu u}{d_p^2}-1.75\dfrac{(1-\varepsilon)}{\varepsilon^3}\times\dfrac{\rho u^2}{dp} \end{array}\right\} \quad (6)$$

A simpler analysis ignores the pressure drop in flow reducing to the conservation equations for mass and energy with reaction kinetics, used by Yuguo [59] and Dashti [25]

$$\frac{dz}{dx}=\frac{\eta R_A}{2F^{o}_{N}/A} \quad (7)$$

$$\rho u C_p \frac{dT}{dx}+(-\Delta H_r)\eta R_A=0 \quad (8)$$

For the reaction kinetics, the Temkin-Pyzhev [25,59] form of the synthesis reaction rate as a function of the pressure, temperature, and activities is used

$$R_A=2k\left[K_a^2 a_N\frac{a_H^{1.5}}{a_A}-\frac{a_A}{a_H^{1.5}}\right] \quad (9)$$

where the activities are defined as $a_i=y_i\phi_i P$. The individual activities are:

$$\phi_H=\exp\left\{e^{(-3.8402T^{0.129}+0.541)}P-e^{(-0.1263T^{0.5}-15.98)}P^2+300\left[e^{(-0.01190T1-5.941)}\right]e^{-P/300}\right\} \quad (10a)$$

$$\phi_N=0.93431737+0.2028538\,X10^{-3}T+0.295896\,X10^{-3}P-0.270727\,X10^{-6}T^2+0.4775207\,X10^{-6}P^2 \quad (10b)$$

$$\phi_A=0.1438996+0.2028538X10^{-2}T+0.4487672X10^{-3}P-0.1142945X10^{-5}T^2+0.2761216X10^{-6}P^2. \quad (10c)$$

The Arrhenius rate form is given as

$$k=k_o\exp\left(-\frac{E}{RT}\right) \quad (11)$$

The specific heat capacities of hydrogen, nitrogen, methane and argon of the syngas (T in Kelvin, C_p in J/mol-K) expressed as:

$$\begin{array}{l} c_pH_2=4.184(6.952-0.04567E-2T+0.09563E-T^2-0.2079E-T^3) \\ c_pN_2=4.184(6.903-0.03753E-2T+0.01930E-5T^2-0.6861E-9T^3) \\ c_pCH_4=4.184(4.75+1.2E-2T+0.303E-5T^2-2.63E-9T^3) \\ c_pAr=4.184*4.9675 \end{array} \quad (12a)$$

For ammonia, the Shomate equations [10],

$$c_pNH_3=A+B*t+C*t^2+D*t^3+\frac{E}{t^2} \quad (12b)$$

T in the range 298-1400 K,

$$t = \frac{T}{1000}$$

$$A = 19.99563; B = 49.77119; C = -15.37599; D = 1.921168; E = 0.189174$$

have been used for the temperature range of interest (500-800K) and compared with simplified expressions [37]:

$$c_P N_2 = 27.27 + 4.93e-3T$$

$$c_P H_2 = 27.01 + 3.51e-3T \qquad (12c)$$

$$c_P N_2 = 29.75 + 25.11e-3T$$

For a compressor, the power requirements [37,50] for isentropic compression, are obtained as

$$W_s = \frac{\gamma}{\gamma - 1} RT_1 \left[1 - \left(\frac{P_2}{P_1} \right)^{(\gamma-1)/\gamma} \right]. \qquad (13)$$

The actual work will of course be larger than W_s and the ratio W_s / W_{actual} will depend on the compressor efficiency. In terms of the initial and final temperatures, the work W_s can also be found from

$$W_s = -\Delta H = C_p (T_1 - T_2). \qquad (14)$$

More generally, for a multi-stage compressor with *n* units, with the compression ratios (*r)* in all the stages equal, the total work can be estimated from

$$W_s = \frac{n\gamma}{\gamma - 1} RT_1 \left[1 - (r)^{(\gamma-1)/\gamma} \right]. \qquad (15)$$

where, for an ideal gas $P_1 V_1 = RT_1$. The above expressions are based on the assumption that specific heats remain constant in the pressure and temperature range. In this analysis, the compression power requirements for a single-stage reciprocating compressor are obtained.

Similar models are also used to determine the compression requirement for recycle in the converter, refrigeration duty, and vaporizer and purge systems. Additional objectives will be to quantify process-variable trade-offs with an aim to progress towards an “optimal design”. Thus, an issue worth exploring is: what percentage change in the plant operating parameters can result in an incremental change in availability of syn gases which can be used to generate electricity at night from the NH_3 synthesis exothermic reaction.

The above model can be used to carry out an energy balance of the Process Flow Diagram (PFD). The ‘energy input’ components are thus the compressors (C-1 and C-2), and the refrigeration systems for condensing liquid ammonia (E-1), while the ‘energy output’ system is the heat recovery system with E-1 or taken separately.

The equilibrium constant is obtained from

$$\log K_a = -2.691122 \log T - 5.51925 X 10^{-5} T + 1.848863 X 10^{-7} T^2 + \frac{2001.6}{T} + 2.689. \qquad (16)$$

The overall synthesis rate (kmol of ammonia produced per hr per unit volume of catalyst) is ηR_A where η is the catalyst effect factor [25]. It is defined as and may have a significant effect on the overall efficiency.

$$\eta = b_o + b_1 T + b_2 Z + b_3 T^2 + b_4 Z^2 + b_5 T^3 + b_6 Z^3 \qquad (17)$$

The resulting equations are coupled non-linear partial differential equations, which are converted to ordinary differential equations and solved by numerical integration [51].

The above model has been used by Siddiq *et al* [11] to obtain the molar flow rates and temperature of the syngas in a single-bed catalyst convertor, and the net power produced by the TSP. For a plant of magnitude similar to that described in Dashti [25] the results for the nitrogen conversion, syngas temperature and molar flow rates are shown in Figs. 4-7.

The resulting equations are coupled non-linear partial differential equations, which are converted to ordinary differential equations and solved by numerical integration [51].

The above model has been used by Siddiq et al [11] to obtain the molar flow rates and temperature of the syngas in a single-bed catalyst convertor, and the net power produced by the TSP. For a plant of magnitude similar to that described in Dashti [25] the results for the nitrogen conversion, syngas temperature and molar flow rates are shown in Figs. 4-7.

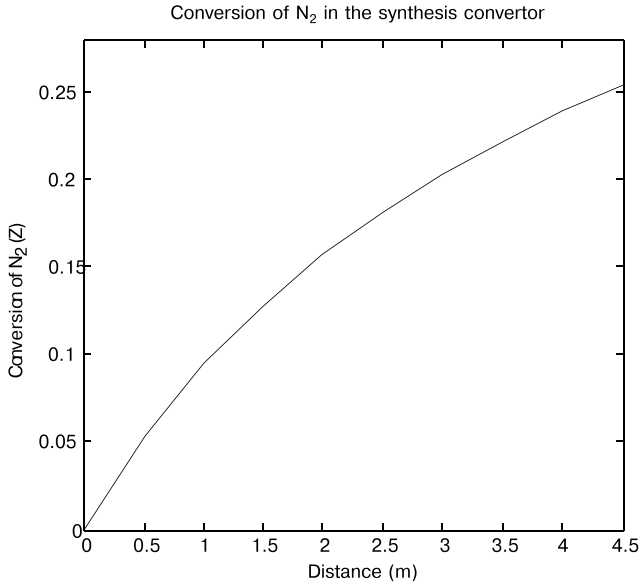

Figure 4: Conversion of Nitrogen along a single-bed catalyst

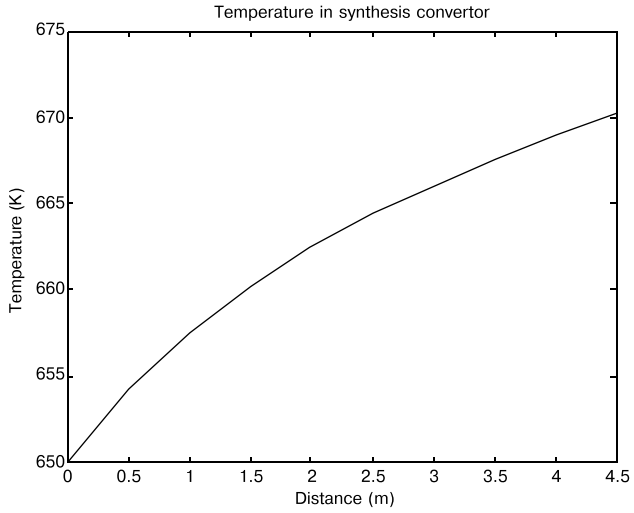

Figure 5: Syngas temperature in converter

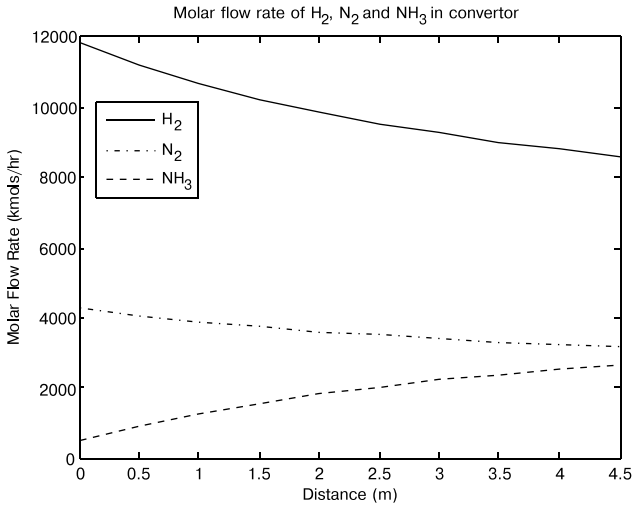

Figure 6: Molar flow rate in converter.

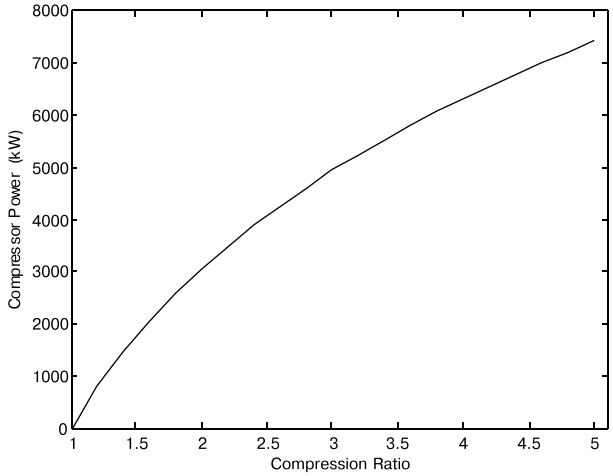

Figure 7: Syngas compression requirement.

It was found that the overall energy availability from the exothermic synthesis of ammonia is of the order of 32.4 MW(th), of which about 50% is available in the top 30% of the convertor. This energy availability was assessed in comparison with the syngas compression requirement shown in Figure 7. As shown, the compressor power is dependent on the syngas flow-rate, the compression ratio and the initial temperature. As a rough guide a compression ratio of 3, typical of industrial multistage compressors, would require of the order of 5 MW(e). The two dominating energy factors of a thermal storage plant based on the endothermic dissociation and exothermic synthesis of ammonia were quantified. It was determined that the syngas compression may greatly exceed the useful work realizable from such a plant. Factors to investigate in greater detail include the hydrogen/nitrogen ratio, the purge gas ratio, the ammonia content of the convertor feed-stream and the catalyst effect. The computer program developed, using the model described above, can investigate all these effects and quantify the sensitivity of each independent parameter on the overall system efficiency, restricted, for the moment to only two important and dominating energy components. Ammonia concentration in the convertor feed, for example, is an important parameter as it determines the ammonia production, recirculation rate, and refrigeration requirement. Yuguo and Changing [59] found that, when inerts and the H_2/N_2 ratio remained constant, for ammonia content increase from 2 to 2.5%, power consumption increased from 6 to 6.1 kW-hr/kmol and ammonia production increased 3% from 985 to 1015 MTD.

Such an analysis can include compressor speed, refrigeration duty and synthesis conversion process. The compressor requirement can also be reduced by an optimization analysis to determine of the number of stages and the suction, and discharge, pressures of each stage. For a three-stage compressor, for example, the objective function to minimize the work requirement is [38].

$$f = \left[\left(\frac{P_2}{P_1} \right)^{(\gamma-1)/\gamma} + \left(\frac{P_3}{P_2} \right)^{(\gamma-1)/\gamma} + \left(\frac{P_4}{P_3} \right)^{(\gamma-1)/\gamma} \right] \quad (18)$$

Optimization

Optimization is a widely used engineering tool for enhancing the energy efficiency, and hence the economic competitiveness, in chemical industry. It is aimed at finding some 'optimal' set of design and operating parameters which enables industry to function in a 'best possible' way.

Design parameters, such as physical dimensions and materials of plant components, are the basis of fabrication and subsequent plant erection. Operating parameters, on the other hand, involve process variables, such as flow rates, pressures and temperatures, which are integrated into the overall plant units. As an example, a urea fertilizer chemical process plant has four large integrated units: reforming, ammonia, urea, and utilities, all of which involve inter-dependent process variables. The overall system is thus not only large in magnitude, but its interdependence in the form of re-cycle streams, for example, renders the determination of optimality as a complex non-linear problem. The process of optimization is thus both theoretical and practical as it is based on mathematical models which are non-linear and utilize material properties at actual plant conditions. These can be obtained from on-line chemical analysis during plant operation. Once formulated, the system of equations needs to be solved by analytical or numerical methods often requiring powerful computer hardware and sophisticated simulation software. Optimization analysis for a solar thermal plant requires a mathematical framework to model the underlying processes, the physical and chemical data of the plant and its materials, and numerical techniques to carry out a simulation to achieve the objective of determining optimality.

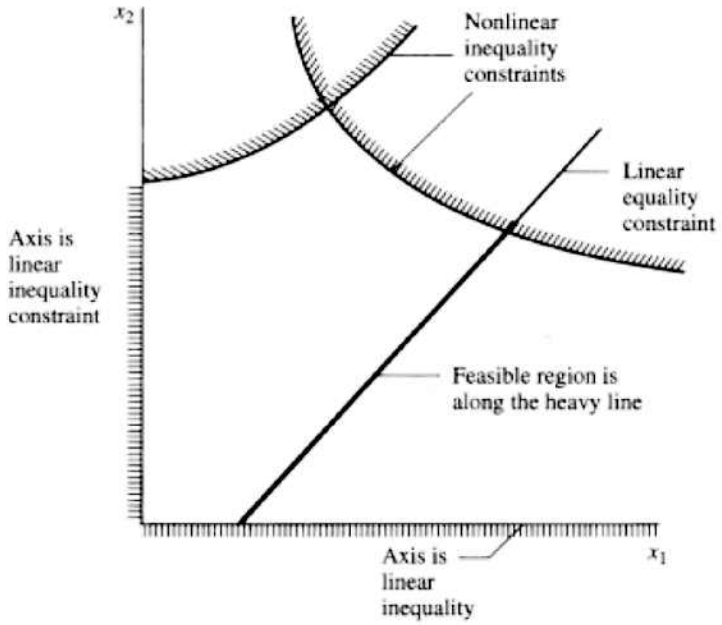

Figure 8: Optimization Process

The objective of optimization studies is to determine optimality which will result in maximum efficiency of the plant, by which it will be taken to mean optimality of the synthesis reactor in the integrated plant. Several other objectives, as diverse as plant and equipment sizing, minimizing inventory charges, and allocating resources among several processes, may be defined [26, 38]. Other terms that are analogously used for objective function, process model, and constraints are economic cost (or profitability) function and feasible solution. An optimization problem, formulated as an objective function $f(x_1, x_2)$ with two independent variables x_1, x_2, subject to an equality constraint $g(x_1, x_2) = 0$ and possibly N inequality constraints of the form $h_i(x_1, x_2) \geq 0, i = 0,1,2 \cdots N$ will then have a feasible region illustrated by Figure 8 [38]. An optimal solution will then be determined as falling in the feasible region defined as satisfying all the constraints and having an extremum. For such a problem, the dashed lines in the figure would show the infeasible regions for the inequality constraints while the solid line would show the equality constraint. Of all the values of the variables x_1, x_2 lying in the feasible region, one would need to determine the particular one set, or a number of sets, which would correspond to the extremum.

Possible obstacles in the optimization process are non-linearities, discontinuities, insensitivity of the objective function to independent variables, and local extrema confused with a global extremum.

The mathematical methodology is then identified to solve the governing equations and carry out a simulation to obtain the optimal set of parameters. These methodologies may be broadly classified as deterministic or stochastic. The former are illustrated in Figure 9 [38]. Thus, numerical techniques such as the Runge-Kutta method for solving a non-linear set of coupled first-order ordinary differential equations may be used, while the latter is based on either an analogous stochastic simulation of the phenomena or on stochastic methods to solve a deterministic set of governing equations. A typical example of a full stochastic simulation is analog, or biased, Monte Carlo simulation, while a typical example of a stochastic technique for a deterministic set of governing equations are random search methods such as Genetic Algorithms (GA).

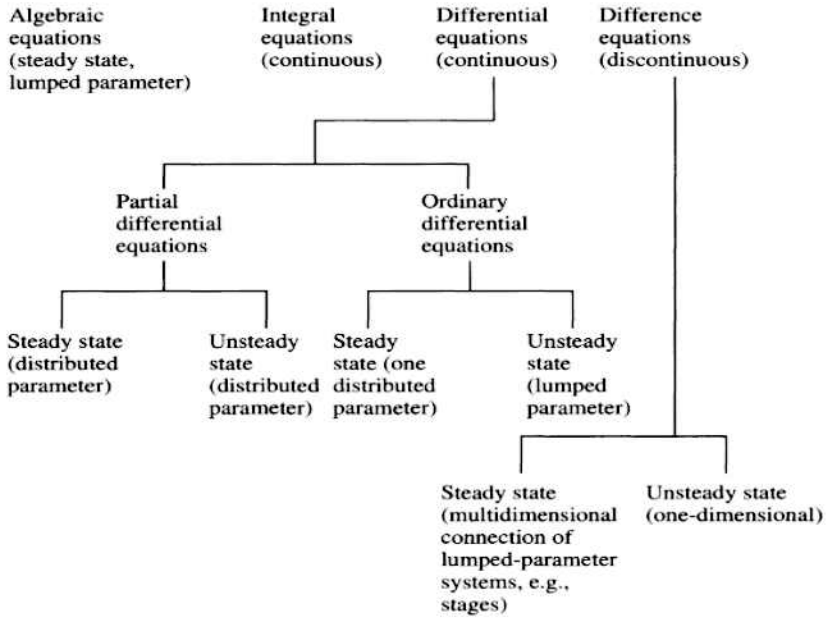

Figure 9: Mathematical Methodology to solve governing equations

One way of classifying modeling problems [38] is from the degrees of freedom $N_f = N_v - N_e$, in terms of the number of variables N_v, and the number of independent equations N_e. When $N_f = 0$ the problem is exactly determined and for a linear set of independent equations, there is a unique solution, while for non-linear equations there may be multiple solutions or no real solution. Such problems do not constitute an optimization problem. When $N_f > 0$, the problem is underdetermined and at least one process variable can be optimized, while for $N_f < 0$. Conversely, $N_f < 0$ constitutes an over-determined problem and the set of equations has no solutions and methods, such as the least squares method, can be used to determine the unknowns.

Widely used optimization methods include the following areas [38]: one-dimensional search, unconstrained multivariable optimization, linear programming, nonlinear programming, optimization involving discrete variables, and global optimization (operations research, including Monte Carlo, heuristic methods, GA and evolutionary methods). Some widely used techniques for obtaining optimality are (i) the deterministic variational functional optimality based on Pontryagin's Maximum Principle, and (ii) the Genetic Algorithm optimization search [32, 38]. The GA search method has been used [26,38] for the optimization of an ammonia synthesis reactor [38] shown in Figure 10.

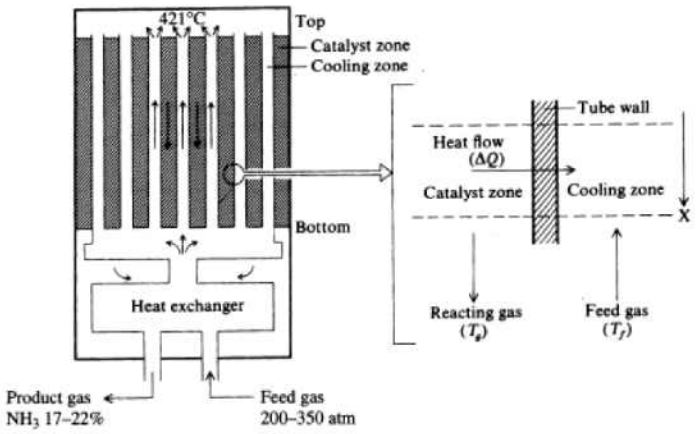

Figure 10: Ammonia Synthesis Reactor

First, the governing equations are numerically solved to obtain the temperature and concentration profiles shown in Figure 11.

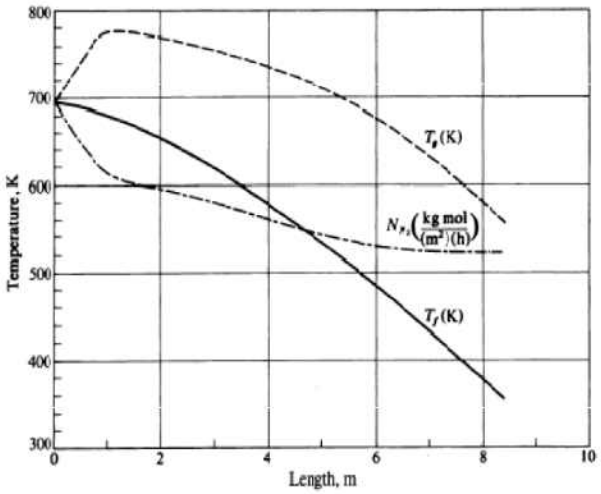

Figure 11: Temperature & Concentration Profiles along Converter Length

The numerical solution is followed by an optimization exercise in which an objective function $f(x, N_{N_2}, T_f, T_g)$ is defined along with the three governing equations, taken as constraints. Thus, the problem has one variable (*x*; the reactor length) one degree of freedom $(N_f = 1)$ and, being underdetermined, can be solved for optimality. The GA search is carried out as shown in Figure 12.

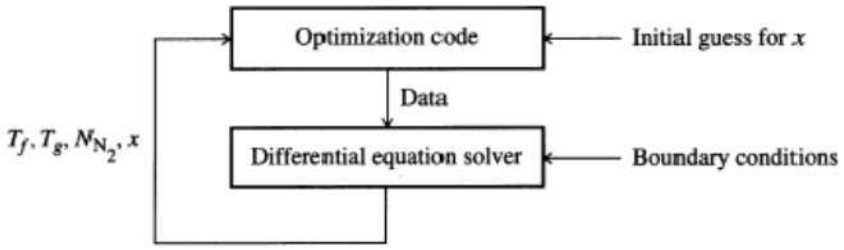

Figure 12: GA Search Algorithm

The optimal solution found for the exit conditions shown in Table 2.

Table 2: Optimal solution for the exit conditions

	Initial guesses	Optimal solution
N_{N_2}	646 kg mol/(m²)(h)	625 kg mol/(m²)(h)
Mole fraction N_2	20.06%	19.4%
T_g	710 K	563 K
T_f	650 K	478 K
x	10.0 m	2.58 m
$f(x)$	8.451×10^5 $/year	1.288×10^6 $/year

The optimization thus concludes that a 10*m* reactor results in an optimal solution for the values given above

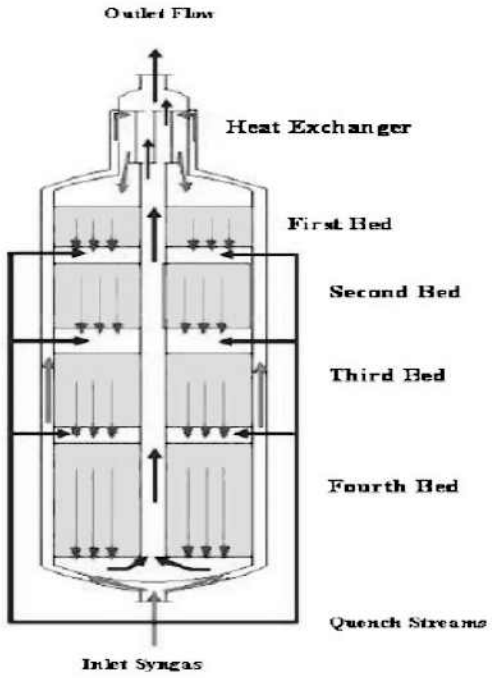

Figure 13: Four-Bed Synthesis Reactor

Sadeghi and Kavianiboroujeni [21] have used the Genetic Algorithm for a 1-D and 2-D optimization of a Kellog-type ammonia plant, located at Khorasan (Iran). The axial reactor (Figure 13) has four promoted-Fe catalytic fixed beds with a heat exchanger at the top. Syngas flows vertically upwards in the spaces between the two walls of the reactor, where it is pre-heated, then turns down through the beds and from the bottom fourth bed again turns upwards, exiting from the top of the reactor. The independent parameters investigated are the quench flow and quench temperature. Between the beds, the hot syngas is mixed with quench streams (shown in three streams between the beds) to control the temperature.

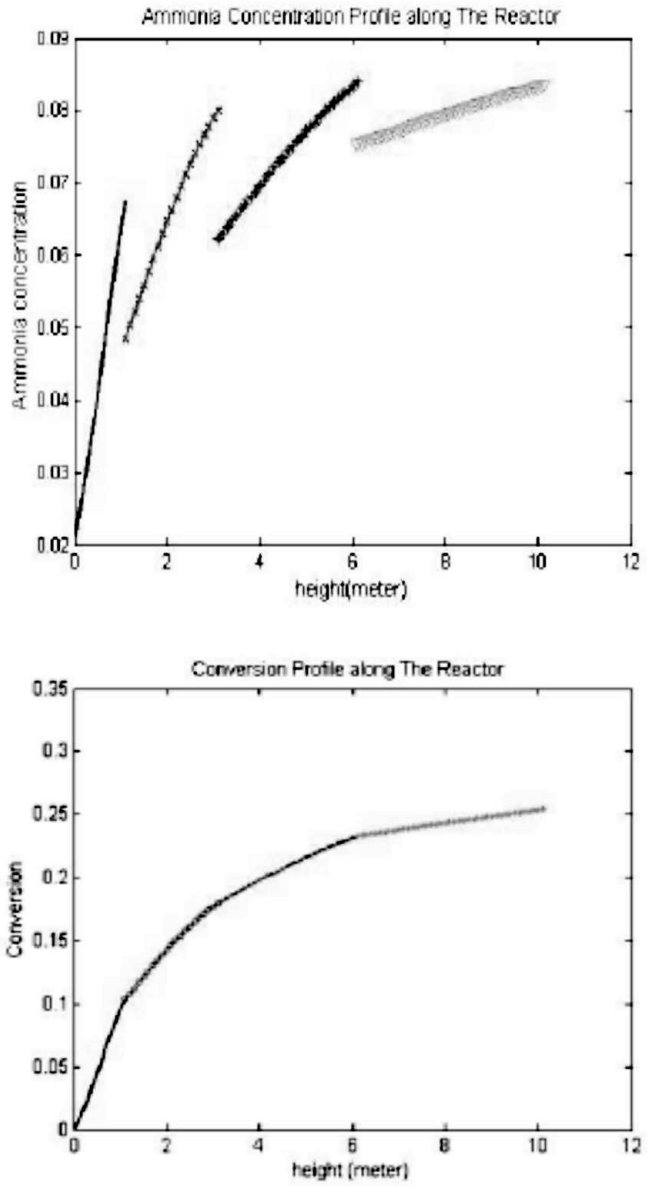

Figure 14: Effect of Quench gas on conversion efficiency

The purpose of injecting the quench streams is, clearly, to increase the ammonia production from the reactor; and since the forward synthesis chemical reaction is favored by high pressure and low temperature, the challenge is to reduce the temperature at every bed exit. The ammonia and nitrogen conversion obtained by Sadeghi and Kavianiboroujeni [21] by a numerical solution of the mass and energy balance equations is shown in the Figure 14. It can be seen that most of the ammonia

conversion takes place in the first bed even though it is the shortest. The effect of the quench gas is to reduce the ammonia conversion after every bed exit but this picks up as flow proceeds.

The paper uses GA for obtaining optimal temperature distribution, in this nonlinear optimization problem, resulting from a given quench flow, and subsequently optimal quench flow given quench temperature. In the optimization problem, the objective function is the ammonia outlet flow-rate, while the constraints are (i) $T < 800K$, in the reactor for avoiding hotspots, (ii) an ascending nitrogen conversion during optimal flow: $Z\,\mathrm{I}_x < Z\,\mathrm{I}_{x+\Delta x}$, and (iii) for the syngas: $T_{in} < T_{out}$.

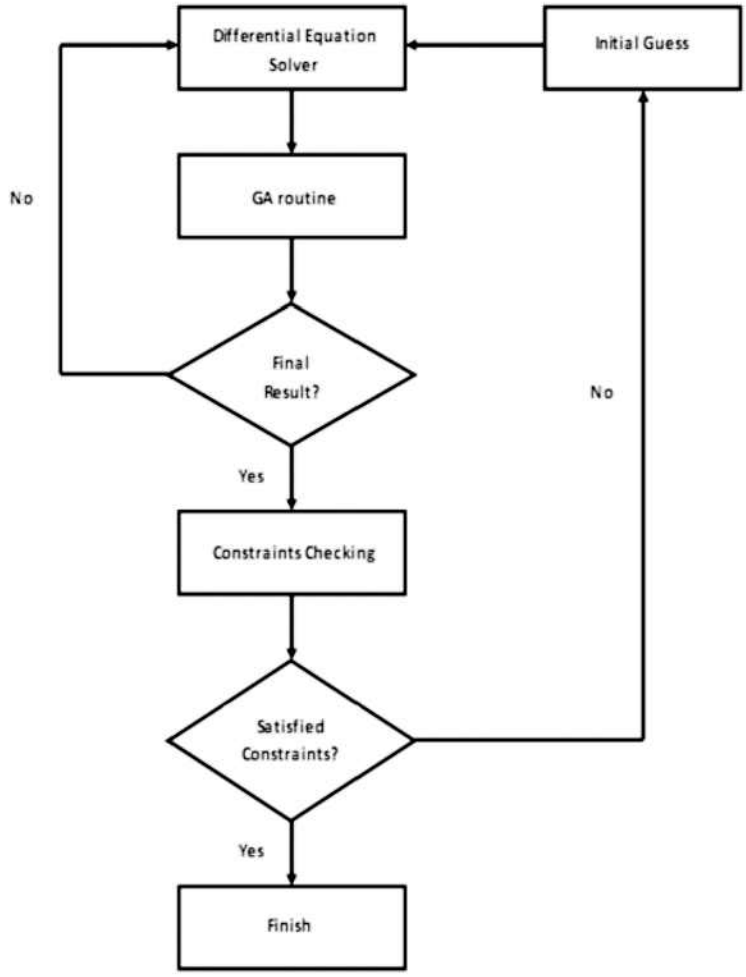

Figure 15: GA Algorithm for obtaining optimal temperature distribution

The flow-chart, Figure 15, for this optimization is reproduced from the paper [21] and their results, in Figure 16, give maximum ammonia conversion at a quench temperature of 650 K and a maximum conversion flow-rate of 47%

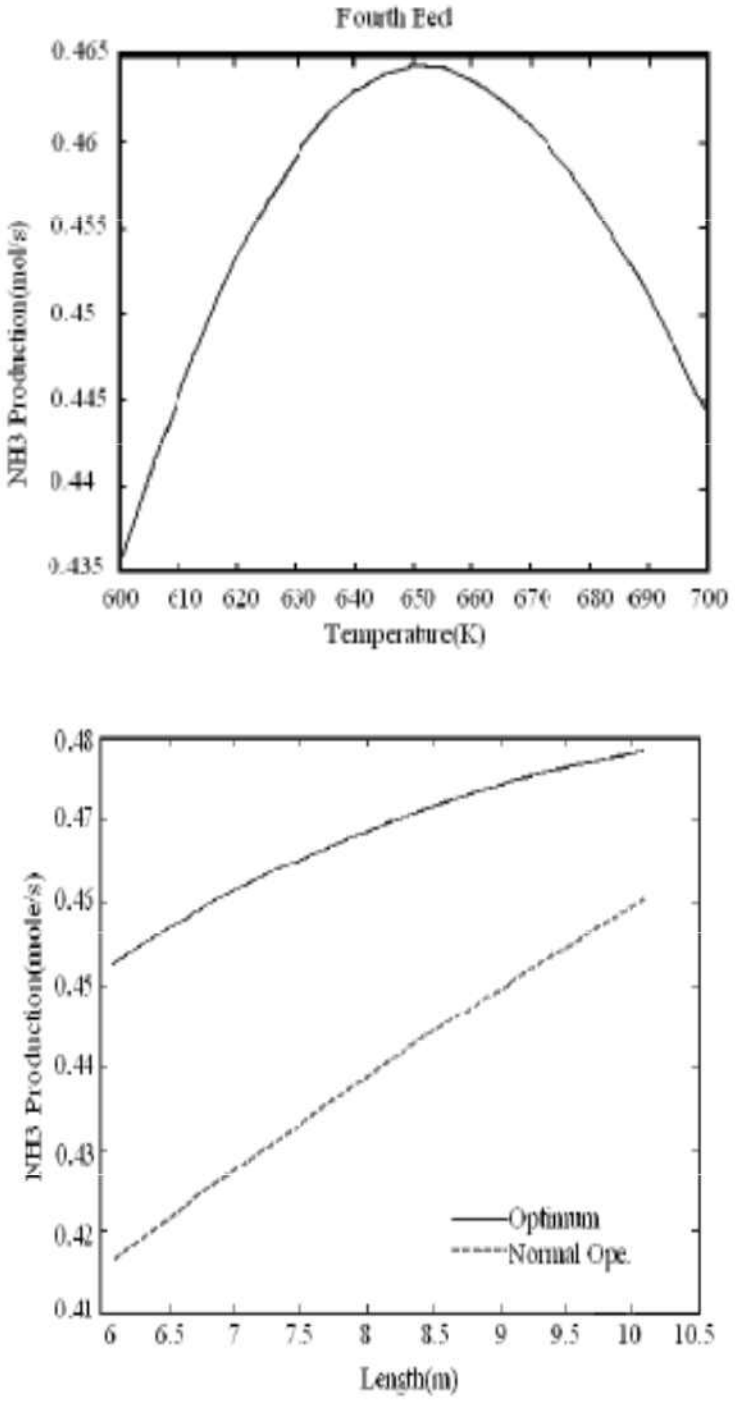

Figure 16: Optimal and Normal Ammonia Production rates

The important changes between normal and optimal operations for nitrogen conversion and reaction rate are shown in Figure 17.

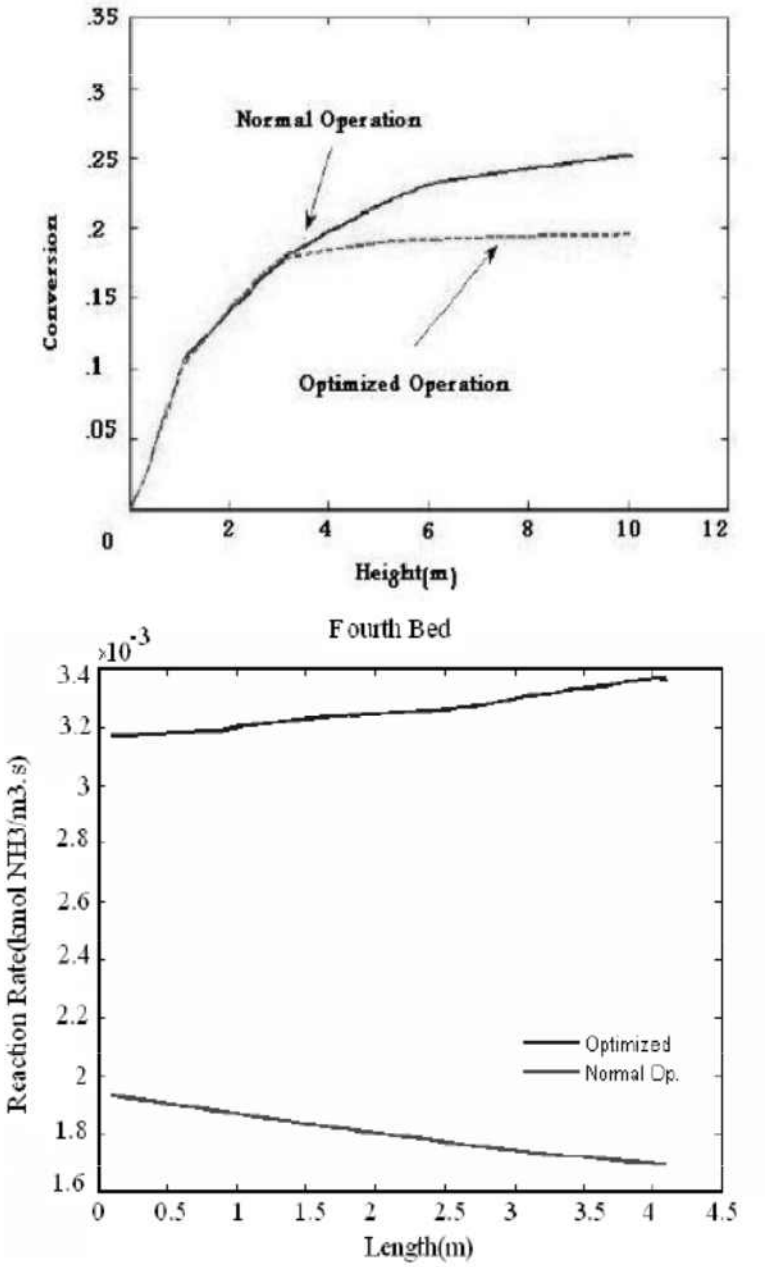

Figure 17: Optimal and Normal Nitrogen Conversion and Reaction rates

GA used for obtaining optimal temperature distribution has increased the ammonia production of the Khorasan plant by 3.3% (8,470 tons per year).

When the reactor is isothermal, different catalysts can be loaded to enhance productivity and when it is non-isothermal i.e. it has temperature gradients, then the catalyst may be non-uniformly loaded or different catalysts may be used for different temperature regions, to enhance productivity. Finding the optimal (spatial) distribution of catalyst is crucial to optimizing the performance. Numerical search can be carried out by dividing the reactor in zones and assuming uniform values of catalyst material in each zone; this will mostly result in a sub-optimal solution.

Variational methods have also been used to find optimal configurations for process variables in a synthesis convertor. These methods originate from the works of Leibniz (1646-1716) and Newton (1643-1727) credited for inventing and formalizing Calculus; followed by "Variational Calculus" attributed to Leonhard Euler (1707-1783) through his published work of 1733. Among the several contributors to variational calculus were Lagrange (1736-1813), Legendre (1752-1833), Gauss (1777-1855), Cauchy (1789-1857), and Poisson (1781-1840).

The field of Optimal Control [68] is an area of optimization in which the "best possible" strategy is chosen using the calculus of variations. While calculus can be used for optimization of a function of variables, calculus of variations is used to obtain the extremum, or stationary condition, of a functional (function of a function) by finding the function which extremizes the functional. The first variational calculus optimal problem was the Brachistochrone (shortest time) Problem solved by Bernoulli in 1696 [71] The formulations used are by Lev Semenovich Pontryagin (1908-1988), who developed the Maximum Principle, and the terminology of "Bang-Bang control" to steer a system with maximum or minimum control parameters, and of Bellman (1920-1984) who extended works of Hamilton (1805-1865) and Jacobi (1804-1851) to the now well-known Hamilton-Jacobi-Bellman (HJB) equations in Dynamic Programming.

Variational calculus [69, 70, 71] is used in areas that include optimal control, particle transport, mechanics, optics and chemical plant design [see *e.g.* 63]. There is a vast range of problems that determine complexity, such as whether the functional involves one or several functions, derivatives of functions, and one or more than one independent variable. Another class of variational calculus problems involves constrained problems with algebraic, integral or differential equation constraints.

Industrial Applications of Modeling and Simulation

The purpose of simulation is to estimate the best possible synthesis conversion, by optimizing the catalyst distribution, to investigate the feasibility of such base-load operation. A TSP will have operational parameters, pressures, temperatures and flow rates, similar to those in the ammonia units of urea fertilizer plants in the chemical process industry. These require pressures in the range of 130-250 bar and temperatures in the range 250-600 ^{o}C. Such high pressures require compression which is expensive in terms of equipment cost as well as energy utilization.

The conventional sequence of process steps are optimized by the introduction of improved catalysts (KM high strength, versatile, stable and poison-resistant catalyst, mainly magnetite Fe_3O_4 with promoters mainly oxides of calcium, aluminum and potassium, operating temperatures 340-550 ^{o}C [7]), new equipment design (such as improved synthesis converters), and process optimization studies. The carbon monoxide concentrations have been minimized at the exit of the shift converters, and a low-energy carbon dioxide removal process (such as selexol) has been used. New syn converters S-250 and S-300 are improved versions of the previous single bed S-50 and two-bed S-200 radial flow converters. Topsoe recommends S-300, developed in 1999, for all new plants [5].

Ammonia converter features, listed in Table 3, are taken from Topsøe [13], and depict the technology improvements over thirty years.

Table 3: Converter features

Type	Basic Design	Comments
S-50	One catalyst bed	Simplest and cheapest
S-200	Two catalyst beds and one interbed heat exchanger	Commissioned in 1979; 130 units installed
S-250	Combination of the S-200 followed by the S-50	
S-300	Three catalyst beds with two interbed heat exchangers	Higher conversion for same catalyst volume of S-250; installed first in 1991.

Modeling can also be used to investigate the effect of system pressure, catalyst activity and catalyst bed physical dimensions in KBR plants using a high-activity graphite supported ruthenium catalyst, typically three stages, after one stage of traditional iron catalyst. This is claimed to increase the activity 10 to 20 times [6] enabling very high conversion at a lower pressure of 90 bar.

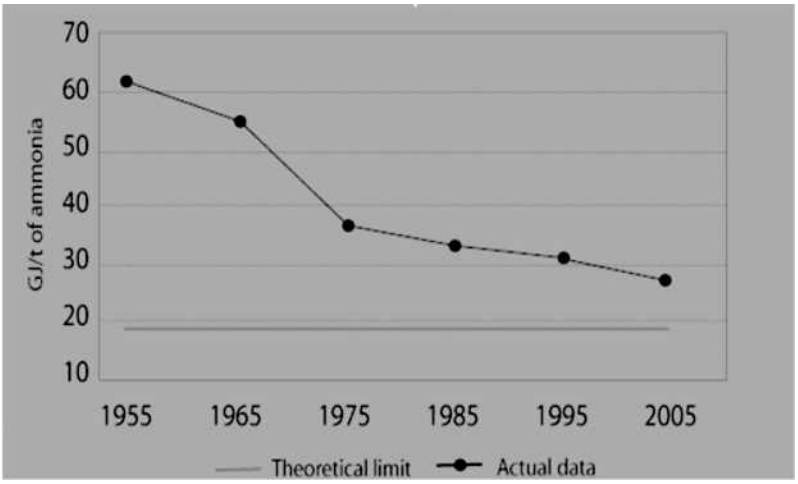

Figure 18: Energy Consumption Trends in the World- Ammonia Plants

A typical 1500 TPD ammonia plant [23], uses 257 TPD hydrogen and 1237 TPD nitrogen. The natural gas feedstock is 36,000 SCFH (2,760 lb-mol/hr), 86,000 SCFH (4,800 lb-mol/hr) air, and 150,000 PPH (8,280 lb-mol/hr) of steam. Modeling can be used to minimize the compression and refrigeration requirements and maximize the synthesis heat recovery.

This plant has an ammonia reactor catalyst bed size 3230 ft^3, and the total catalyst requirements are approximately 15,000 ft^3 (including reformers, HTS, LTS, methanator, de-sulpherizer). The total material cost of catalyst is approximately US$ 8 million (assuming catalyst is acquired once per year).

At a natural gas price of US$ 7.06 per MMBtu, the gas price is US$ 40 million per year. These two material costs account for about 98% of the total material cost, the remainder being the plant water for steam production.

Such a plant results in a production cost of US$ 195/tonne compared with the purchase cost of ammonia of US$ 330/tonne. Accounting for electric and indirect costs, the profit of such a plant is in the range of US$ 60-70 million per year depending on the number of days for plant turnaround in a year. The energy consumption quoted in the report is 5.3 MMBtu/tonne Ammonia = 5.6 GJ/MeT (1Btu = 1055 J). This is a useful figure-of-merit, and as shown in Figure 18, has improved by a factor of two over the last fifty years.

Optimal control methods have also been used to obtain the optimal temperature and concentration profiles in ammonia synthesis reactors [61, 62].

Process simulation, based on the laws of conservation of mass, momentum and energy, together with equations of state and thermo-physical or chemical kinetics data, can be used to carry out steady-state as well as dynamic simulation, depending on whether the focus is on solving for process variables in stationary or time-dependent environments. The aim, of course, is to optimize design and operations so that systems perform with maximal efficiencies translating into maximizing organizational profitability.

Dynamic simulation can be used for a wide range of operational and trouble-shooting issues in chemical industry, such as on-line simulation to control a plant or for training plant operator, and for off-line dynamic simulation is used for process optimization, or to study a process change

In the 1960s, process simulation consisted of solving conservation equations by extensive number-crunching with computer programs written in FORTRAN on large main-frame computers such as VAX, IBM and CDC. Many of these were converted into C++ for object-oriented software environments. This was followed by user-friendly GUI software carrying out essentially the same computations but in an easy-to-use manner.

The current trend in industry is to use commercial process simulation suites or custom designed process simulators to simulate the large, complex and inter-connected industrial processes that represent an actual chemical plant. This ranges from small batch plants to large process fertilizer and petrochemical industry. The commercial suites currently in extensive use include ASPEN HYSYS, CHEMCAD, HYSIM, and WINSIM. ASPEN Plus includes Basic engineering (simulation to PFD, PFD to P&ID).

Conclusions

Mathematical modeling and simulation has been used for the design of ammonia plants and to optimize their performance. The models are based on the laws of conservation of mass, momentum and energy for multi-species mixtures. The chemical reactions are modeled by appropriate thermodynamics and kinetic rate laws. The resulting equations are thus non-linear, coupled, partial differential equations which require numerical computing methods to solve for the process variables.

This paper reviews the mathematical models and the simulation that has been carried out for ammonia synthesis. Optimization methods, both deterministic and stochastic, are also reviewed. These, as well as variational optimal control methods, have been aimed at maximizing the ammonia conversion, and hence the overall efficiency of a thermal storage plant, by estimating optimal process variables.

References

[1] BP Statistical Review of World Energy 2011, available on-line at http :// www.bp .com /live assets/bp_internet/globalbp/globalbp_uk_english/reports_and_publications/statistical_energy_review_2011/STAGING/local_assets/pdf/primary_energy_section_2011.pdf

[2] World Energy Outlook 2011, International Energy Agency (IEA), Paris, France. available on-line at http://www.worldenergyoutlook.org/

[3] Ammonia Casale, available on-line at http://www.casale.ch/extra/ammonia.html

[4] Developments in Ammonia Production Technology, IFFCO, 2010. available on-line at http://www.iffco.nic.in/applications/iffcowebr5.nsf/0/4c4c41bda8dce6c7652570c40047bd41?OpenDocument

[5] Haldor Topsoe, 2010, available on-line at http://www .topsoe. com/business _areas/ ammonia/ processes/ammonia_synthesis.aspx.

[6] KBR 2010: A Global Engineering, Construction and Services Company, available on-line at http://www.kbr.com/Technologies/Proprietary-Equipment/KAAP-Ammonia-Synthesis-Converter

[7] KM1/KM1R, Topsøe Technology A/S, Ammonia Synthesis Catalysts 2010, available on-line at http://www.topsoe.com/business_areas/ammonia/processes/~/media/PDF%20files/Ammonia/Topsoe_ammonia_km1.ashx.

[8] Plant Technical Data, Chashma Nuclear Power Plant-I, Pakistan Atomic Energy Commission, 2010. available on-line at http://www.paec.gov.pk/chasnupp1/planttd.htm

[9] Ministry of Industries and Production, Fertilizer Production page, available on-line at http:// www. moip.gov.pk/fertilizerProduction.html.

[10] National Institute of Standards and Technology (NIST) Handbook 2010, available on-line at http://webbook.nist.gov/cgi/cbook.cgi?ID=C1333740&Units=SI&Mask=1.

[11] Sadaf Siddiq, S. Khushnood, Z. U. Koreshi and M. T. Shah.2010. “Solar Thermal Energy Storage using Liquid Ammonia Systems in Industry”, International Conference on Energy Systems Engineering, ICESE-2010, Islamabad, Pakistan.

[12] The Linde Group, 2010. Available on-line at http:// www. lindeeng ineering.com /en/ process_plants/hydrogen_and_synthesis_gas_plants/gas_products/ammonia/index.html.

[13] Topsøe Technology, Radial Flow Ammonia Synthesis Converters 2010, available on-line at http://www.topsoe.com/business_areas/ammonia/processes/~/media/PDF%20files/Ammonia/Topsoe_radial_flow_converters.ashx

[14] A Transient Systems Simulation Program, 2010 (TRNSYS™).

[15] Uhde GmbH Company, 2010, available on-line at http://www.uhde.eu

[16] Renewables Global Status Report: 2009 Update (Paris: REN21 Secretariat), copyright Deutsche Gesselschaft für Technische Zusammenarbeit (GTZ) GmbH.

[17] Copenhagen conference, 7- 18 December 2009, Copenhagen Denmark

[18] International Fertilizer Industry Association 2009, available on-line at http:// www.fertilizer. org /ifa/Home-Page/ABOUT-IFA

[19] Nextera Energy Resources USA, 2009. available on-line at

a. http://www.nexteraenergyresources.com

[20] Doerte Laing and Carsten Bahl.2008. “Concrete Storage for Solar Thermal Power Plants and Industrial Process Heat”, IRES III 2008, 3rd International Renewable Energy Storage Conference, Berlin.

[21] M. T. Sadeghi and A. Kavianiboroujeni.2008. “The Optimization of an Ammonia Synthesis Reactor using Genetic Algorithm”, International Journal of Chemical Reactor Engineering, Vol. 6, Article A113.

[22] C. W. Forsberg, P. F. Peterson, and H. Zhao.2007. "High-Temperature Liquid Fluoride Salt Closed Brayton Cycle Solar Power Towers", Journal of Solar Energy Engineering, Transactions of ASME, Vol. 129, pp. 141-146.

[23] Jared Crawford, Britni Ellifritz and Benjamin Root, "Process Design of an Anhydrous Ammonia Production Facility for Dyno Nobel", available on-line at http:// digital.uwyo.edu/ Undergraduate_Research_Day_Exhibits/2007023_Crawford_Ellifritz_Root.pdf.

[24] W. L. Luyben.2007. Chemical Reactor Design and Control, John Wiley and Sons, Inc.

[25] Ali Dashti, Kayvan Khorsand, Mehdi Ahmadi Marvast, Madjid Kakavand.2006. "Modeling and Simulation of Ammonia Synthesis Reactor", Petroleum and Coal, Vol. 48(2), pp. 15-23.

[26] B. V. Babu.2006. Process Plant Simulation, Oxford University Press.

[27] Hans Müller-Steinhagen.2006. "The storage of solar heat", First International Renewable Energy Storage Conference, IRES I, Gelsenkirchen.

[28] P. K. Johnson and D. S. Hervol.2006. "Experimental Validation of a Closed Brayton Cycle System Transient Simulation", NASA/CR-2006-214239.

[29] Peter Schossig.2006. "Conclusion on thermal storages", First International Renewable Energy Storage Conference, IRES I, Gelsenkirchen.

[30] Peter Scwarzbohl, Reiner Buck. Chemi Sugarmen, Arik Ring, M Jesus Marcox Crespo, Peter Altwegg, Juanne Enrile.2006. "Solar gas turbine systems: Design, cost and perspectives", Solar Energy, Vol. 80, pp. 1231-1240.

[31] B. Swaminathan.2004. Fertiliser Association of India, and Kristen E. Sukalac, International Fertilizer Industry Association (IFA), "Technology Transfer and Mitigation of Climate Change: the Fertilizer Industry Perspective" IPCC Expert Meeting on Industrial Technology Development, Transfer and Diffusion Tokyo, Japan, 21-23, available on-line at http: //www. iccwbo. org/ uploadedFiles/ICC/policy/Environment/TechTransferFertilizerInd.doc

[32] L. K. Silva, D. C. Mariani, N. R. C. F. Machado, M. A. S. S. Ravagani, "A Genetic Algorithm for Synthesis and Optimization of Reactor System", 2nd Mercosur Congress on Chemical Engineering, 4th Mercosur Congress on Process Systems Engineering, Brazil.

[33] Yu-Ting Wu, Jianxun Ren, Zengyuan Guo, Chongfang Ma. 2004. "Dynamic Simulation of Closed Brayton Cycle Solar Thermal Power System", SET2004 , 3rd International Conference on Sustainable Energy Technologies, Nottingham, UK, 28-30.

[34] Lars Nummedal, Signe Kjelstrup and Monica Costea.2003. "Minimizing the Entropy Production Rate of an Exothermic Reactor with a Constant Heat-Transfer Coefficient: The Ammonia Reaction", Ind. Eng. Chem. Res., Vol. 42, 1044-1056.

[35] R. Byron Bird, Warren E. Stewart and Edwin N. Lightfoot.2003. Transport Phenomena, Second Edition, J. Wiley and Sons, Inc.

[36] Yu-Ting Wu, Jian-Xun Ren, Zeng-Yuan Guo, Xin-Gang Liang.2003. "Optimal Analysis of a space solar dynamic power system", Solar Energy, Vol. 74, pp. 205-215.

[37] K.V. Narayanan.2001. A Textbook of Chemical Engineering Thermodynamics, Prentice-Hall of India Ltd., New Delhi.

[38] T. F. Edgar, D. M. Himmelblau and L. S. Lasdon.2001. Optimization of Chemical Processes, 2nd edition McGraw-Hill chemical engineering series.

[39] Ammonia in Australia 2000, available on-line at http://www.chemlink.com.au/ammonia-summary.htm

[40] Dian Phylipsen, Dan Einstein and Nathan Martin.2000. "Energy Use and Energy Intensity of the U.S. Chemical Industry", Ernst Worrell, , LBNL-44314, University of California, Berkeley. available on-line at http://www.energystar.gov/ia/business/industry/industrial_LBNL-44314.pdf

[41] A. Luzzi, K. Lovegrove, E. Fillipi, H. Fricker, M. Schmitz-Goeb, M. Chandapillai and S. Kaneff.1999.

"Techno-Economic Analysis of a 10 MWe Solar Thermal Power Plant using Ammonia-Based Thermochemical Energy Storage", Solar Energy, Vol. 66 , No. 2, pp. 91-101.

[42] H. Kreetz and K. Lovegrove.1999. "Theoretical Analysis and Experimental Results of a 1 KW Ammonia Synthesis Reactor for a Solar Thermochemical Energy Storage System", Solar Energy, Vol. 67, Nos. 4-6, pp. 287-296.

[43] Irven Rinard.1999. "Material Balance Notes", Revision 3, Department of Chemical Engineering, City College of CUNY and Project ECSEL.

[44] W. L. Luyben, B. D. Tyréus and M.L. Luyben.1999. Plantwide Process Control, McGraw-Hill Companies Inc.

[45] Kerslake, T. W. and D. A. Jacqmin, "Radiation heat transfer modelling improved for phase-change thermal energy storage systems", available on-line at

[46] http://www.lerc.nasa.gov/WWW/RT1997?6000/6920kerslake3.htm

[47] Kyoto Protocol to the United Nations Framework Convention on Climate Change (UNFCC), United Nations 1998. Available on-line at http://unfccc.int/resource/docs/convkp/kpeng.pdf

[48] Costa, M., A. Oliva.1997. et al., "Three dimensional numerical study of melting inside an isothermal horizontal cylinder", Numerical Heat Transfer an International Journal of Computation and Methodology, Vol. 32(5), pp. 531-553.

[49] Costa, M., D. Buddhi.1997. et al., "Numerical simulation of a latent heat thermal energy storage system with enhanced heat conduction", Energy Conversion Management, Vol. 39(3/4), pp. 319-330.

[50] Kang, Y. H., Kwak, H.Y.1997. et al, "Numerical heat transfer analysis of heat storage board with microcapsule using phase change material" [online]. Available on-line at: http://oxford.elsevier.com

[51] Irving Granet.1996. Thermodynamics and Heat Power, Fifth Edition, Prentice-Hall Inc.

[52] William L. Luyben.1996. Process Modeling, Simulation and Control for Chemical Engineers, Second Edition, McGraw-Hill Publishing Company.

[53] Bansal, N. K. and D. Buddhi.1992. "Performance equations of a collector cum storage system using phase change materials", Solar Energy, Vol. 48, pp. 185-194.

[54] Hoogendoorn, C. J. and G. C. J. Bart.1992. "Performance and modeling of latent heat stores", Solar Energy, Vol. 48, pp. 53-58.

[55] Jotshi, C. K., D. Y. Goswami.1992. et al., "Solar thermal energy storage in phase change materials", Proceedings of Solar 92: The 1992 AM. Solar Energy Society Annual Conference, pp. 174-179.

[56] Ghoneim, A. A., S. A. Klein.1991. et al., "Analysis of collector-storage building walls using phase-change materials." Solar Energy, Vol. 47(3), pp. 237-242.

[57] Farid, M. M. and A. Kanzawa.1989. "Thermal performance of a heat storage module using PCM's with different melting temperatures: mathematical modeling", Journal of Solar Engineering, Vol. 111, pp. 152-157.

[58] Firoz Ahmad.1989. "Solar Radiation Studies at Karachi Pakistan, PhD Thesis", Department of Physics, University of Karachi, Pakistan.

[59] Yanadori, M. and T. Masuda.1989. "Heat transfer study on a heat storage container with a phase change material (Part2. heat transfer in the melting process in a cylindrical heat storage container)", Solar Energy, Vol. 42, pp. 27-34.

[60] Yu Yuguo and Wang Changying.1989. "Steady-State Simulation of Ammonia Synthesis Loop", Journal of Chemical Industry and Engineering (China), Vol. 4, No. 2.

[61] Bansal, N. K. and D. Buddhi.1988. "Solar thermal storage systems using phase change materials", International Journal of Energy Research, Vol. 12, pp. 547-555.

[62] J. S. Buchanan and S. Sundaresan.1987. "Optimal Catalyst Distribution and Dilution in Nonisothermal Packed Bed Reactors", Chem. Eng. Comm., Vol. 52, pp. 33-51

[63] Bengt Mansson and Bjarne Andresen.1986. “Optimal Temperature Profile for an Ammonia Reactor”, Ind. Eng. Chem. Process Des. Dev., Vol. 25, pp. 59-65

[64] Ralph W. Pike.1986. Optimization for Engineering Systems, Louisiana State University, Van Nostrand Reinhold, New York. (Open Library)

[65] Eftekhar, J., A. Haji-Sheikh.1984. “Heat transfer enhancement in a paraffin wax thermal storage system”, Solar Energy Engineering, Vol. 106, pp. 203-210.

[66] Michaels, I. A.1978. “An overview of the USA Program for the development of thermal energy storage for solar energy applications”, Solar Energy, Vol. 27, pp. 159-167.

[67] Morrison, D. J. and S. I. Abdel-Khalik.1978. “Effects of phase change energy storage on the performance of air-based and liquid-based solar heating systems”, Solar Energy, Vol. 20, pp. 57-67.

[68] Rajagopal, D., Krishnajwamy. 1978. “A simulation study of phase change energy store”, Proceedings of the Int. Solar Energy Society Congress, New Delhi, India.

[69] Kirk, D.E.1970.Optimal Control Theory: An Introduction, Prentice Hall, Inc., Englewood Clifffs, New Jersey.

[70] M.M. Denn.1970.Optimization by Variational Methods, McGraw-Hill Book Company, New York.

[71] Sagan Hans.1969.Introduction to the Calculus of Variations, McGraw Hill Book Co., New York.

[72] Forray, M. J.1968.Variational Calculus in Science and Engineering, McGraw-Hill Book Company, New York.

[73] Klaus Fuchs, “Pressure dependence of the equilibrium constant of Ammonia”, Proceedings of the Royal Society, Vol. 179 (1942), pp. 433-438.

Comparative Study Of Power Take-Off Units of OWC Based Wave Energy Power Plants

Zahid Suleman[1] and Hammad Bin Khaleeq[2]

Abstract

Ocean wave energy is one of the most abundant sources of renewable energy in the world. Current energy crisis of the world in usual and Pakistan in particular requires full exploitation of potential source of wave energy. To capture wave energy majority of the devices are based on oscillating water column (OWC) technique. Onshore OWC based wave energy power plants have shown great promise in converting raw wave energy into useful electricity in different parts of the world. So far most of the wave energy projects are using the Wells turbine as power take-off unit. But Wells turbine has some inherent disadvantages associated with it. On the other hand the Impulse turbine with fixed guide vanes has presented far better results than the Wells turbine. In this paper comparative study is presented that concludes on to the selection of impulse turbine with fixed guide vanes as power take-off unit for ultimate design of an onshore OWC based wave energy power plant. It is observed that the wave power of intensity about 15 kW/m of wave crest may be incident on Pakistani coastline.

Key Words: Wave Energy, Impulse Turbine, Wells Turbine, Oscillating Water Column.

Introduction

Energy is the indispensable want of life. From earliest times it can be seen that energy has been used in three forms; low temperature heat for comfort of human beings, force required for motion and high-temperature heat in order to work on materials and lightening purposes. These forms of energy are still in extensive use. After industrial revolution, there was need of more energy and hence extensive use of fossil fuels started to meet the growing energy demands [1].

Being inexpensive and easily available, the fossil fuels lead towards the wide usage in machinery. However, fossil resources are limited and are rapidly depleting. Therefore, there is a need to exploit renewable energy resources. The various types of renewable energy resources are solar, wind, geothermal, hydel, biomass, tidal and wave energy of ocean.

Wave energy is generated by wind passing over stretches of water. As the wind is originally derived from solar energy, it can be taken as to be the high-density form of solar energy. The World Energy Council estimates that a total of 2TW of energy could be harnessed from the world's oceans, the equivalent of twice the world's electricity production.

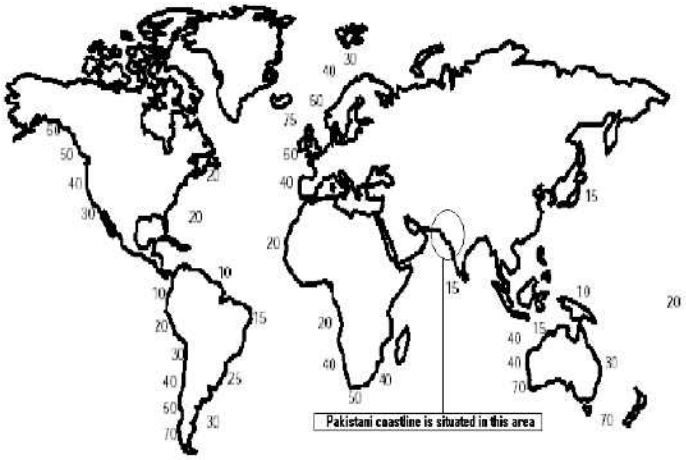

Figure 1: Global distribution of annual wave power level in kW / m wave crest [5]

[1] Mechanical Engineering Dept., University of Engineering and Technology, [2] Engineering Systems Pak, Islamabad.

Among the renewable energy resources, ocean wave energy is an abundant, persistent and clean source of power and is available round the clock. Wave energy technology is an emerging technology [2, 3, 4]. Currently world is facing very serious energy crisis. Especially in Pakistan the situation regarding energy is the worst. The shortage of the energy is badly affecting the economy of the homeland. In this scenario wave energy resource should be exploited to meet the energy demand. Pakistan is gifted with long coastline of about 1000 kilometer by Allah. Global distribution of annual wave power level in kW/ m wave crest is shown in Fig. 1 [5]. Region of Pakistani coastline is highlighted by the authors in Fig.1. More wave power is available on headlands and it is 15 kW/m of wave crest on the nearest headland in Fig.1.

Therefore, it is estimated that the wave power of intensity slightly less than 15 kW/m of wave crest may be incident on Pakistani coastline.

Wave Energy Technology

A number of device concepts have been used to capture wave energy over the period and to convert it into useful form of energy. Practical application of different techniques or device concepts in prototypes in the sea indicated that only one technique i.e., the Oscillating Water Column or OWC could be thought of near to full development or ripeness [6, 7].

Oscillating Water Column (OWC)

The OWC based wave energy power plant consists of a concrete or steel structure which is partially submerged in the sea water. This structure has an opening towards the sea below the water line, therefore enclosing air above the column of water as shown in Fig. 2. When waves of sea water travel and reach the structure, they cause the water column inside the chamber of the structure to rise and fall. This rise and fall i.e., oscillation of water column causes the air to exhale and inhale. The exhaling and inhaling air is allowed to pass to and from the atmosphere through a self-rectifying turbine which drives an electric generator [8, 9, 10, 11].

The self-rectifying turbines are those turbines that are capable to rotate in one direction only irrespective of the direction of airflow passing over them. This characteristic of self-rectifying turbine is due to their specially designed symmetric blade profiles. Over the period of time many different types of turbines have been developed. Among them the two prominent self- rectifying turbines used for wave energy power conversion are discussed below [12].

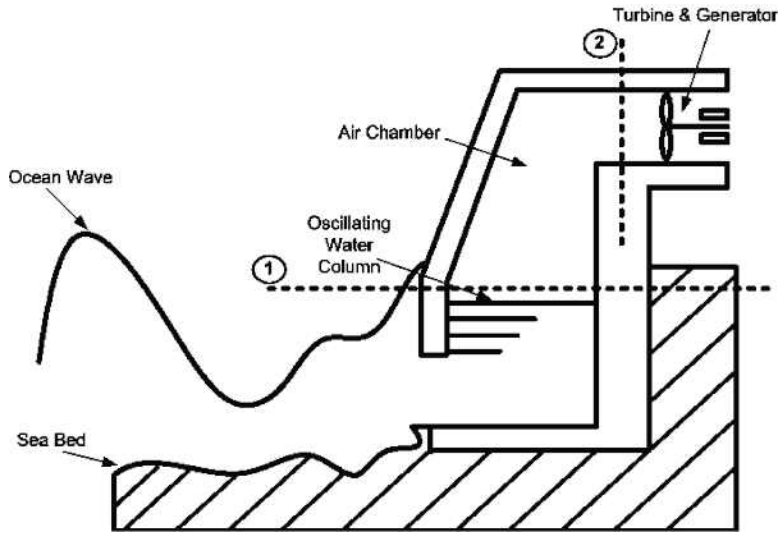

Figure 2: Schematic of onshore OWC based wave energy power plant [11]

The Wells Turbine

Dr. A.A Wells of Queen's University, Belfast, UK, invented the Wells turbine in 1976, (Fig. 3). This turbine is an axial flow self- rectifying turbine and is suitable for wave energy conversion in an oscillating water column. This turbine has a symmetric blade shape commonly based on NACA four digit profiles. It works on the basic aerofoil theory. The lift over the aerofoil creates a tangential torque component that makes the turbine to rotate. It is a high-speed turbine and operates between 700 to 1500 rpm.

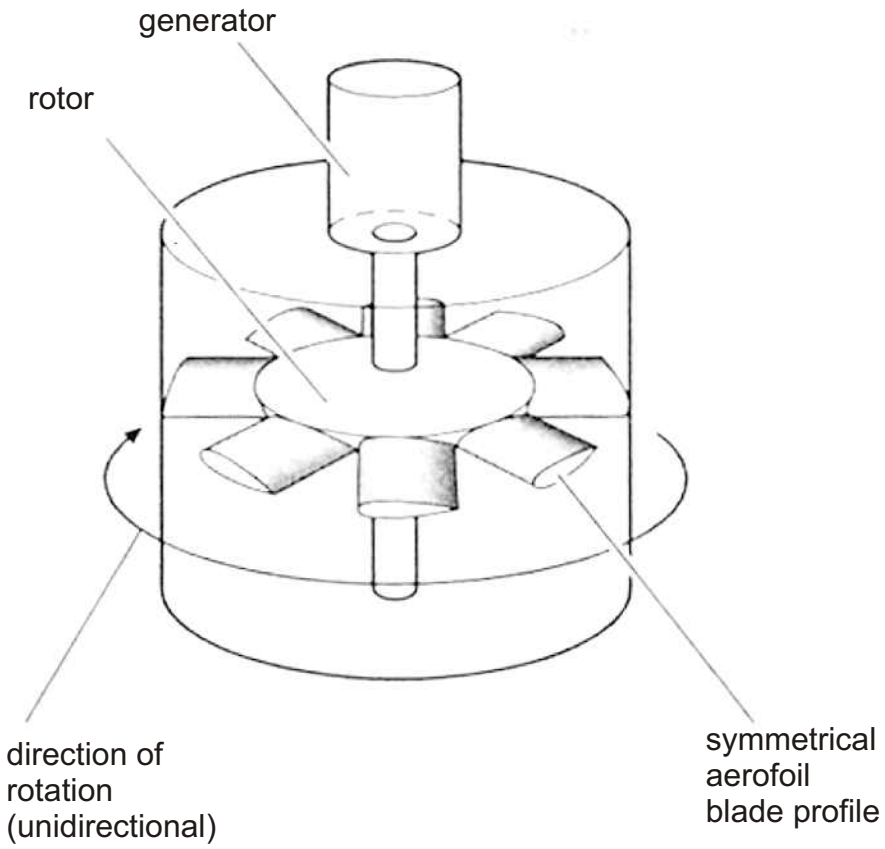

Figure 3: The Wells turbine schematic diagram [12]

Several reports describe the performance of Wells turbine. According to these reports it is established that the Wells turbine has some inherent disadvantages that are narrow range of flow rates at which it operates at useful efficiencies, poor starting characteristics, high speed operations and consequent noise and high axial thrust [12]. So far some new versions have been tried to overcome these weak points. Some other types of the Wells turbine are given in the following.

(i) Wells turbine with guide vanes (WTGV) Fig. 4

(ii) Turbine with self-pitch-controlled blades (TSCB) Fig. 5

(iii) Biplane Wells turbine with guide vanes (BWGV) Fig.6.

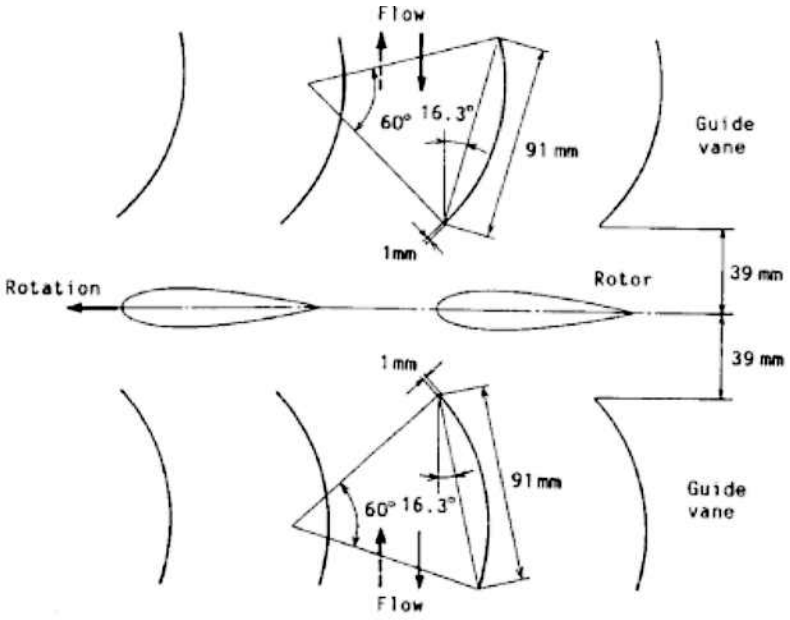

Figure 4: Wells turbine with guide vanes (WTGV) [13]

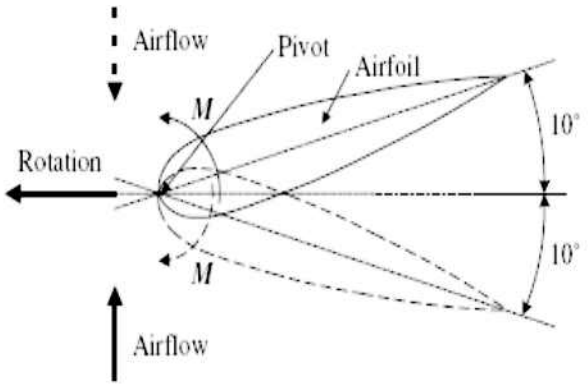

Figure 5: Turbine with self-pitch-controlled blades (TSCB) [13]

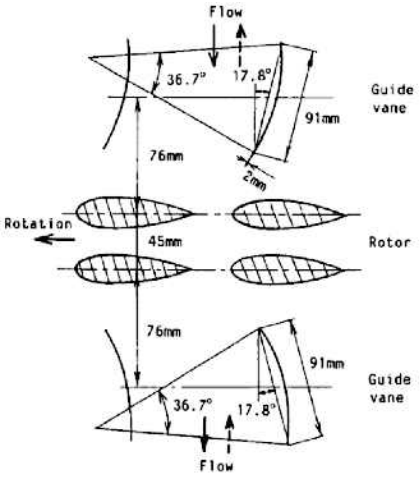

Figure 6: Biplane Wells turbine with guide vanes (BWGV) [13]

As mentioned earlier the Wells turbine is the most commonly used self- rectifying turbine on OWC based wave energy power plants so far, but its inherent disadvantages led to the shift towards other self-rectifying turbines.

The Impulse Turbine

By the time of introduction of the Impulse turbine by Kim and his team, in 1988, the research on both turbines was in progress in Japan. The most important contribution in this research work was added by Professor T. Setogouchi and his team at Saga University of Japan in Collaboration with other Universities and Institutions of Japan, Asia and Europe.

Fig. 7 shows the rotor of the Impulse turbine. This rotor is surrounded by two sets of guide vanes on either side. Under the action of these two sets of guide vanes the turbine becomes capable of rotating in one direction only in a bidirectional air flow.

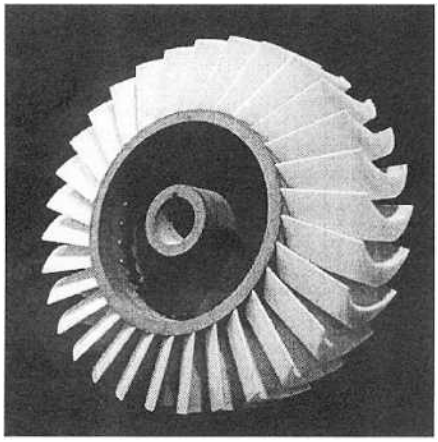

Figure 7: Rotor of the Impulse turbine [12]

A number of Impulse turbines for the wave power conversion have been presented so far. Among them three important impulse turbines are as follows.

I. impulse turbine with self-pitch-controlled guide vanes (ISGV) (Fig. 8)

II. impulse turbine with self-pitch-control linked guide vanes (Fig. 9)

III. impulse turbine with fixed guide vanes (IFGV) (Fig. 11)

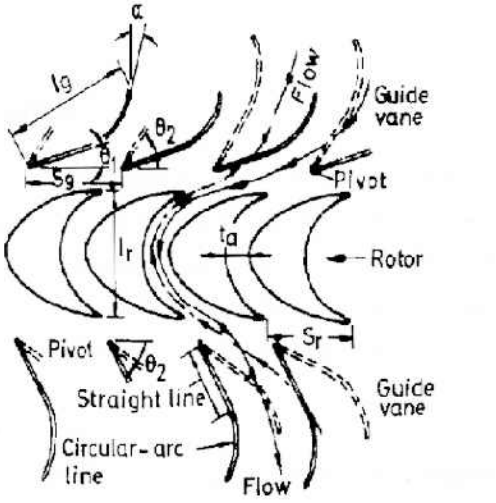

Figure 8: Impulse turbine with self-pitch controlled guide vanes [13]

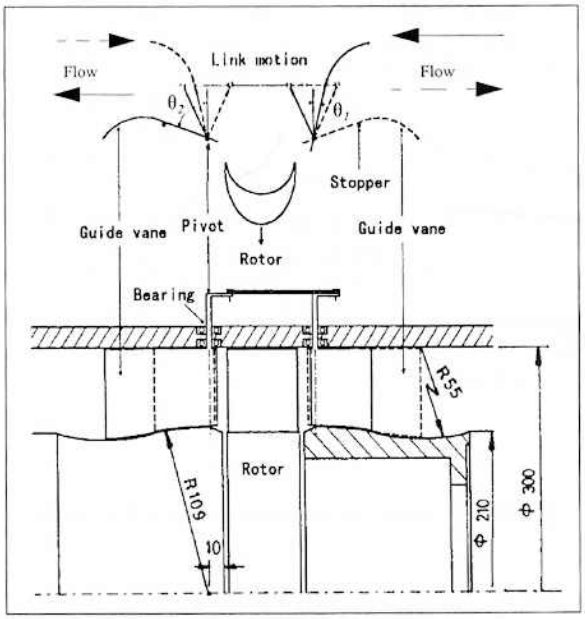

Figure 9: Meridional section of Impulse turbine with self-pitch-control linked guide vanes [13]

For same guide vane geometry parameters, other than links, as used for the Impulse turbine with self-pitch-controlled guide vanes it was found that the efficiency of turbine with linked guide vanes was superior (Fig.10).On the other hand this configuration has its own disadvantage of enlarged maintenance due to presence of larger number of moving parts. Consequently this lead towards the impulse turbine with fixed guide vanes.

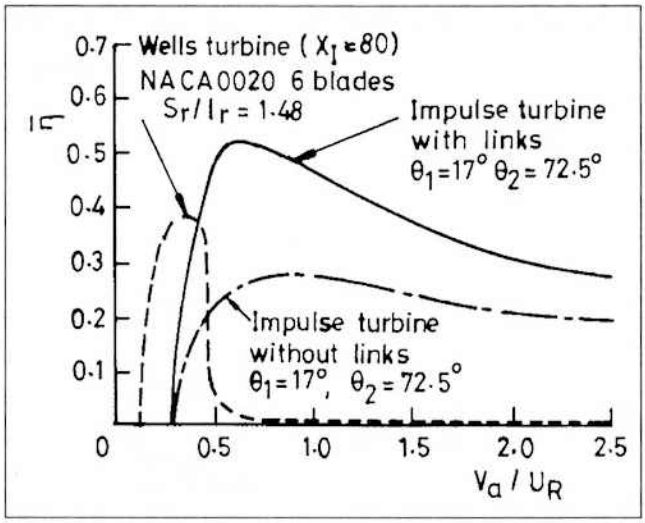

Figure 10: Comparison of mean efficiency [12}

Impulse Turbine with Fixed Guide Vanes

Due to large number of moving parts in complex design of moving guide vanes with links frequent maintenance was the major problem. Therefore, it was proposed by the researchers that if the guide vanes were fixed on both ends at an optimum angle, this problem could be overcome. Although this configuration will affect the peak efficiency of the turbine but the simple design can compensate for the slight drop in the overall performance. In this configuration, there are two rows of symmetrically placed fixed guide vanes on both sides of the rotor with a fixed inlet/outlet angle Fig.11.

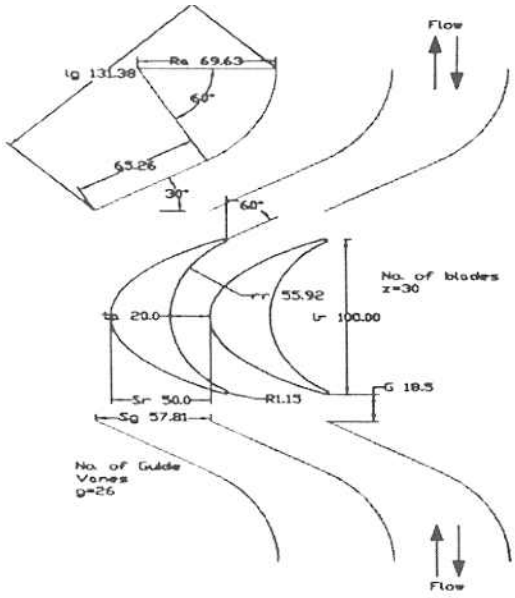

Figure 11: Impulse turbine with fixed guide vanes [12]

Efficiency Comparison of Impulse Turbine with Fixed Guide Vanes and the Wells Turbine

Comparison of both Wells and Impulse turbines with similar tip diameter of 0.6m and a hub to tip ratio of 0.6 under regular flow conditions is presented here. The experimental data used for the Wells and Impulse turbines for this analysis is taken from the work carried out by Bajeet, 2001[14] and Khaleeq, 2002 [12] respectively.

For the comparison of the two turbines, experimental data under uni-directional steady flow conditions were used. The data for the Impulse turbine was based on a constant rotational speed of 350 rpm and for the Wells turbine, at a constant rotational speed of 1700 rpm.

The plot shown in the (Fig. 12) gives the comparative efficiency curves for both turbines based on experimental data. It can be observed that the Wells turbine is giving a peak efficiency of 74% as compared to 48.73% achieved by the impulse turbine. It can also be observed that the Wells turbine stalls at a flow coefficient of 0.38 whereas the impulse turbine keeps on giving useful output for higher flow coefficient.

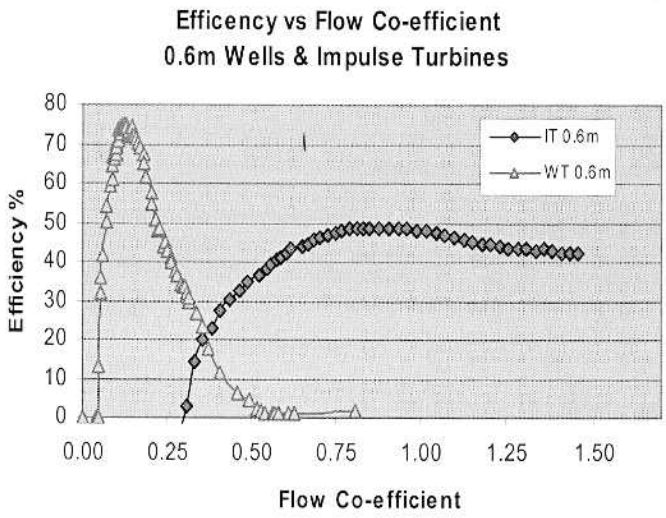

Figure 12: Efficiency Comparison under regular flow conditions [12]

Therefore, it can be said that the Impulse turbine has a far better range of efficient and stable operation as compared to the Wells turbine. Its wide operational range compensates for its lower maximum efficiency (48.73% compared to 74% for the Wells turbine). Therefore, it is believed that the Impulse turbine is capable of coping up with high intensity waves, the conditions where the Wells turbine is believed to stall. This also shows the Impulse turbine can operate at lower rotational speed whereas the Wells turbine is a high speed turbine and therefore has its disadvantages from maintenance problems as well as high noise operation. Although, this particular configuration of the Wells turbine showed that it is self-starting, as compared to the other configurations, the Impulse turbine is inherently self-starting, which gives it another edge over low-solidity vaneless Wells turbines [12].

Comparison of conversion efficiencies and starting characteristics of Impulse type and Wells type turbines

An important study was carried out by Setoguchi and Takao in 2005 [13] to compare the performances of self rectifying turbines under irregular wave conditions which are prevailed in real sea conditions. The performances were evaluated numerically.

In Fig.13 comparison of conversion efficiencies of five above mentioned turbines is presented. Conversion efficiency may be defined as the product of the efficiencies of the air chamber and the turbine. It can be seen that conversion efficiency for impulse type turbines is higher than the Wells type turbine.

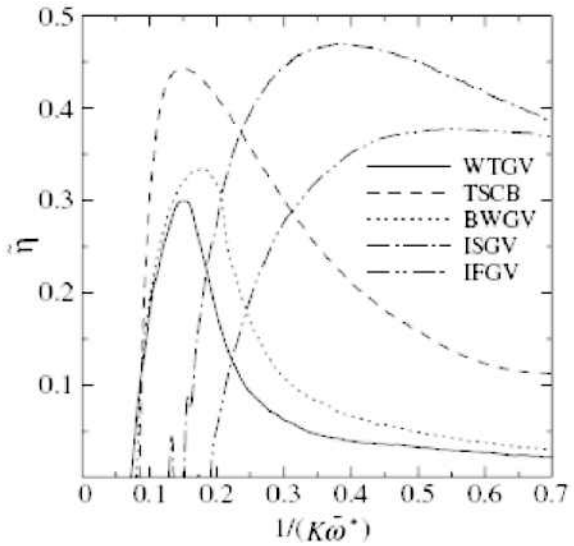

Figure 13: Comparison of conversion efficiency of wave energy [13]

In Fig.14 starting characteristics under irregular sea conditions are presented. Analysis of the figure shows that the impulse turbine can start in short time than the Wells turbine. This means that the generating time of a generator with the impulse turbine is more than that of the Wells turbine. Also the operational speed of the impulse turbine is less than that of the Wells turbine which is helpful in noise reduction. It can be concluded that the impulse turbine is superior to that of the Wells turbine in starting and running characteristics [13]. Summary of the comparison of the two turbines can be presented in the tabular form as given in table 1.

Conclusions

It can be concluded from the above presented study that the impulse type turbines are superior to the Wells type turbines. The Wells turbine has high operational speed, therefore produces more noise while the impulse turbine has low operational speed which is merit in noise reduction. The study also indicates that

Table 1: Summary of comparison

Sr.No.	Wells Turbine	Impulse Turbine
1	High operating speed	Low operating speed
2	High axial thrust	Low axial thrust
3	High noise	Low noise
4	Low solidity	High Solidity
5	Poor starting characteristics	Good starting characteristics
6	Narrow range of flow rates	Wide range of flow rates
7	Delivers maximum output /efficiency at a particular value of flow coefficient	Delivers useful output/efficiency at wide range of flow coefficient
8	It stalls at high flow coefficients	There are no stall conditions
9	Can not cop up with high intensity waves	Can cop up with high intensity waves
10	Poor range of efficient and stable operation	Better range of efficient and stable operation
11	Poorer starting and running characteristics	Superior starting and running characteristics

the conversion efficiency of the impulse type turbines is superior to the Wells type turbines. Starting and running characteristics of the impulse type turbines are better than the Wells type turbines. The Wells turbine delivers maximum output or efficiency at a particular value of flow coefficient above which it stalls. The impulse turbine delivers useful output or efficiency at a wide range of flow coefficient and there are no stall conditions. The Wells turbine does not respond well in high intensity waves, whereas the impulse turbine performs well in this situation.

If the performance of the impulse turbine with self-pitching guide vanes is compared with the performance of the impulse turbine with fixed guide vanes it is found that the former is superior to the later. But on the other side it is seen that due to presence of larger number of moving parts in self-pitching guide vanes configuration frequent maintenance is problematic. This difficulty can be mitigated by compromising on a little reduced efficiency or performance by adopting the impulse turbine with fixed guide vanes. Reduced maintenance will result in longer operational life and less cost. Therefore, the impulse turbine with fixed guide vanes is a better choice, as power take-off unit for an onshore OWC based wave energy power plant, in comparison to the Wells turbine. The impulse turbine with fixed guide vanes has a far better range of efficient and stable operation as compared to the Wells turbine. It delivers useful efficiency over a wide range of flow coefficient.

It is required to promote R & D in the wave energy and its technology in Pakistan so that the potential source of wave energy can be exploited to reduce the energy crisis. This will contribute towards the strengthening of the economy of the homeland.

References

[1] Alexander, G., 1996. Chapter 1, Overview - The Context Of Renewable Energy Technologies, in: Renewable Energy – Power for a Sustainable Future, Boyle, G., Ed, 1 – 40, Oxford, UK: Oxford University Press.

[2] [Zhang, D., Li W., and Lin Y., “Wave Energy in China: Current Status and Perspectives”, Renewable Energy, Volume 34, pp. 2089-2092, 2009.

[3] Flanes, J., "A review of wave-energy extraction", Marine Structures, Volume 20, pp. 185-201, 2007.

[4] Liu, Z., Hyun, B.S., Hong, K.Y., and Lee, Y. Y., "Investigation on Integrated System of Chamber and Turbine for OWC Wave Energy Converter", Proceedings of the Nineteenth (2009) International Offshore and Polar Engineering Conference, Osaka, Japan, June 21-26, 2009.

[5] Richard Boud, 2003. Department of Trade and Industry, UK, Status and Research and Development Priorities/2003, Wave and Marine Current Energy, 24 report number FES-R-132, AEAT report number AEAT/ENV/1054.

[6] The Marine Institute and Sustainable Energy Ireland, Options for the Development of Wave Energy in Ireland, A Public Consultation Document, November 2002.

[7] Neumann, F., IST-MARETEC, Turbomaquinas, P., and Av. Rovisco Pais, "Advanced Coastal Structures Incorporating Wave Energy Caissons", e-mail frank@hidro1.ist. utl.pt

[8] Thakker, A., Jarvis, J., and Sahed, A., "Quasi-Steady Analytical Model Benchmark of an Impulse Turbine for Wave Energy Extraction", International Journal of Rotating Machinery, Volume 2008,pp. 1-12, 2008.

[9] Conde, J.M.P., and Gato, L.M.C., "Numerical study of the air-flow in an oscillating water column wave energy converter", Renewable Energy, Volume 33, pp. 2637-2644, 2008.

[10] Anand, S., Jayashankar, V., Nagata, S., Toyota, K., Takao, M., and Setoguchi, T., "Turbines for wave energy plants", Proceedings of the 8th International Symposium on Experimental and Computational Aerothermodynamics of Internal Flows, pp. 1-7, Lyon, July, 2007.

[11] Suleman, Z., and Khaleeq, H.B., "Design Analysis of Power Extracting Unit of an Onshore OWC based Wave Energy Power Plant using Numerical Simmulation", Mehran University Research Journal of Engineering & Technology, volume 30, pp. 397-404, University of Engineering and Technology, Mehran, Jamshoro, Sindh,Pakistan, July, 2011.

[12] Khaleeq, H. B., 2002."Design Analysis of the Impulse Turbine with Fixed Guide Vanes for Wave Energy Power Conversion", Ph. D. Thesis, University of Limerick, Republic of Ireland.

[13] Setoguchi T., & Takao M., 2006, "Current status of self rectifying air rectifying for wave energy conversion", Energy Conversion & Management, ELSEVIER, pp. 2382-2396.

[14] Bajeet, E. S., 2001. Performance analysis of Wells Turbine for Wave Energy Conversion. Ph. D. Thesis. University of Limerick, Republic of Ireland.

Guidelines And Information For Authors

General

Papers may be submitted any time throughout the year. After having received a paper it is sent to three referees, at least one from a technology advanced countries. Papers reviewed and declared fit for publication before 31 December are published next year before 31 March every year. Papers must be submitted on a CD with FOUR Hard copies to the editor Technical journal, University of Engineering and Technology Taxila. Soft copy by e-mail to the following address is preferred.

technical.journal@uettaxila.edu.pk

Authors are required to read the following carefully for writing a paper.

Text

Text should be type-written with M.S word, Arial Font size 10.at single space and with margins as 1.5 inch top, 1 inch right, 1 inch left and 1 inch bottom, on an A-4 size, paper. The title page should include; the title; the name/names of the authors and their addresses, an abstract of about 200 words and keywords followed by the introduction. The text of the paper may be divided into introduction, methodology/Analysis results and discussion, conclusion, references and acknowledgment (if any). All pages should consist of single columns text.

Length

Research paper should not exceed 15 pages as per specifications given above.

Elements of Paper

The basic elements of paper are listed below in the order in which they appear: Title, names of the author and affiliations, Abstract, Body of paper, Acknowledgments, Nomenclature, references, Appendices.

Title

The title of the paper should be concise and definitive.

Names of Authors and Affiliations

Names of authors should consist of first name (or initial), middle initial and last name. The author affiliation should consist of his full address.

Abstract

An abstract up to a maximum of 200 words should open the paper. The abstract should give a clear indication of the objectives, scope and results, the abstract text may be organized to include the background, methods, results and conclusions.

Keywords

Keywords should be included on a separate line at the end of the abstract.

Body of the Paper

Body of the paper may include introduction and literature review, materials and methods, modeling/experimentation, results-discussions and conclusions.

Originality

Only original contributions to engineering and Science literature should be submitted for publication. It should incorporate substantial information not previously published.

Accuracy

All the technical, scientific and mathematical information contained in the paper should be checked with great care.

Use of SI Units

Preferably SI units of Measurements be included.

Mathematics

Equations should be numbered consecutively beginning with (1) to the end of the paper. The number should be enclosed in parentheses (as shown above) and set flush right in the column on the same line as the equation. This number then should be used for referring the equation within the text. Equation may be referenced within the text as “E q. (x)”.”When the reference to an equation begins a sentence, it should be spelled out fully, as “Equation (x).in all mathematical expressions and analyses, symbols (and the units in which they are measured) not previously defined in nomenclature should be explained.

Figures

All figures (graphs, line drawings, photographs, etc.) should be numbered consecutively and have a caption consisting of the figure number and a brief title or description of the figure. This number should be used when referring to the figure in the text. Figure references should be included within the text in numerical order according to their order of appearance. Figure may be referenced within the text as “Fig.-x”. When the reference to a figure begins a sentence, the abbreviation “Fig,” should be spelled out e.g.,” Figure-x”

Tables

All tables should be numbered consecutively. Tables should have a caption consisting of the table number and brief title. This number should be used when referring to the table in text. Table references should be included within the text in numerical order according to their order of appearance. Table should be inserted as part of the text as close as possible to its first reference.

Acknowledgments

All individuals or institutions not mentioned elsewhere in the work who have made an important contribution should be acknowledged.

References

Within the text, references should be cited with name of the author and year in parenthesis. The reference list will be arranged alphabetically.

Example

Chamber (1959) has described a method and Wormleaton (2006) used this method. In case of two authors, name of both the authors will appear with year. For example Khan and Ghumman (2008) studied hydrodynamic modeling for water-saving strategies in irrigation canals. In case of three or more authors it will be cited as: Ghumman et al. investigated use of numerical modeling for management of canal irrigation water in case of continuous references, the references may be separated by comma”,” See the list of sample references.

List of References

References to original source of the cited material as given above as sample reference should be listed together at the end of the paper, footnotes should not be used for this purpose. References should be arranged in alphabetic order. Each reference should include the last name of each author followed by his initials.

1. Reference to journal articles and paper in serial publication include :Last name of each author followed by their initial, Year of publication, Full title of the cited article, Full name of the publication in which it appears, Volume number (if any) in boldface, Issue number (if any) in parentheses, Inclusive page number of the cited article.
2. Reference to the text books and monographs should include: Last name of each author followed by their initial, Year of publication, Full title of the publication, Publisher, City of publication, Inclusive page number of the work being cited, Chapter number(if any).
3. Reference to original conference papers, papers in compiled conference proceedings or any other collection of woks by numerous authors should include: Last name of each author followed by their initial, Year of publication, Full title of the cited paper in quotes, individual paper number (if any) ,Full title of the publication , Initial followed by the name of the editor (if any),followed by the abbreviation, "eds" ,Publisher, City of publication, Volume number (if any),Inclusive Page number of the work being cited.
4. Reference to thesis and technical reports should include: Last name of each author followed by their initial, Year of publication, Full title in quotes, title capitalization, Report number(if any) Publisher or the institution name, City.

Sample References

[1] Bievere B.D Alvarado, A.Timbe, L. Celleri and J. Feyen 2003.Night irrigation reduction for water saving in medium-sized system, Journal of irrigation and Drainage Engineering, ASCE Vol.129, N0.2.337-348.

[2] Chamber R.1988. Managing canal irrigation: Practical Analysis from South Asia, Institution of Development Studies, Oxford & IBH Publishing Co. Ltd.

[3] Strelkof T.1969.One-dimentional equations of open-channel flow. J. Hydraulics Div., ASCE, Vol.95 (HY3):861-876

[4] Khan,M.Z. 2006. Investigation of the optimal operation strategies for irrigation systems. Ph.D.Dissertation. Department of Civil Engineering, University of Engineering and Technology Taxila.

[5] Ghumman, A.R., M.Z. Khan, and M.J. Khan.2006.Use of numerical Modeling for Management of Canal Irrigation Water. Irrigation and Drainage.Wilay Intersciencez. : 445-458.

[6] Khan M. Z. and Ghumman A. R.2008, Hydrodynamic Modeling For Water-Saving Strategies In Irrigation Canals.